Biophysical and functional consequences of sequence changes on dystrophin and utrophin

A DISSERTATION
SUBMITTED TO THE FACULTY OF
UNIVERSITY OF MINNESOTA
BY

Jackie Lynn McCourt

IN PARTIAL FULFILLMENT OF THE REQUIREMENTS
FOR THE DEGREE OF
DOCTOR OF PHILOSOPHY

Adviser, James M. Ervasti

April, 2017

Acknowledgements

I would like to thank my thesis advisor, Jim Ervasti, for teaching and mentoring me towards my career goals how and demonstrating excellence in scientific scholarship. I could not have asked for a better mentor.

To the Ervasti Lab, both past and present - thank you. Thank you to Joe and Dana for training me in; to Chris, Alli, JT, Xiaobai, D'anna, Preston, and Tung, for helping me with experiments, for excellent discussions and suggestions, and for generally putting up with me.

I would like to thank Murti Salapaka, Sayan Ghosal, and Sivaraman Rajaganapathy for being such excellent collaborators.

I would like to thank the wonderful graduate students from my year who have helped me survive classes, prelims, and the graduation process. Thank you to Darlene Toedter, Sarah Dittrich, and Sue Knoblauch, the program administrators, who have guided me through all the graduate school and program requirements.

I would like to acknowledge Dave Thomas and the Minnesota Muscle Training grant, the U of MN Muscular Dystrophy Center, the Minnesota ARCS Foundation, the Ryan's Quest Foundation, the Mary Dempsey, Amstrong-Pothapragada, Cyrus Barnum, and Ross A. Gortner Fellowhips for supporting my graduate career.

I would like to thank my committee members, Carrie Wilmot, Dave Thomas, Tom Hays, Melissa Gardner, and Scott Dehm for your helpful criticisms and advice on my project over the years.

To my close friends from Minnesota, Young Life, Bethlehem, Arizona, California, and China - they know who they are - thank you for cheering me on through graduate school and life.

I am especially grateful to my family who have offered me never-ending love and support. To my parents, Jeff and Peggy, - thank you for your continuous prayers, housing, and meals. To my siblings Alisa, Aaron, Kara, and Preston - thank for your encouragement, humor and kindness and for giving me the cutest and most loving nieces and nephews.

Finally, I would like to thank God - my Creator, Redeemer, and Sustainer.

Dedication

This dissertation is dedicated to my grandparents, Dorothy and Leslie Griffee and Jan and Michael McCourt.

Abstract

Mutations in the DMD gene result in Duchenne (DMD) and Becker (BMD) muscular dystrophies. The DMD gene encodes the protein, dystrophin that is predominantly expressed in skeletal muscle. Dystrophin is part of a larger protein complex known as the dystrophin-glycoprotein complex (DGC) and, as part of the DGC, provides a mechanical link between the sub-sarcolemmal cytoskeleton and the extracellular matrix. BMD is typically caused by mutations that maintain the reading frame and most often produce variable levels of internally truncated, partially functional dystrophin wheras DMD is most frequently characterized by a complete loss of dystrophin protein or disruption of key ligand binding domains. Utrophin has a highly similar overall structure to dystrophin and is part of the homologous utrophin-glycoprotein complex (UGC) present during fetal development and is localized to neuromuscular and myotendinous junctions in adult muscle.

Our lab has previously demonstrated that dystrophin protein *in vitro* thermal stability is sensitive to disease-causing missense mutations and internal deletions. In contrast, utrophin displays uniform stability upon internal deletion or terminal truncation. Several therapeutic strategies to treat DMD utilize internally deleted dystrophins, including the recently FDA approved exon-skipping drug, eteplirsen, as well as adeno-associated virus (AAV) mediated delivery of therapeutic micro-dystrophins. Here, we characterized therapeutically relevant, internally truncated dystrophin constructs that have been proposed by leading scientists in the field. We show that, as a group, gene therapy micro-dystrophins are significantly less stable *in vitro* than full-length dystrophin whereas exon-skipped dystrophins have stability profiles congruent with full-length dystrophin.

To address the consequences of dystrophin instability *in vivo*, we generated two novel transgenic mouse models expressing missense mutant dystrophins reported in human DMD (L54R) and BMD (L172H) patients. The L54R and L172H missense mutants were previously evaluated in cultured myoblasts and shown to have missense-mutant dystrophin levels that were inversely proportional to *in vitro* stability and disease severity of the corresponding patients. Analysis of the L54R and L172H mouse lines as well as a homozygous L172H mouse reveal that disease severity inversely correlates with expression levels of dystrophin protein. Based on the increase of mutant dystrophin upon proteasome inhibition in cultured myoblasts, our hypothesis is that missense dystrophin proteins are being targeted to the proteasome for degradation through the ubiquitin-proteasome pathway. To determine the specific ligases involved in targeting missense dystrophins to the proteasome, we screened an siRNA library of over 500 ubiquitin-conjugating enzymes in cultured myoblasts and identified five putative dystrophin-specific E3 ligases. Two of the identified ligases, Amn1 and FBXO33, were observed in our transgenic mouse lines, with Amn1 protein levels showing significant increases correlating with the amount of missense dystrophin present. Our future studies will continue to evaluate the impact of Amn1 and FBXO33 activity on dystrophin protein levels in order to identify potential therapeutic targets.

In addition to the characterization of dystrophin and utrophin stability, we have begun to interrogate a long-hypothesized but understudied function of dystrophin and utrophin, namely, their roles as molecular springs to mechanically stabilize the muscle membrane during muscle contraction. Using atomic force microscopy (AFM), we show here the first mechanical characterization of utrophin and functionally relevant utrophin fragments. Our data reveal striking differences in the mechanical properties of N- and C-terminal halves of utrophin despite having nearly identical thermal stabilities and high

structural homology. The high unfolding forces observed in utrophin and the evidence of stiffening spring behavior suggest that utrophin may be acting as a stiff elastic element in series with the giant muscle protein, titin, at the myotendinous junction. Future studies will include evaluation of myotendinous defects in utrophin-deficient mice as well as mechanical characterization of full-length dystrophin.

Table of Contents

List of Tables

List of Figures

Chapter 1

Introduction

Duchenne Muscular Dystrophy and the DMD gene

Disruptions in the structural components of the muscle fiber result in a wide variety of muscular dystrophies (Cohn and Campbell, 2000). One subtype, Duchenne muscular dystrophy (DMD), is an X-linked recessive disease and is the most prevalent of the muscular dystrophies affecting 1 in 4000 born males (Mendell et al., 2012). DMD, like many muscular dystrophies, is characterized by progressive muscle weakness and loss of motor function. The progression of DMD is typically high plasma levels of creatine kinase (CK) at birth (Zellweger and Antonik, 1975), muscle fiber hypertrophy during early childhood (Dennett et al., 1988), weakness of the proximal muscles (Gowers, 1886), loss of ambulation, and pulmonary and cardiac dysfunction towards the end of the second decade leading to death (Kohler et al., 2009). While there are some treatments to manage symptoms and improve quality of life, there is still no cure for DMD.

The gene mutated in DMD was identified in 1987 on the X chromosome and is the largest gene found in nature, spanning over 2.4 million base pairs (Koenig et al., 1987). The DMD gene is transcribed into several different tissue specific transcripts from internal promoters and its full-length isoform contains 79 exons (Muntoni et al., 2003). The full length transcript encodes the protein dystrophin (discussed in greater detail below), which is predominantly expressed in skeletal muscle (Hoffman et al., 1987). One-third of DMD patients have *de novo* germline mutations with the remaining two thirds having heritable mutations passed down from asymptomatic or mildly affected female carriers (Flanigan, 2014).

Mutations in the DMD gene can also lead to a milder form of the disease, Becker muscular dystrophy (BMD), which is typically caused by mutations that maintain the reading frame and most often produce variable levels of internally truncated, partially

functional dystrophin (Monaco et al., 1988; Koenig et al., 1989). In contrast, DMD is most frequently characterized by a complete loss of dystrophin protein or disruption of key ligand binding domains. Mutation types for DMD and BMD vary with 68.5% of patients harboring large deletions (>1 exon), 11% with duplications (>1 exon), 10% with non-sense mutations, 6% with smaller deletions or insertions (<1 exon), 3% with splice-site mutations, and the remaining patients with rare mid-intronic or missense mutations (Figure 1.1, Bladen et al., 2015). Two mutational hot spots have been identified in exons 2-20 and exons 45-55, with 80% of large deletions and 65% of duplications found in these regions (Oudet et al., 1992; Bladen et al., 2015). The genetic and phenotypic diversity found in DMD and BMD patients makes studying and treating the diseases very challenging but has also stimulated efforts to determine mechanisms of disease and to develop personalized therapies.

Dystrophin and Utrophin

Dystrophin is a 427kDa rod-shaped protein comprised of an amino-terminal actin binding domain (ABD1), a central rod domain, a cysteine rich domain, and a carboxy-terminal domain (Koenig et al., 1988). Due to its large size, a high-resolution structure of full-length dystrophin has not been determined, however, the crystal structures of individual domains have been solved. The amino terminus contains a tandem calponin homology (CH) domain that binds actin filaments. The crystal structure revealed an α-helical globular fold of the individual CH domains connected by an α-helix linker (Norwood et al., 2000). The carboxy terminus is composed of a cysteine rich (CR) region containing two EF-hand modules, a WW domain, and a ZZ domain, all of which are required for binding to the transmembrane protein β-dystroglycan. The central rod domain is the largest domain of dystrophin, containing 24 spectrin-type repeats. Spectrin repeats are independent motifs of left-handed, antiparallel, triple-helical coiled coils (Pascual et al., 1997). The dystrophin sequence was mapped using the spectrin repeat model that predicted similar triple-helical bundles but revealed unique, interspersed proline-rich regions within the dystrophin central rod domain (Koenig and Kunkel, 1990). These regions are designated as “hinges” and are thought to add flexibility to the rod-like structure or delineate three separate sub-domains (Legardinier et al., 2008). One proposed model for the structure of the central rod domain is that the spectrin-type repeat motifs are structurally “nested” within each other (Mirza et al., 2010). The crystal structure of dystrophin’s first repeat supports this model by revealing an extension of the structural domain at the C-terminus (Muthu et al., 2012).

Dystrophin is thought to function as a mechanical link between the cortical cytoskeleton and the extracellular matrix and has been shown to interact with a variety of

different proteins and lipids (Figure 1.2). At the N-terminus are binding domains for actin and keratin 19 (Way et al., 1992; Stone et al., 2005). Within the central rod is a second actin-binding domain (Rybakova et al., 1996) as well as domains for binding phospholipids, Par1b, neuronal nitric oxide synthase (nNOS), synemin, and microtubules (Legardinier et al., 2009b; Prins et al., 2009; Yamashita et al., 2010; Lai et al., 2013; Belanto et al., 2014). The cysteine-rich and C-terminal domains bind plectin, phospholipids, ankrin B/G, dystrobrevin, syntrophin, and β-dystroglycan (Suzuki et al., 1992; Albrecht and Froehner, 2002; Hijikata et al., 2003; Ayalon et al., 2008; Legardinier et al., 2009b). Through these interactions, dystrophin is part of a larger, sub-sarcolemmal protein assembly enriched at costameres, known as the dystrophin-glycoprotein complex (DGC) (Figure 1.3, Ervasti and Campbell, 1991; Ervasti, 2007, 2003). The core components of the DGC are dystrophin, α-dystrobrevin, and syntrophin, the sarcoglycans, sarcospan, β-dystroglycan, and α-dystroglycan. Mutations in many of the DGC proteins or proteins involved in their post-translational processing cause various forms of muscular dystrophy (reviewed in Rahimov and Kunkel 2013). Without the proper formation, localization, or function of the DGC, the sarcolemma becomes destabilized and more prone to contraction-induced damage with downstream effects of increased sarcolemmal permeability, cell death, and muscle degeneration. It is hypothesized that as a part of the DGC, dystrophin may potentially act as a molecular spring or “shock absorber” to mechanically stabilize the sarcolemma during muscle contraction (Ervasti, 2007).

The protein utrophin was originally named dystrophin-related protein based on high sequence homology with dystrophin (Love et al., 1989). Due to its detection in tissues other than muscle and nerve (Khurana et al., 1990), it was later renamed utrophin, for ubiquitous dystrophin (Blake et al., 1992). The utrophin protein has a similar

organizational structure to dystrophin with an N-terminal actin binding domain, a large central rod domain of spectrin-like repeats with interspersed “hinge” regions, and CR and C-terminal domains (Figure 1.2). Some properties in which utrophin differs from dystrophin include two fewer spectrin-like repeats, a contiguous actin binding domain from the N-terminus to repeat 10 (Rybakova et al., 2006), lack of microtubule binding (Belanto et al., 2014) and nNOS localization activities (Li et al., 2010). Like dystrophin, utrophin forms a homologous utrophin-glycoprotein complex (UGC), but is most abundantly expressed during fetal development and subsequently replaced by dystrophin at the sarcolemma after birth (Rigoletto et al., 1995). In adult skeletal muscle, utrophin localizes to the neuromuscular and myotendinous junctions (Ohlendieck et al., 1991).

Therapeutic Strategies to Treat DMD

Genetic approaches to treat DMD have shown tremendous promise in pre-clinical studies and many have been fast-tracked to clinical trials where there has been variable success. Traditional gene therapy approaches of replacing the mutated DMD gene have focused on the use of an adeno-associated viruses (AAV). The limited capacity of AAV vectors requires the use of miniaturized dystrophins (or "micro-dystrophins") with large internal deletions in the central rod domain, of which there have been several proposed constructs showing efficacy in dystrophin-deficient animal models (Wang et al., 2000, 2007; Lai et al., 2009; Banks et al., 2010; Lai et al., 2013). One micro-dystrophin was used in a clinical trial that reported no recombinant dystrophin expression (Mendell, 2010) but improved constructs are now in the clinical trial pipeline. Another genetic approach involves restoring the reading frame of DMD transcripts carrying deletions using exon-skipping technologies of antisense oligonucleotides or phosphorodiamidate morpholino oligomers (van Deutekom et al., 2007; Aartsma-Rus et al., 2009; Kinali et al., 2009). Like gene therapy constructs, exon-skipping produces an internally truncated but partially functional dystrophin and both approaches aim to yield a Becker-like phenotype in DMD patients. The exon-skipping drug eteplirsen was recently approved by the FDA to treat patients with out-of-frame deletions corrected by exon 51 skipping (Aartsma-Rus and Krieg, 2017). An additional genetic approach is "read-through" drugs that suppress nonsense mutations which result in premature codons in dystrophin transcripts. The read-through drug ataluren was used in a clinical trial and was shown to be safe but did not show clinical efficacy (Bushby et al., 2014). Other read-through drugs have been developed and are moving into clinical trials (Karijolich and Yu, 2014).

With the advancement of gene editing technologies, recent studies have applied the CRISPR/Cas9 gene editing system to correct DMD gene mutations (reviewed in Hotta, 2015). Proposed CRISPR/Cas9 therapeutic approaches include transplantation of gene edited human induced pluripotent stem cells (hIPSCs) as well as AAV delivery of Cas9 and guide RNAs (gRNAs). Initial studies demonstrating proof of concept showed partial gene editing and dystrophin restoration in *mdx* mice and DMD patient myoblasts (Long et al., 2014; Ousterout et al., 2015). CRISPR/Cas9-mediated deletion of the DMD gene in hiPSCs carrying mutations surrounding exons 44 and 51 demonstrated expression of frame-corrected dystrophin and restoration of DGC components in hiPSC-derived cardiomyocytes and myotubes (Young et al., 2016). Multiple groups utilizing AAV mediated delivery of Cas9 and gRNAs in *mdx* mice have shown dystrophin protein restoration to varying degrees and improvement in the dystrophy phenotype (Xu et al., 2016; Long et al., 2016; Nelson et al., 2016; Tabebordbar et al., 2016; Bengtsson et al., 2017). While still in pre-clinical stages, CRISPR/Cas9-mediated correction of the DMD gene is a promising therapeutic strategy and in the case of AAV delivery, could establish a more permanent correction.

Utrophin replacement and upregulation therapies have been in development to compensate for the absence of dystrophin in DMD. AAV-delivery of a micro-utrophin and TAT-mediated protein transduction of full-length or micro-utrophins in *mdx* mice resulted in improvement of muscle function, demonstrating that utrophin can functionally substitute for dystrophin (Odom et al., 2008; Sonnemann et al., 2009; Call et al., 2011). Additionally, pharmacologic upregulation of endogenous utrophin has shown efficacy in *mdx* mice and the utrophin modulator drug SMT C1100 is currently in clinical trial (Tinsley et al., 2011; Ricotti et al., 2016). Other therapy approaches of note include stimulation of muscle regeneration (Campbell et al., 2016), sarcolemmal stabilization

(Heller et al., 2015), and inhibition of inflammatory and fibrosis pathways (Heier et al., 2013; Bodanovsky et al., 2014).

Biophysical Characterization of Dystrophin and Utrophin

There is a significant body of research that has focused on understanding the thermodynamic properties of dystrophin, particularly of the spectrin-like repeats in the central rod domain because of their unique sequence and structure compared to other spectrin repeats (Nicolas et al., 2014a) and because of their unclear functional significance (Legardinier et al., 2008). A meta-analysis of literature reports on the thermodynamic stability of dystrophin fragments, repeats, and deletion constructs using circular dichroism melting temperature as a common parameter is summarized in Figure 1.4 (Henderson et al., 2010, 2011; Bhasin et al., 2005b; Legardinier et al., 2008, 2009b; Mirza et al., 2010; Singh et al., 2010; Ruszczak et al., 2009; Krieger et al., 2010a; Sahni et al., 2012). From this meta-analysis, it is evident that there exists substantial heterogeneity among spectrin-like repeats of dystrophin. It also demonstrates that the stability of tandem repeat fragments does not necessarily reflect the stability of the individual repeats that compose them and that stability is context dependent. Despite this heterogeneity, full-length dystrophin appears to behave as a single unit as evidenced by its cooperative unfolding during thermal denaturation (Henderson et al., 2010), a property that is likely important for dystrophin's function.

Similar thermodynamic analyses of disease-causing missense mutations in the N-terminal actin binding domain and internal deletions have shown increased instability and insolubility *in vitro* (Singh et al., 2010; Henderson et al., 2010, 2011), suggesting that dystrophin is sensitive to sequence mutations and deletions. In contrast, utrophin exhibits remarkably consistent stability regardless of terminal sequence truncation or internal deletion (Henderson et al., 2011). Whether differences in the *in vitro* thermodynamic properties of dystrophin and utrophin impact their stability and function *in vivo* is still unclear but there is evidence that the instability of disease-causing missense

mutations *in vitro* inversely correlates with expression levels of missense mutant proteins in cultured myoblasts (Talsness et al., 2015).

In conjunction with biophysical characterization, there have been efforts to evaluate the mechanical behavior of dystrophin given its proposed role as a molecular shock absorber. The mechanical stability of proteins differs from thermodynamic stability in that the free energy required for unfolding is dependent on spatial distribution (Rief et al., 1999). Forced mechanical unfolding data as measured by atomic force microscopy for dystrophin central rod domain fragments revealed mechanical properties similar to those measured for spectrin, a cytoskeletal scaffolding protein required for plasma membrane integrity (Rief et al., 1999; Law et al., 2003b; a; Bhasin et al., 2005b; Krieger et al., 2010a). Since dystrophin fragments display considerable heterogeneity in thermodynamic stability compared to the full-length protein, it would be important to mechanically characterize full-length dystrophin as well as utrophin in order to compare with established biophysical characterization.

The *mdx* mouse model of DMD

Experiments in animal models of DMD have been critical for therapy development and for substantiating hypotheses about dystrophin function emerging from *in vitro* studies. The most widely used mouse model for DMD is the naturally occurring *mdx* mouse (named for X-chromosome linked muscular dystrophy) that was first discovered in 1984 (Bulfield et al., 1984). Thus, the muscular dystrophy phenotypes of the *mdx* mouse have been well documented.

At the molecular level, *mdx* mice have a nonsense mutation in exon 23 of the DMD gene, rendering it a dystrophin-deficient mouse and resulting in the reduction of other DGC components at the sarcolemma (Hoffman et al., 1987; Sicinski et al., 1989; Ohlendieck and Campbell, 1991). The histopathology of *mdx* skeletal muscle is consistent with what is reported in patients, showing increases in central nucleation, indicating muscle degeneration and regeneration, and decreases in fiber size (Briguet et al., 2004). *Mdx* mice show elevated serum creatine kinase levels and increased uptake of cell-impermeable dyes in skeletal muscle, suggesting a loss of sarcolemmal integrity (Bulfield et al., 1984; Moens et al., 1993; Consolino and Brooks, 2004). Physiologically, *mdx* mice have reductions in grip strength and whole body tension (Connolly et al., 2001), show marked inactivity after mild exercise (Kobayashi et al., 2008), and demonstrate eccentric contraction-induced force loss both *in vitro* and *in vivo* (Petrof et al., 1993; Consolino and Brooks, 2004).

Even though *mdx* mice display hallmark signs of DMD muscle pathology compared to wild-type mice, the phenotype is considerably milder than what is seen in DMD patients (Tanabe et al., 1986). A possible explanation for the milder phenotype is that mice compensate for lack of dystrophin through upregulation of utrophin (Matsumura et al., 1992; Dowling et al., 2002), a hypothesis supported by the more

severe phenotype seen in utrophin-deficient *mdx* mice and the rescue of dystrophic phenotype upon utrophin overexpression (Grady et al., 1997; Deconinck et al., 1997; Tinsley et al., 1998). Another possible explanation is that the mice have an enhanced muscle regeneration response that may be dependent on the murine genetic background (Fukada et al., 2010). *Mdx* mice bred onto a background with decreased regenerative capacity (DBA/2) exhibit a more severe phenotype (Fukada et al., 2010; Rodrigues et al., 2016). Furthermore, *mdx* mice lacking MyoD, a transcription factor required for muscle regeneration, have a marked increase in dystrophic pathology (Megeney et al., 1996). Despite its imperfections as a model of DMD, the *mdx* mouse has been a critical resource in elucidating mechanisms of dystrophy and in the development of therapies that are now approved or in clinical trial.

Additional animal models of DMD have been identified or developed to address the limitations of the *mdx* mouse. Mouse lines with different mutation types, modulated levels of dystrophin, or on different backgrounds have been particularly valuable (McGreevy et al., 2015). Non-mammalian animal models of dystrophin deficiency include *C. elegans* (Chamberlain and Benian, 2000), drosophila (Lloyd and Taylor, 2010), and zebrafish (Kunkel et al., 2006). Larger mammalian models that have been identified as naturally occurring are a golden retriever muscular dystrophy (GRMD) model that has become a standard for pre-clinical testing for DMD therapies (Valentine et al., 1986; Cooper et al., 1988; Kornegay et al., 2012) and a BMD porcine model with a missense mutation (Nonneman et al., 2012).

Questions Addressed by this Thesis

Our lab has previously demonstrated that the thermal stability of dystrophin is sensitive to disease-causing point mutations and internal deletions (Henderson et al., 2010, 2011). Several therapeutic strategies to treat DMD utilize internally deleted dystrophins, including the recently FDA approved exon-skipping drug, eteplirsen (Aartsma-Rus and Krieg, 2017), and viral delivery of therapeutic micro-dystrophins (Sakamoto et al., 2002; Wang et al., 2000). Thus my thesis seeks to answer the question: "**How do deletions present in therapeutically relevant, internally truncated dystrophins affect *in vitro* protein stability?'**

My analysis of thermal stablity *in vitro* showed that micro-dystrophin gene therapy constructs are significantly less stable than full-length dystrophin whereas the exon-skipped dystrophins have stability profiles congruent with full-length dystrophin (McCourt et al., 2015). My *in vitro* thermal studies also reinforce the need to better understand how differences in protein stability *in vitro* translate to therapeutic efficacy *in vivo*. A recent study in cultured myoblasts suggested that dystrophin proteins bearing DMD or BMD-causing missense mutations, the mutant proteins are targeted to the proteasome for degradation resulting in reduced steady state dystrophin protein levels (Talsness et al., 2015). Using the cell culture models and novel transgenic mice expressing missense dystrophins, we answered the questions: **How are missense dystrophin proteins regulated in murine models of DMD and BMD missense mutants?**

While dystrophin stability is sensitive to missense mutations and internal deletions, the fetal homologue of dystrophin, utrophin, maintains stability upon terminal or internal deletions (Henderson et al., 2011). However, differences in thermodynamic

properties between dystrophin and utrophin do not address their proposed function as molecular springs to mechanically stabilize the muscle membrane during muscle contraction (Ervasti, 2007). Our aim is to use atomic force microscopy to address the question: **What are the mechanical properties of full-length utrophin and functionally relevant utrophin fragments?**

Figures

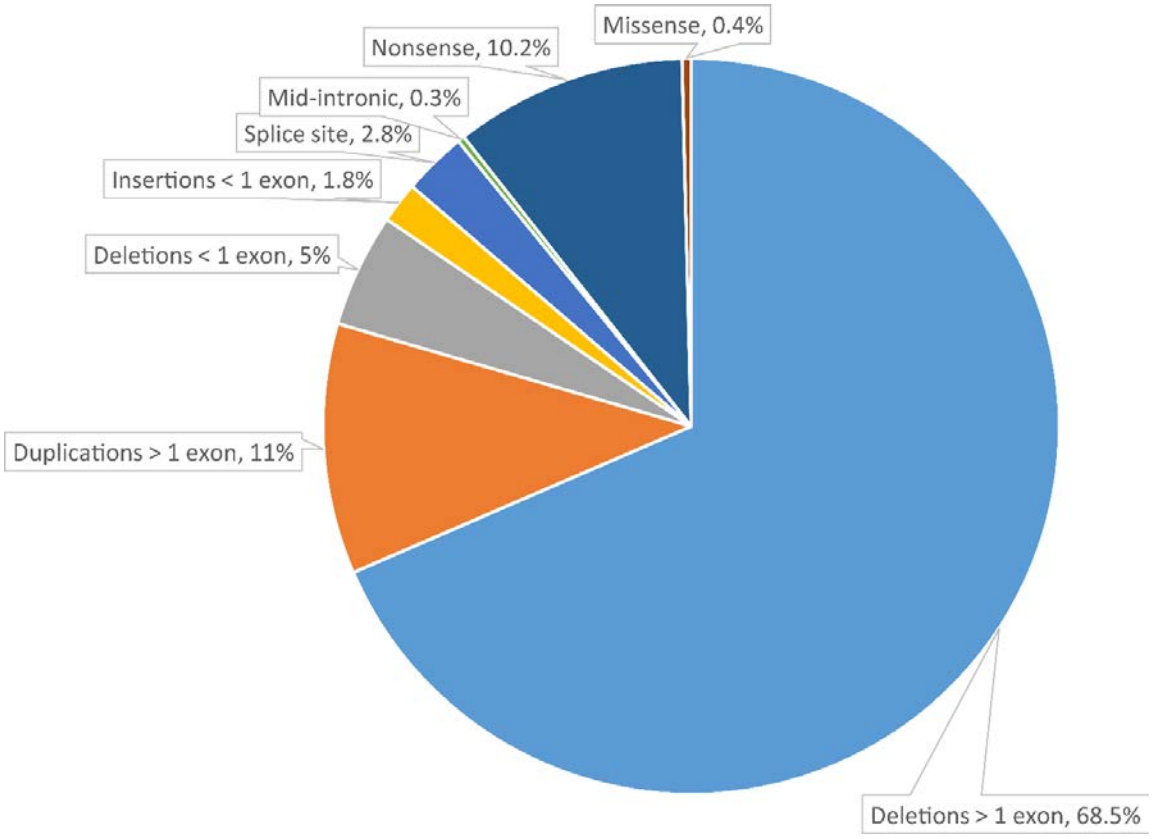

Figure 1.1: Frequency of DMD/BMD mutation types. Data compiled from the Treat-NMD DMD Global Database (Bladen et al., 2015).

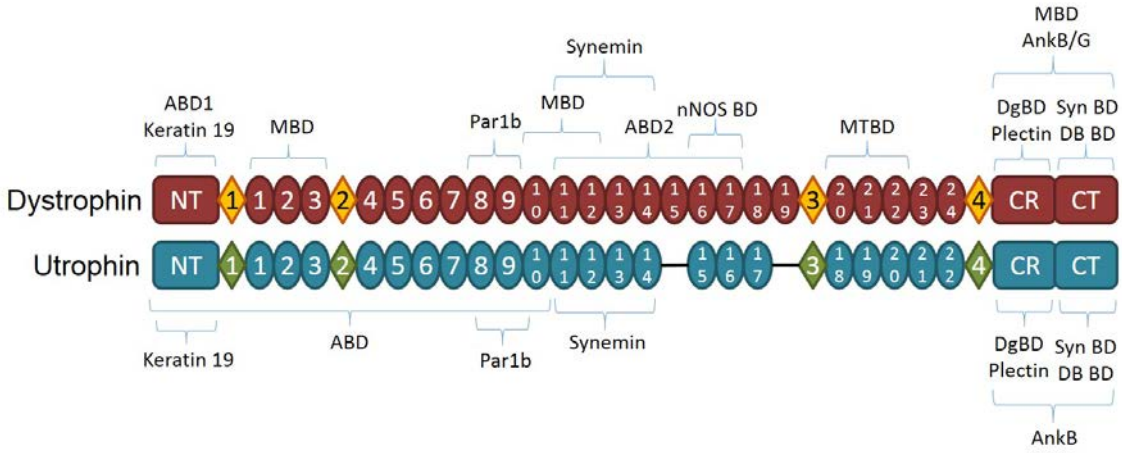

Figure 1.2: Dystrophin and utrophin protein interacting domains. NT – amino terminus; CR – cysteine rich domain; CT – carboxy terminus; ovals – spectrin-like repeats; diamonds – unstructured “hinge” regions; ABD – actin binding domain; MBD – membrane binding domain; nNOS – neuronal nitric oxide synthase; MTBD – microtubule binding domain; DgBD – dystroglycan binding domain; AnkB/G – ankyrin B/G; Syn BD – syntrophin binding domain; DB BD – dystrobrevin binding domain.

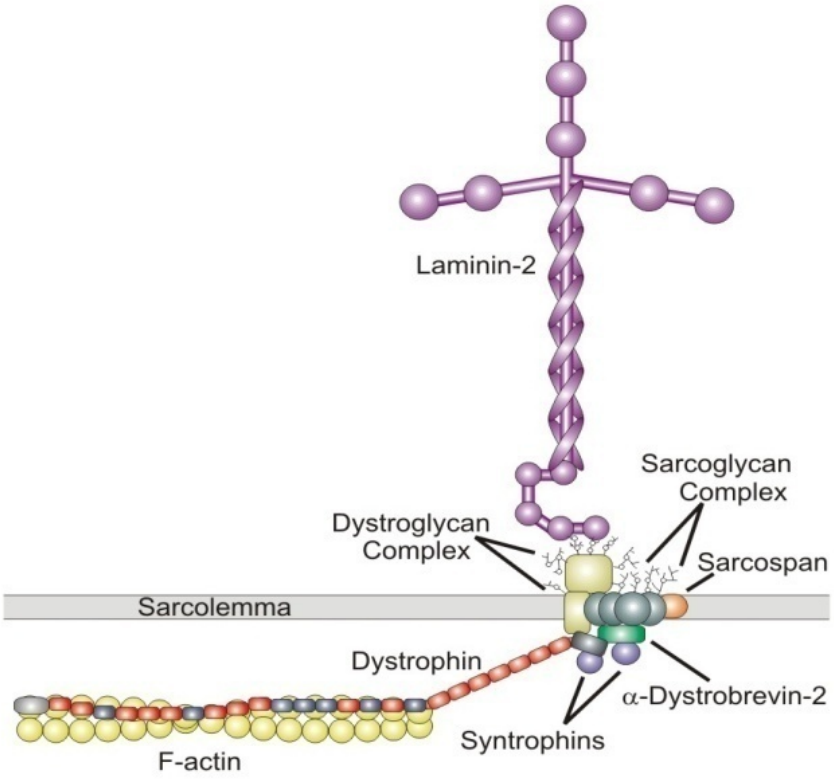

Figure 1.3: The Dystrophin-Glycoprotein Complex. Diagram of the core members of the dystrophin-glycoprotein complex at the sarcolemma. On the inside of the cell are dystrophin, syntrophins, and α-dystrobrevin-2. Spanning the membrane are β-dystroglycan, sarcospan, α-, β-, γ-, and δ-sarcoglycan. On the extracellular side are α-dystroglycan, and laminin-2.

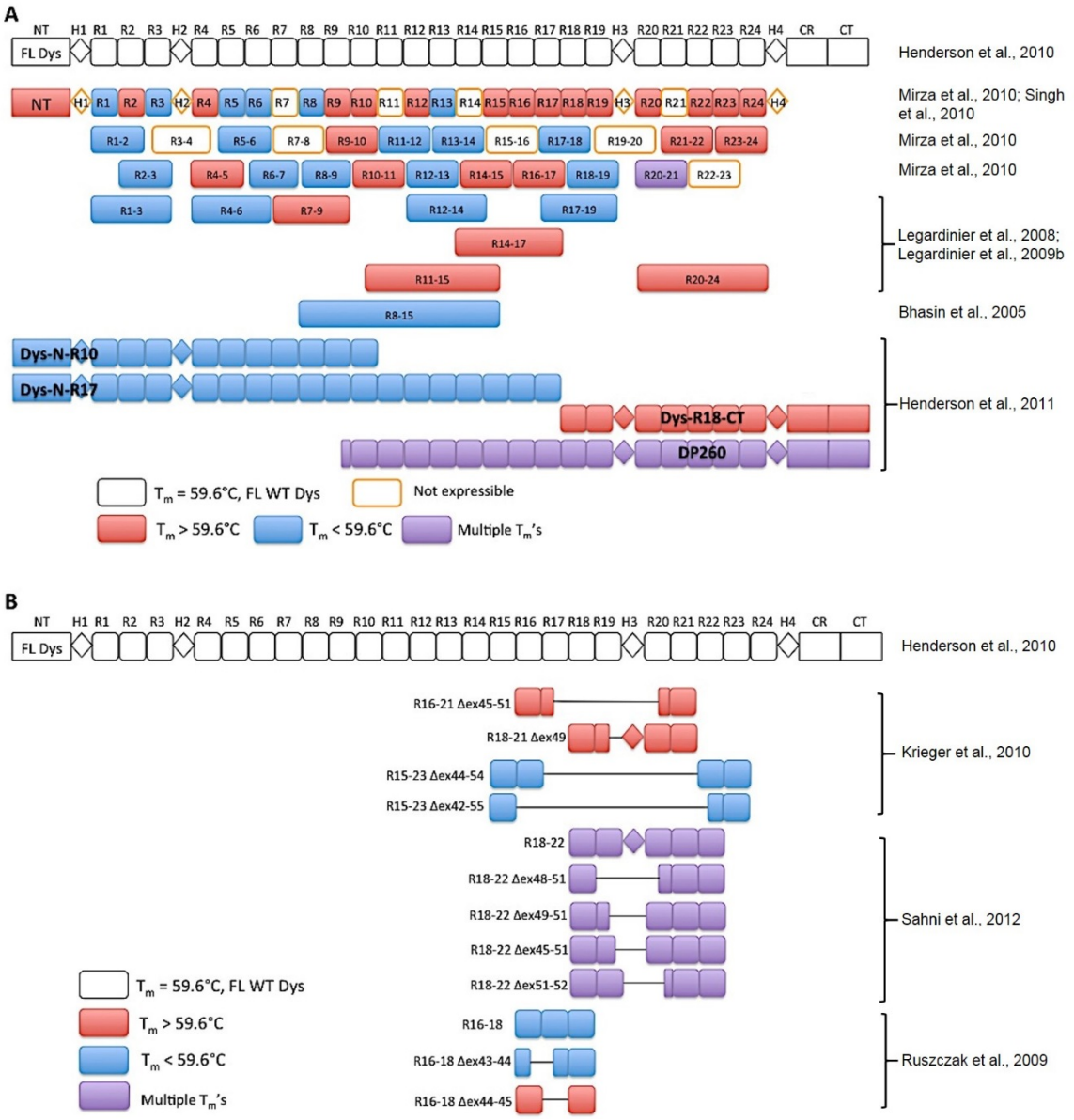

Figure 1.4: Meta-analysis of melting temperatures of dystrophin fragments (A) and exon-skipped constructs (B). Individual spectrin-type repeats are represented by rounded squares, hinge regions represented by diamonds. White boxes represent full-length dystrophin with a melting temperature of 59.6°C. Blue and red shaded boxes indicate repeats/fragments that had melting temperatures below or above 59.6°C,

respectively; purple shaded boxes indicate constructs that had multiple melting temperatures; orange bordered boxes indicate constructs that were not expressible.

Chapter 2

In vitro stability of therapeutically relevant, internally truncated dystrophins*

* McCourt, Jackie L, Katrina K Rhett, Michele A Jaeger, Joseph J Belanto, Dana M Talsness, and James M Ervasti. 2015. “In Vitro Stability of Therapeutically Relevant, Internally Truncated Dystrophins.” *Skeletal Muscle* 5. England: 13

Jackie McCourt carried out molecular cloning of exon 51 constructs, performed protein expression/purification and biophysical assays, carried out the data and statistical analysis, and drafted the manuscript. Katrina Rhett carried out protein expression/purification and biophysical assays of gene therapy and utrophin proteins. Michele Jaeger aided in molecular cloning of utrophin and dystrophins skipped around exon 45, and protein expression/purification, and biophysical assays for dystrophins skipped around exon 45. Joseph Belanto carried out the molecular cloning for gene therapy and utrophin constructs and edited the manuscript. Dana Talsness established the DSF instrument and protocol and edited the manuscript.

Synopsis

The X-linked recessive disease Duchenne muscular dystrophy (DMD) is caused by mutations in the gene encoding the protein dystrophin. Despite its large size, dystrophin is a highly stable protein, demonstrating cooperative unfolding during thermal denaturation as monitored by circular dichroism spectroscopy. In contrast, internal sequence deletions have been associated with a loss of the cooperative unfolding and cause *in vitro* protein aggregation. Several emerging therapy options for DMD utilize internally deleted micro-dystrophins and multi-exon skipped dystrophins that produce partially functional proteins but the stability of such internally-truncated proteins has not been investigated. In this study, we analyzed the *in vitro* stability of human dystrophin constructs skipped around exon 45 or exon 51, several dystrophin gene therapy constructs, as well as human full-length and micro-utrophin. Our results reveal that not all gene therapy constructs display stabilities consistent with full-length human dystrophin. However, all dystrophins skipped in-frame around exon 45 or exon 51 show stability profiles congruent with intact human dystrophin. Similar to previous studies of mouse proteins, full-length human utrophin also displays stability similar to human dystrophin and does not appear to be affected by a large internal deletion. Our results suggest that the *in vitro* stability of human dystrophin is less sensitive to smaller deletions at natural exon boundaries than larger, more complex deletions present in some gene therapy constructs.

Introduction

The X-linked disease Duchenne muscular dystrophy (DMD) is caused by mutations in the gene encoding the protein dystrophin (Hoffman et al., 1987). Mutations causing this disease are variable with 65% of DMD patients harboring deletions which span exons, 5-15% having duplications, and the remaining populations having either point mutations or deep intronic deletions (Muntoni et al., 2003). Becker muscular dystrophy (BMD) is a milder allelic form of dystrophy typically caused by in-frame gene deletions that maintain reading frame, but presumably cause disease through diminished abundance or functionality (Koenig et al., 1989).

The dystrophin protein is a critical molecular component of the dystrophin-glycoprotein complex (DGC) that functions to maintain skeletal muscle integrity during contraction (Rybakova and Ervasti, 1997; Ervasti, 2007). Dystrophin provides a structural link between the sub-sarcolemmal cytoskeleton and the extracellular matrix through interactions with actin (Rybakova et al., 1996, 2000), intermediate filaments (Stone et al., 2005; Bhosle et al., 2006; Rezniczek et al., 2007), microtubules (Prins et al., 2009; Belanto et al., 2014) and the membrane-associated dystroglycan complex (Jung et al., 1995; Ishikawa-Sakurai et al., 2004). The observation that milder BMD patients harbor deletions in the central rod domain suggests that dystrophin can tolerate such deletions to some degree and that the central rod domain is less critical to the function of dystrophin.

Two avenues of therapeutic research have focused on producing internally truncated, Becker-like dystrophins in DMD patients. Exon-skipping approaches aim to restore the reading frame of mutated DMD transcripts using antisense oligonucleotides (ASOs) or phosphorodiamidate morpholino oligomers (PMOs), producing an internally truncated but partially functional protein (van Deutekom et al., 2007; Aartsma-Rus et al.,

2009; Kinali et al., 2009). Alternatively, adeno-associated viral (AAV) gene therapy is under active investigation to express miniaturized dystrophin constructs in DMD patients due to the large size of the dystrophin gene and the limited capacity of AAV vectors(Harper et al., 2002; Sakamoto et al., 2002; Wang et al., 2000).

The stability of the corresponding proteins produced from dystrophin exon skipping or AAV-mediated delivery of micro-dystrophins is unknown and may be an important factor to maximize therapeutic efficacy. Previous *in vitro* work has demonstrated that the stability of mouse dystrophin was sensitive to disease-causing missense mutations and internal deletion (Henderson et al., 2010, 2011), raising the question of whether the stabilities of micro-dystrophins or exon-skipped dystrophins relevant to DMD therapies might also be compromised. In contrast, the stability of mouse utrophin, a fetal homologue of dystrophin, was insensitive to both terminal and internal deletion (Henderson et al., 2011).

Here, we expressed and purified five dystrophins skipped around exon 45 or 51 with an exon 43-skipped control, five recombinant dystrophin gene therapy constructs, and two utrophin constructs. The selected constructs represent the leading therapy approaches that have been shown to ameliorate the dystrophic phenotype in *mdx* mice with transition to clinical trials underway (Wang et al., 2000; Sakamoto et al., 2002; Lu et al., 2005; Alter et al., 2006; Odom et al., 2008; Sonnemann et al., 2009; Banks et al., 2010; Call et al., 2011). In the current study, all constructs were expressed from human sequences, as opposed to the mouse constructs used previously (Henderson et al., 2010, 2011). Our biophysical analysis revealed that the dystrophin gene therapy constructs exhibited more variable stabilities *in vitro* while exon-skipped dystrophin constructs showed stabilities not different from full-length dystrophin. Consistent with previous mouse studies, utrophin maintained stability despite internal deletion.

Methods

Cloning

Full-length human dystrophin was obtained from the DNASU vector repository in the pE223 Gateway entry vector. Human utrophin and micro-utrophin were cloned from HEK293 cells into the pENTR/D-TOPO vector (Invitrogen™) and sequence verified. An 8-amino acid FLAG-tag (DYKDDDDK) was added to the N-terminus of both human dystrophin and utrophin constructs for use in purification. All human dystrophin deletion constructs were PCR amplified using primers designed around adjacent exons, repeats, or domains for the desired deletion based on reported repeat and domain boundaries(Winder et al., 1995). The PCR products were circularized using T4 polynucleotide kinase and T4 DNA ligase (New England BioLabs) and sequence verified. Using the Gateway Recombination system (Life Technologies), the deletion constructs were recombined into the pDEST8 destination vector and subsequently transformed into DH10Bac competent *E. Coli* and purified according to the manufacturer's protocol.

Protein expression and purification

Sf9 insect cells were maintained at 1 x 10^6 cells/mL in Sf-900™ II SFM (Life Technologies). Purified Baculovirus was transfected using Cellfectin® II (Life Technologies) and high-titer viral stocks were generated through successive infections of Sf9 cells in 3.5 cm plates (P0), 10 cm plates (P1), and 250 mL of 1 x 10^6 cells/mL suspended cells (P2). Ten mL of P2 virus were used to infect 250 mL of 1 x 10^6 cells/mL and cultured for 72-hour post-infection to maximize protein expression. Infected cells were centrifuged at 1,000 x *g* for 3 minutes and re-suspended in phosphate buffered saline (PBS) containing a cocktail of protease inhibitors [100nM Aprotinin, 10mg/mL E-64, 10μM Leupeptin, 1mM PMSF, 1μg/mL Pepstatin]. Cells were lysed by sonication, 5

bursts of 30 seconds using a BioLogics Ultrasonic Homogenizer set at 30% power. The lysate was centrifuged at 14,000 x *g* for 10 min at 4ºC and the supernatant applied to an anti-FLAG M2 agarose column (Sigma Aldrich). The column was washed with >10 column volumes of PBS and bound protein eluted with PBS containing protease inhibitors and 100μg/mL FLAG peptide. After dialysis overnight in 2L of PBS at pH 7.5, the purified protein was concentrated using the Amicon Centrifugal Filter unit (UFC801024) and protein concentration was determined using A_{280} and extinction coefficients calculated from the amino acid compositions for each construct. Concentrated proteins were run on a 3-12% SDS polyacrylamide gradient gel and run at 150V for 1 hour. Gels were stained with Coomassie blue stain and visualized using Licor's Odyssey® Infrared Imaging System.

Tandem purification of full-length human dystrophin

To optimize the purification of full-length human dystrophin, a Twin-Strep-tag® (IBA), with amino acid sequence SA-WSHPQFEK$(GGGS)_2$GGSAWSHPQFEK, was cloned onto the C-terminus of pE223 dystrophin in addition to the N-terminal FLAG-tag. The dual-tagged dystrophin was then recombined into the pDEST8 expression vector and expressed in the *Sf9* baculovirus system as described above. The cell lysate was applied to a *Strep*-Tactin ® Superflow ® high capacity resin (IBA), eluted with 100 mM Tris-HCl, 150 mM NaCl, 1 mM EDTA, 2 mM desthiobiotin, pH 8, and the eluent immediately applied to an anti-FLAG M2 agarose column as described above.

Western Blotting

Purification fractions from the tandem purification were run on a 3-12% SDS polyacrylamide gradient gel at 150V for 1 hour. The gel was transferred onto a polyvinylidene difluoride (PVDF) membrane at 100V for 1 hour. The PVDF membrane

was blocked using 5% milk in 1X PBS, 0.1% Tween and blotted using mouse monoclonal anti-FLAG M2 (Sigma Aldrich, F1804) and rabbit polyclonal anti-Strep-tag II (Abcam, ab76949) antibodies at 1:1000 dilution. The blot was visualized using anti-mouse DyLight™ 800 (green channel) and anti-rabbit DyLight™ 680 (red channel) conjugate antibodies in Licor's Odyssey® Infrared Imaging System.

High-speed sedimentation

Each purified protein was diluted to 0.3 mg/mL (for exon 51 skipped dystrophins) or 0.5 mg/mL (for all other proteins) with PBS in a final volume of 120 µL and 60 µL was immediately aliquoted into 12 µL 6X LSB to prepare a "total" fraction. The remaining 60 µL was centrifuged at 100,000 x *g* for 30 minutes at 4ºC. The supernatant was transferred into 12 µL 6X LSB and the pellet re-suspended in 72 µL of 1X LSB. Triplicate fractions were run on a 3-12% gradient polyacrylamide gel at 150V for 1 hour and stained with Coomassie blue stain. Gels were scanned using Licor's Odyssey® Infrared Imaging System and band density calculated with Odyssey Software v2.1. Full-length human dystrophin was used as a control at both 0.3 mg/mL and 0.5 mg/mL concentrations and did not show any significant difference in percent aggregation between the different concentrations (17.6% ± 7.39 and 17.4% ± 7.30, respectively).

Circular dichroism

Each purified protein was centrifuged at 14,000 x *g* for 10 minutes at 4ºC and the supernatant diluted to 0.5 mg/mL (for gene therapy and utrophin proteins) or 0.3 mg/mL (for exon-skipped and full-length dystrophins) using PBS. Absorption spectra were acquired with a Jasco J-815 spectropolarimeter, initially at 20°C as controlled by a Peltier device, from 200 to 260nm wavelength. Spectra were then acquired at 1°C temperature intervals from 20-90°C and the characteristic ellipticity at alpha-helical wavelength (θ_{222}) recorded. Molar ellipticity, [θ], was calculated using the following

equation: $[\theta] = \theta / (10 \times c \times l)$ where c is the molar concentration of the sample (mole/L) and *l* is the path-length in cm. Molar ellipticity (with units of degrees, cm squared per decimole) was plotted against wavelength for the circular dichroism (CD) spectra. Ellipticity at 222nm (θ_{222}) was normalized, plotted against temperature, and fit by regression analysis in Sigma Plot (Systat Software, Inc.) using equations for two state or three state unfolding (Legardinier et al., 2009a).

Differential scanning fluorimetry

Our method closely followed that described by Niesen *et al*(Niesen et al., 2007). Briefly, the fluorescent dye SYPRO Orange (Life Technologies™ #S6650) was incubated at a ratio of 1:1000 (w/w) with 0.5 mg/mL (or 0.3 mg/mL for exon-skipped proteins) of purified protein in PBS. The dye/protein solution was aliquoted into 50µL-technical triplicates and an emission of 610nm was measured in a real time PCR instrument (iCycler, Bio-Rad) as the temperature was increased from 20° to 90°C at 1°C temperature intervals. The fluorescence was normalized from 0 to 1, plotted against temperature, and fit by regression analysis in Sigma Plot (Systat Software, Inc.) using an equation for a two state unfolding model(Legardinier et al., 2009a).

Statistical analysis

Data for percentage aggregation and melting temperatures of single transition melt curves from CD and differential scanning fluorimetry (DSF) were analyzed using a one-way analysis of variance (ANOVA) with a Tukey's post hoc test in Prism software (GraphPad), all compared to full-length human dystrophin.

Results

Basis for Choice of Recombinant Proteins and Gel Analysis

The choice of constructs to analyze was based on current models for exon-skipping and gene therapy in pre-clinical testing and clinical studies (Figure 2.1). The exon 45-skipped and exon-51 skipped dystrophins were analyzed because they could potentially treat 8% and 13% of DMD patients, respectively (Aartsma-Rus et al., 2009) and ASO and morpholino drugs targeting these exons are currently in clinical trials (Phase IIb Study of PRO045 in Subjects With Duchenne Muscular Dystrophy, A Study of the Safety, Tolerability & Efficacy of Long-term Administration of Drisapersen in US & Canadian Subjects). Therefore, we expressed a subset of exon-45 and exon-51 skipped human dystrophins, ∆ex44-45, ∆ex45-46, ∆ex45-51, ∆ex51-52, ∆ex51-63, as well as ∆ex43-44, a control deletion that has been previously speculated to cause decreased stability (Ruszczak et al., 2009). While we initially attempted to generate a larger array of exon-51 skipped constructs, we analyzed the three (∆ex45-51, ∆ex51-52, and ∆ex51-63) that yielded products in the first stages of cloning.

The gene therapy constructs μH2 hDys and μH3 hDys contain spectrin-like repeats (SLRs) 1-3 and 24 with hinge 2 or hinge 3, respectively. These constructs have been shown to ameliorate the dystrophic phenotype in *mdx* mice (Banks et al., 2010) and μH2 also showed significant expression with muscle improvement in the GRMD dog model of DMD (Wang et al., 2007, 2012). The ∆3990 hDys construct corresponds to the AAV-delivered micro-dystrophin used in a clinical trial that reported minimal recombinant dystrophin expression associated with a strong immune response to dystrophin (Wang et al., 2000; Mendell, 2010). Constructs ∆H2-R15/∆CT hDys and ∆R3-15/18-23/∆CT hDys are miniaturized dystrophins that retain SLRs 16 and 17 necessary for

sarcolemmal localization of neuronal nitric oxide synthase (nNOS) (Lai et al., 2009, 2012). Full-length human utrophin and a micro-utrophin (μH2 hUtr, homologous to μH2 hDys) correspond to constructs that are under investigation for gene, cell, and protein-based therapies (Odom et al., 2008; Sonnemann et al., 2009; Call et al., 2011; Filareto et al., 2013).

While gel analysis of the FLAG affinity-purified recombinant proteins revealed a predominant band of the expected molecular weight for each purified dystrophin gene therapy and utrophin constructs, full-length and exon skipped human dystrophins exhibited a near-stoichiometric contaminating fragment at ~230 kDa (Figure 2.2A) that was not previously observed in preparations of full length mouse dystrophin (Henderson et al., 2010) and was not present in gene therapy or utrophin preparations (Figure 2.2A). To identify the contaminating fragment, we generated and expressed a dual-tagged, full-length human dystrophin containing a C-terminal Twin-Strep-tag® (IBA) in addition to the N-terminal FLAG-tag. Western blot analysis after tandem affinity purification of the dually-tagged dystrophin revealed that the near-stoichiometric, ~230 kDa contaminating fragment present in the FLAG affinity-purified samples was an N-terminal fragment (green band, Figure 2.2B) and was mostly likely caused by a cleavage from a protease in our expression system. The cleavage event was further confirmed by the presence of the corresponding C-terminal fragment in the load and elution fractions of the Strep-tag purification (red band, Figure 2.2B). The absence of the contaminating N-terminal fragment in constructs with deletions preceding repeat 16 combined with its presence in constructs with deletions after repeat 16 suggests that the proteolytic cleavage site resides within repeat 14 or 15, which would yield the predicted N-terminal fragment of ~230 kDa. While the tandem purification was successful in identifying the contaminating

fragments and a more purified full-length dystrophin was recovered (yellow band), the resulting yield was not sufficient to support the planned biochemical or biophysical analyses. Therefore, single FLAG affinity-purified proteins were used in all subsequent analyses.

Protein Aggregation

High-speed sedimentation is a facile *in vitro* technique to quantify aggregation of purified proteins. Full-length human dystrophin exhibited 17.6% aggregation (Figure 2.3, Table 2.1), which is similar to the 14% aggregation previously reported for full-length mouse dystrophin(Henderson et al., 2010). Exon-skipped dystrophin proteins did not show significant increases in aggregation relative to full-length human dystrophin, however ∆ex43-44 showed a significant decrease in aggregation (gray bars, Figure 2.3). Four of the five gene therapy proteins showed a significant increase, with percent aggregation ranging from 31.7 to 44.4% (white bars, Figure 2.3, Table 2.1). Interestingly, the ∆3990 protein was the only gene therapy construct that exhibited protein aggregation congruent with full-length dystrophin. Similar to the exon-skipped dystrophins, utrophin and micro-utrophin did not vary significantly from full-length dystrophin aggregation (lined bars, Figure 2.3).

Assessment of Secondary Structure Unfolding

To assess secondary structure and protein unfolding, we analyzed the purified proteins by circular dichroism (CD) spectroscopy. All of the constructs exhibited CD spectra characteristic of proteins with high alpha-helical content and minima at 208 and 222 nm (Figure 2.4A-C). As the temperature was increased, loss of secondary structure (or unfolding) was monitored at 222nm to generate melt curves (Figure 2.4D-F) with a calculated melting temperature or temperatures (Table 2.1). Full-length human

dystrophin exhibited a single transition melt curve with a melting temperature of 48.1°C (Table 2.1, Figure 2.4), which is in contrast to the 59.6°C melting temperature reported for full-length mouse dystrophin (Henderson et al., 2010). Upon closer inspection of the melt curves from the previous report, it is apparent that full-length mouse dystrophin exhibited an additional melting transition similar to the dystrophin isoform DP260 (Henderson et al., 2011), a property that is absent in CD melt curves of human dystrophin. Exon-skipped dystrophins exhibited single transitions all with comparable melting temperatures to full-length dystrophin (Figure 2.4D, Table 2.1). Two of the gene therapy constructs, Δ3990 and ΔR3-15/18-23/ΔCT, also displayed a single transition but Δ3990 had a significantly higher melting temperature of 56.1°C. However, the other gene therapy constructs displayed a second transition with two calculated melting temperatures ranging from 47° to 85°C (Figure 2.4E, Table 2.1). This indicates that the protein is either not unfolding cooperatively, or is composed of two populations of folded and unfolded states. Full-length human utrophin and μH2 hUtr displayed single transition melt curves with melting temperatures of 46.2 and 47°C, respectively (Figure 2.4F, Table 2.1). These values are not significantly different from full-length dystrophin and are consistent with previously reported melting temperatures for mouse full-length and micro-mouse utrophins (Henderson et al., 2011).

Assessment of Tertiary Structure Unfolding

Differential scanning fluorimetry (DSF) utilizes a fluorescent dye that increases its fluorescence emission upon binding to hydrophobic moieties in proteins, which become more exposed and accessible as a protein unfolds during thermal denaturation (Niesen et al., 2007). Like CD, DSF can be used to obtain protein melt curves, but unlike CD, the signal measured reflects changes in tertiary structure rather than secondary structure.

By DSF analysis, full-length human dystrophin displayed a melt curve with a single transition at 45.7°C (Figure 2.5). This temperature was lower than that seen in CD, consistent with the concept that tertiary structure will be lost before secondary structure. Exon-skipped dystrophins displayed single transitions with similar melting temperatures to full-length dystrophin ranging from 43.7° to 48.1°C (Figure 2.5A, Table 2.1). In contrast to the CD data, all of the gene therapy constructs exhibited single transitions with melting temperatures ranging from 45.8° to 50.4°C (Figure 2.5B, Table 2.1). Both Δ3990 and ΔH2-R15/ΔCT hDys had significantly right-shifted melt curves from full-length dystrophin with melting temperatures of 50.4° and 49.8°C, respectively. Full-length and micro-utrophin both show a left-shifted melt curve with melting temperatures of 43.4° and 42.9°C, respectively, but, like exon-skipped dystrophins, these values are not significantly different from full-length dystrophin (Figure 2.5C, Table 2.1).

Discussion

In this study, we have analyzed the biophysical properties of several therapeutically relevant, internally truncated dystrophins and utrophins. Therapies that produce internally deleted dystrophins are based on observations that patients with the milder BMD can harbor large deletions in the central rod domain. In addition to conferring elasticity or flexibility to dystrophin (Koenig and Kunkel, 1990; Ervasti, 2007; Saadat et al., 2006), it is known that the central rod domain encodes a second actin binding domain (Rybakova et al., 1996; Amann et al., 1998; Warner et al., 2002), as well as domains for localizing nNOS to the sarcolemma (Lai et al., 2009, 2012), for *in vitro* binding to phospholipids (Legardinier et al., 2008, 2009b), intermediate filaments (Bhosle et al., 2006), and microtubules (Prins et al., 2009; Belanto et al., 2014).

The biophysical properties of individual and tandem repeats of the rod domain have been extensively investigated and these findings demonstrate a wide range of stabilities (Mirza et al., 2010; Legardinier et al., 2008, 2009b; Bhasin et al., 2005b), whereas full-length dystrophin has remarkable cooperative stability (Henderson et al., 2010). Additionally, there is evidence that certain internal deletions of the central rod domain are associated with increased protein aggregation and instability (Henderson et al., 2011). Together, these studies suggest that the stability of individual or tandem repeat fragments does not necessarily reflect that of larger fragments or full-length dystrophin proteins and that protein stability of individual regions within dystrophin is context dependent.

Several groups have investigated the biophysical consequences of exon-skipping on dystrophin fragments within the central rod domain, particularly those spanning exons 43 to 51 (Ruszczak et al., 2009; Krieger et al., 2010b; Sahni et al., 2012; Nicolas et al., 2012). For constructs skipping exon 51, they concluded that some protein fragments are

more stable than others. Our results, however, suggest that for dystrophins skipped around exon 51, there is little measureable change in stability *in vitro* between exon-skipped proteins and full-length human dystrophin. This conclusion is consistent with the conclusions of a recent report that assessed the structural differences and stability profiles of human dystrophin fragments with deletions around exon 51 (Nicolas et al., 2014b). They found that while there were marked structural differences between the different deletion fragments, the stability was not significantly affected.

For the common, out-of-frame deletion of exon 45 (Δ45) in patients, exon-skipping therapies are being designed to either delete exon 44 (Δex44-45) or exon 46 (Δex45-46) to correct the reading frame. Based on another recent report, it was speculated that the Δex45-46 dystrophin protein might be highly unstable because this in-frame deletion is associated with the more severe DMD phenotype in patients (Findlay et al., 2015), and therefore a Δex44-45 skipping strategy would be more beneficial. However, based on our *in vitro* data, there does not appear to be any significant difference in stability between Δex44-45 and Δex45-46 and full-length dystrophin proteins. These different conclusions from the clinical and *in vitro* studies indicate that the source of pathogenesis from the exon 45-46 deletion may not depend on the stability of the resulting protein, but perhaps is caused by a regulatory or functional perturbation.

Interestingly, *all* of the exon-skipped dystrophins evaluated in our study displayed *in vitro* stabilities congruent with full-length dystrophin, including the Δex43-44 protein that exhibited decreased stability when previously evaluated in the context of a smaller recombinant fragment encompassing SLRs 16-18 (Ruszczak et al., 2009). Because dystrophy-causing missense mutations also cause less dramatic instability in full-length dystrophin compared to small fragments (Henderson et al., 2010; Singh et al., 2010), it

seems possible that long-range and cooperative intra-protein communication may serve to buffer dystrophin against the destabilizing effects of sequence changes and deletions.

We also expressed internally deleted human micro-dystrophins that are currently under investigation for gene therapy. We showed that several of these constructs have significantly different stability compared to the full-length human dystrophin protein. Both micro-dystrophins μH2, hDys, and μH3 hDys displayed increased aggregation and additional melting transitions upon secondary structure unfolding. One of the sarcolemmal nNOS-localizing constructs, ΔH2-R15/ΔCT hDys, displayed similar behavior. Interestingly, the more truncated nNOS-localizing construct, ΔR3-15/18-23/ΔCT, exhibited a single melting transition similar to full-length dystrophin but also increased aggregation. These data suggest that the *in vitro* stability of dystrophin gene therapy constructs may be dependent on the stability of the non-native junction created by the internal deletion. The Δ3990 hDys construct was the only gene therapy construct that exhibited wild-type aggregation and it displayed significantly increased melting temperatures for both CD and DSF, suggesting that the Δ3990 protein is *more* stable than full-length dystrophin. However, a small clinical trial for AAV-mediated delivery of the Δ3990 was not successful (Mendell, 2010).

Utrophin replacement therapies are also currently under investigation, therefore we analyzed the stability of full-length human utrophin and a micro-utrophin. A previous study demonstrated that mouse utrophin is a highly stable protein that does not appear to be sensitive to terminal truncation or internal deletion (Henderson et al., 2011). Consistent with these results, our data showed that both full-length and micro-utrophin have similar protein aggregation to dystrophin and maintain melting temperatures that are not significantly different from full-length human dystrophin. Investigation of utrophin

as a dystrophin substitute therapy for DMD (Odom et al., 2008; Sonnemann et al., 2009; Call et al., 2011; Filareto et al., 2013) is based on its ability to rescue most phenotypes of the *mdx* mouse when transgenically overexpressed (Tinsley et al., 1998) and also the positive correlation between increased utrophin expression with improved prognosis in a small cohort of DMD patients (Kleopa et al., 2006). Utrophin maintains some functional properties of dystrophin, such as forming an analogous utrophin-glycoprotein complex (Matsumura et al., 1992) and binding actin filaments (Rybakova et al., 2006), but lacks the ability to localize nNOS to the sarcolemma (Li et al., 2010; Lai et al., 2012) and organize the sub-sarcolemmal microtubule lattice (Belanto et al., 2014). While utrophin cannot completely substitute for dystrophin in terms of protein-protein interactions, our results suggest that utrophin and micro-utrophin proteins are appealing as therapeutic targets in terms of protein stability, especially when compared to dystrophin gene therapy proteins.

While the recombinant dystrophin and utrophin proteins used in this study were expressed in a eukaryotic cellular environment, their purification and characterization in more simple buffers leaves open the possibility that they exhibit unfolding and aggregation properties *in vitro* that are different from how they behave in the complex environment of a mammalian muscle cell. It will therefore be important to develop both cell and tissue-based model systems to better understand how deletions in dystrophins and utrophins affect stability *in vivo*.

Our *in vitro* analysis of the biophysical consequences of internal deletion on dystrophin and utrophin suggests that dystrophin stability is context-dependent: relatively unaffected by small deletions at natural exon boundaries, but sensitive to larger and more complex rearrangements from deletions present in gene therapy constructs. In contrast, utrophin maintains uniform stability despite large internal deletion. Moreover,

our results also highlight the need to better understand how differences in protein stability *in vitro* translate to therapeutic efficacy *in vivo*.

Figures

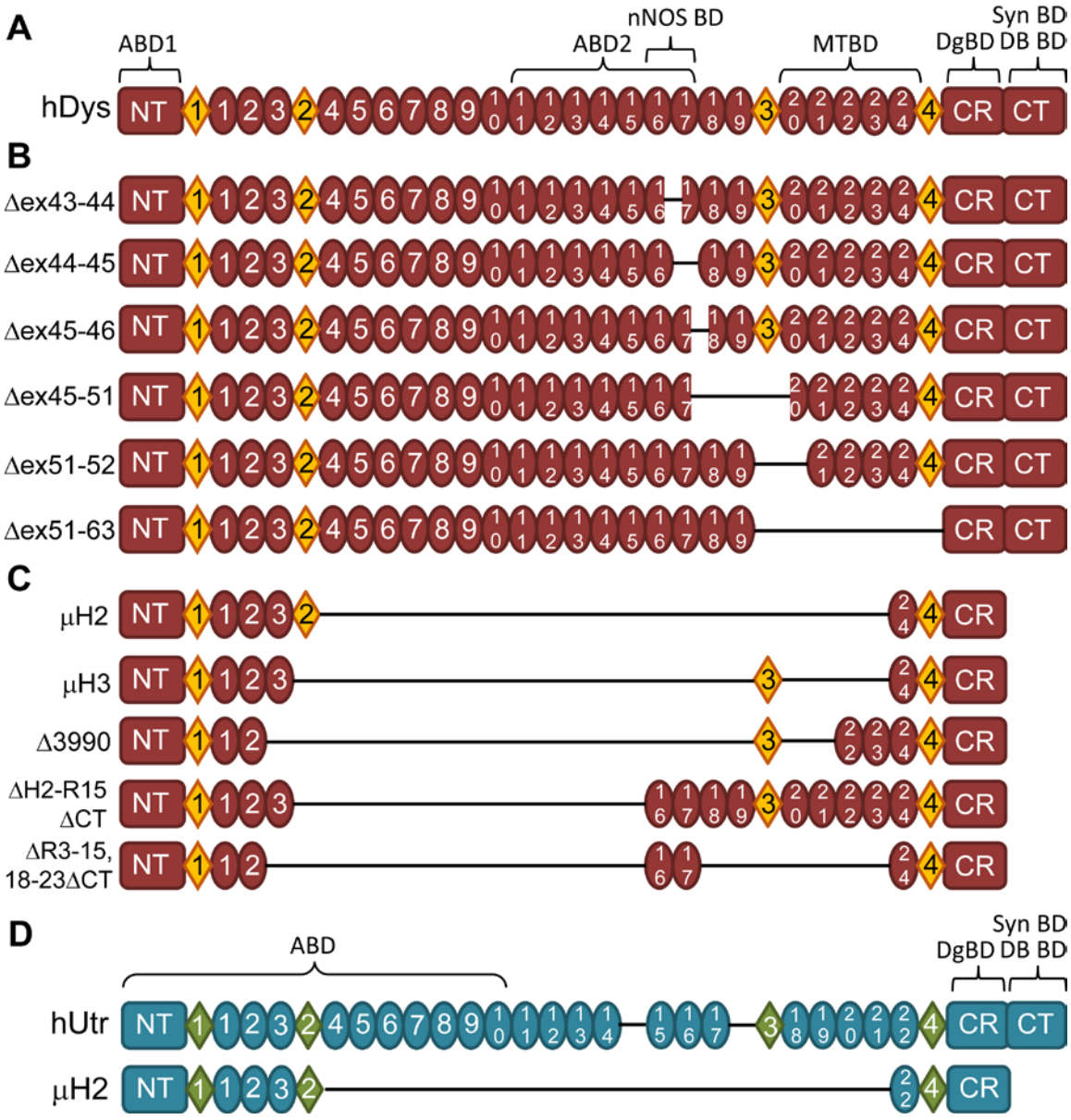

Figure 2.1: Dystrophin and utrophin constructs analyzed. A Diagram of full-length human dystrophin (hDys); NT – N-terminus, CR – cysteine-rich domain, CT – C-terminus, circles – spectrin-like repeats, diamonds – unstructured "hinge" regions, ABD1/2 – actin binding domains, nNOS BD – neuronal nitric oxide synthase binding

domain, MTBD – microtubule binding domain, DgBD – dystroglycan binding domain, Syn BD – syntrophin binding domain, DB BD – dystrobrevin binding domain. **B** Diagrams of exon-skipped human dystrophin constructs analyzed. **C** Diagrams of gene therapy human dystrophins analyzed. **D** Diagrams of full-length human utrophin (hUtr) and a micro-utrophin (µH2 hUtr) analyzed.

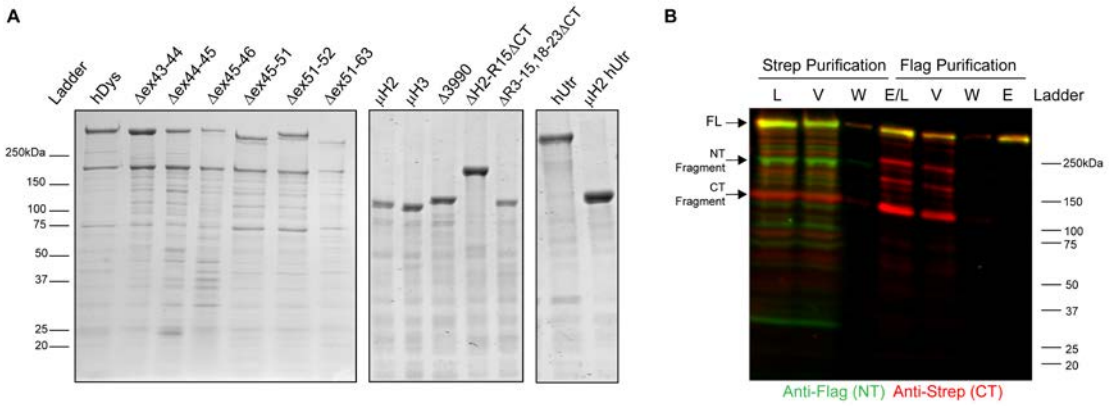

Figure 2.2: Gel analysis of purified recombinant proteins. A Representative Coomassie-stained gels with 5 μg of exon-skipped dystrophins, gene therapy dystrophins, and utrophins loaded for comparison. **B** Western blot of purification fractions from tandem purification of dual-tagged full-length human dystrophin with N-terminal (NT) FLAG-tag (green channel) and C-terminal (CT) Strep-tag (red channel); fractions from Strep affinity purification and FLAG affinity purifications: load (L), void (V), wash (W), and elute (E).

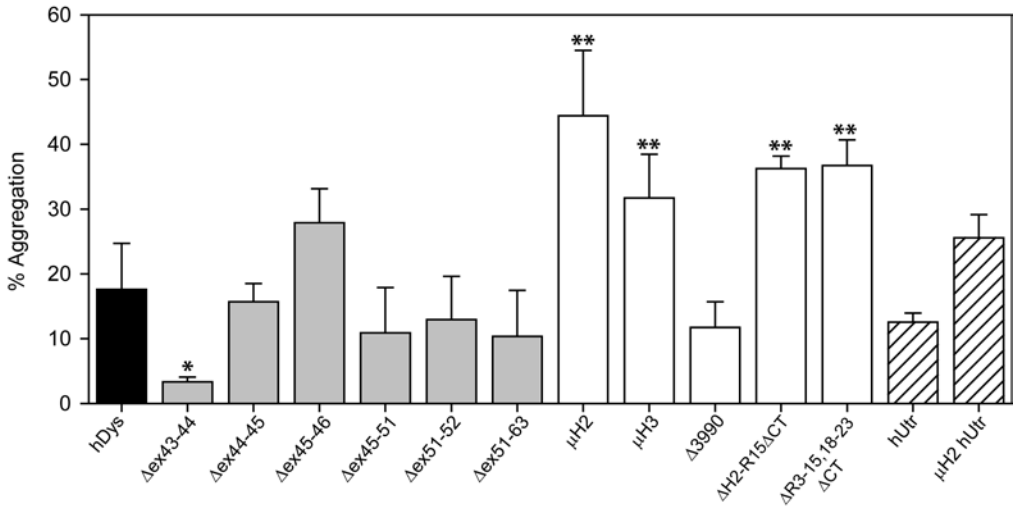

Figure 2.3: Analysis of protein aggregation by high-speed sedimentation. Quantification of high-speed sedimentation assay of supernatant (S) and pellet (P) fractions where % aggregation = S/(S+P); full-length human dystrophin (hDys) in black bar, exon-skipped dystrophins in gray bars, gene therapy dystrophins in white bars, and utrophins in lined bars; * $p<0.05$, ** $p< 0.0001$ using ANOVA statistical analysis compared to full-length human dystrophin.

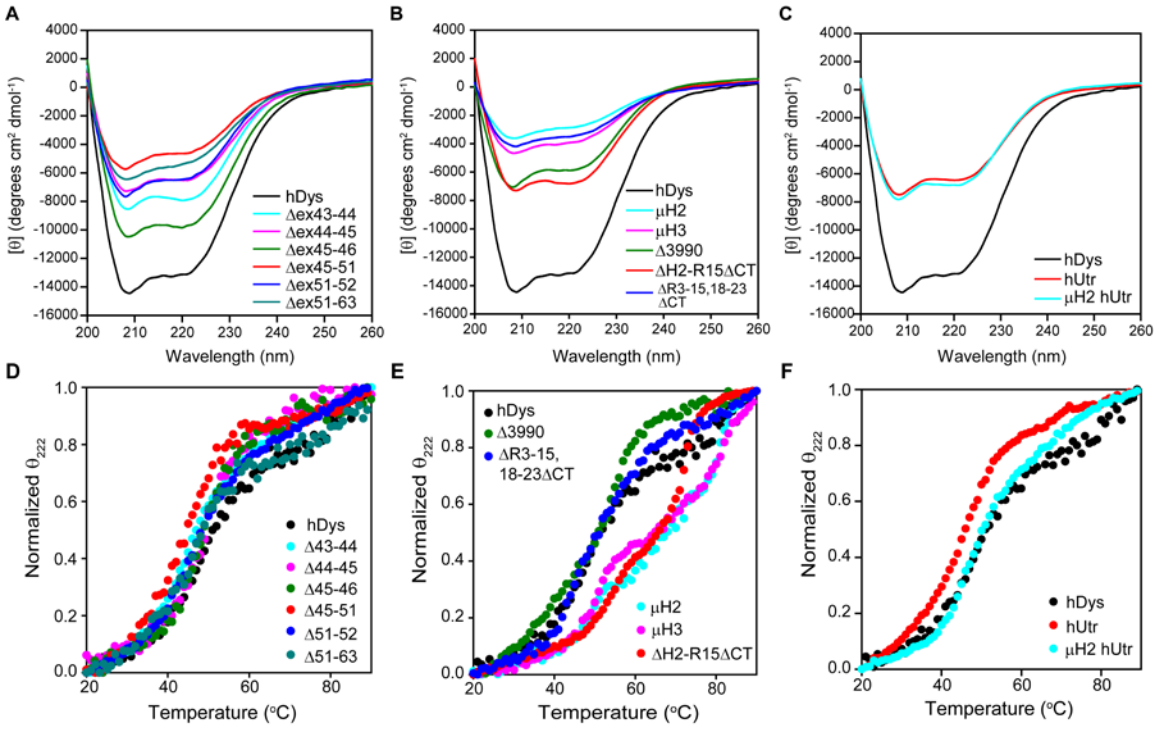

Figure 2.4: Spectra and melt curves obtained by circular dichroism spectroscopy. **(A-C)** Circular dichroism absorption spectra from 200 to 260 nm for exon-skipped dystrophins (**A**), gene therapy constructs (**B**), and utrophins (**C**). Molar Ellipticity [θ], with units of degrees cm^2 per decimole, was calculated as θ / (10 x *c* x *l)* where c is the molar concentration of the sample (mole/L) and *l* is the path-length in cm. **(D-F)** CD absorption spectra monitored at 222nm from 20°C to 90°C for exon-skipped dystrophins (**D**), gene therapy dystrophins (**E**), and utrophins (**F**). Melt curves were normalized to θ_{222} from 0-1 fraction unfolded and a representative curve plotted. See Table 1 for melting temperatures (CD T_m1 and T_m2).

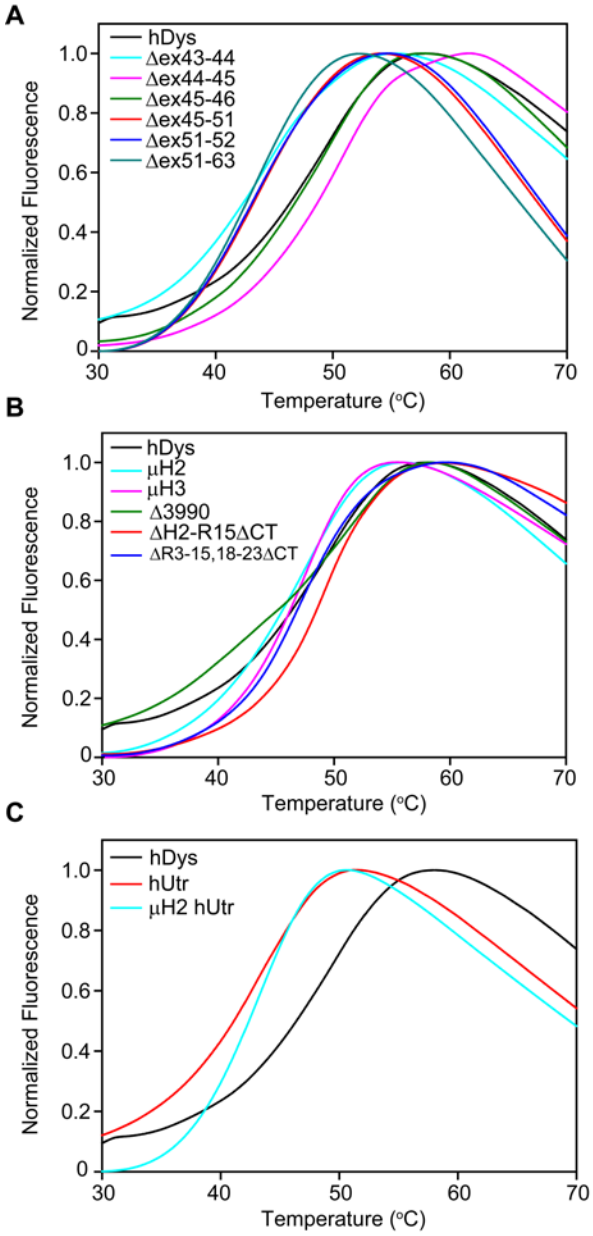

Figure 2.5: Melt curves obtained by differential scanning fluorimetry. Differential Scanning Fluorimetry (DSF) melt curves for exon-skipped dystrophins (**A**), gene therapy dystrophins (**B**), and utrophins (**C**). Fluorescence monitored at 610nm from 20°C to 90°C and fluorescence normalized from 0-1 fraction unfolded and a representative curve plotted. See Table 2.1 melting temperatures (DSF T_m).

Construct	Molecular Weight (kDa)	CD Tm1 (ºC)	CD Tm2 (ºC)	DSF Tm (ºC)	% Aggregation
hDys	427	48.1 ± 1.17	-	45.7 ± 2.62	17.6 ± 7.11
Δex43-44	414	46.7 ± 0.70	-	44.3 ± 0.35	3.4 ± 0.73*
Δex44-45	413	51.7 ± 1.51	-	48.1 ± 1.54	15.7 ± 2.83
Δex45-46	414	48.4 ± 2.38	-	46.0 ± 2.60	27.9 ± 5.28
Δex45-51	385	47.9 ± 4.07	-	44.6 ± 1.63	10.9 ± 7.00
Δex51-52	414	47.2 ± 0.87	-	43.8 ± 0.31	12.9 ± 6.70
Δex51-63	351	48.6 ± 3.08	-	43.7 ± 1.15	10.4 ± 7.11
μH2	139	47.3 ± 1.25	85.1 ± 4.14	46.0 ± 1.28	44.4 ± 10.10**
μH3	137	49.5 ± 1.78	79.0 ± 2.82	45.8 ± 0.86	31.7 ± 6.72**
Δ3990	154	56.1 ± 1.97**	-	50.4 ± 1.91*	11.7 ± 3.97
ΔH2-R15ΔCT	242	53.7 ± 1.51	72.9 ± 4.11	49.8 ± 0.54*	36.2 ± 1.95**
ΔR3-15,18-23 ΔCT	146	45.8 ± 2.96	-	47.3 ± 0.07	36.7 ± 3.96**
hUtr	399	46.2 ± 1.42	-	43.4 ± 0.36	12.5 ± 1.40
μH2 hUtr	138	47.0 ± 1.16	-	42.9 ± 0.25	25.6 ± 3.58

Table 2.1: Biophysical properties of human dystrophin and utrophin constructs.

All values are mean values of at least 3 experiments with standard deviations. CD T_m1 and T_m2: Circular dichroism melting temperatures; DSF T_m: Differential scanning flourimetry melting temperatures. * $p < 0.05$; ** $p < 0.0001$ using ANOVA statistical analysis compared to full-length human dystrophin.

Chapter 3

Ubiquitin Proteasome Pathway in Novel Mouse Models of Missense Mutant Dystrophins*

*Manuscript of co-first author paper with Dana M. Talsness to be submitted to *Human Molecular Genetics* in May of 2017.

The initial siRNA screen was performed collaboratively with Dana Talsness and Robert Arpke with subsequent validation done by Jackie McCourt. Initial mouse-line development and analyses were performed by Dana Talsness collaboratively with Dawn Lowe, John Olthoff, Paul Chatterton, and Chris Chamberlain. Development of the homozygous mouse line and subsequence analyses was performed by Jackie McCourt with physiological analysis done in collaboration with Angus Lindsay.

Synopsis

Missense mutations in the dystrophin protein are thought to cause Duchenne (DMD) or Becker (BMD) muscular dystrophy in 0.4% of patients through an undefined pathomechanism. *In vitro* studies suggest that missense mutations in the N-terminal actin binding domain (ABD1) cause protein instability and decreased expression levels in cultured myoblasts that were restored to wild type by treatment with ubiquitin proteasome inhibitors. To identify the specific ubiquitin-conjugating enzymes responsible for targeting dystrophin to the proteasome, we screened a myoblast cell line expressing GFP-tagged L54R mutant dystrophin with an siRNA library of E1, E2, and E3 ligases. The screen identified five putative dystrophin-specific E3 ligases. To further elucidate the role of the ubiquitin proteasome pathway in missense dystrophin biology and the effects of missense dystrophins *in vivo*, we generated two missense dystrophin mouse lines on the *mdx* background – L54R and L172H – corresponding to DMD- and BMD- associated mutations identified in human patients. The biochemical, histological, and physiological parameters measured for these new mouse models demonstrate that disease severity is inversely proportional to the amount of missense protein present in the muscle. While treatment of the mice with proteasome inhibitors was not effective at increasing missense dystrophin protein, increased expression of missense L172H dystrophin through the generation of homozygous mice revealed further improvements in muscle histology and physiology. Additionally, protein levels for one of the five putative dystrophin-specific E3 ligases identified in our screen showed increased levels correlating with the amount of missense mutant dystrophin present in each mouse model. This work establishes two novel mouse models representing DMD or BMD where the level of dystrophin expression exceeds the accepted therapeutic level for wild type protein, and highlights the ubiquitin-proteasome pathway as a mechanism of

dystrophin protein regulation relevant for understanding the etiology of DMD/BMD and potential therapies.

Introduction

The X-linked recessive disease Duchenne muscular dystrophy (DMD) is caused by mutations in the DMD gene encoding for the 427 kDa protein dystrophin(Koenig et al., 1988). Dystrophin is predominantly expressed in muscle cells and is a critical component of the dystrophin-glycoprotein complex (DGC) that functions to stabilize the muscle cell membrane during muscle contraction (Ervasti, 2003; Rybakova et al., 2000). Disease-causing mutations in the DMD gene vary with 68.5% of patients harboring large deletions (>1 exon), 11% with duplications (>1 exon), 10.2% with non-sense mutations, 6% with smaller deletions or insertions (<1 exon), 3% with splice-site mutations, 0.3% with mid-intronic mutations, and 0.4% with missense mutations (Bladen et al., 2015). Typically, mutations that result in the absence of dystrophin protein (i.e. through nonsense mutations or out-of-frame deletions) cause the severe phenotype of Duchenne muscular dystrophy (DMD) whereas mutations that result in a partially functional dystrophin cause a milder form known as Becker muscular dystrophy (BMD) (Koenig et al., 1989). Exceptions to this categorization include the subset of patients with missense mutations that result in only one amino acid change. A patient with an L54R mutation in the N-terminal tandem calponin homology (CH) actin binding domain (ABD1) was reported as having a severe form of dystrophy diagnosed as DMD (Prior et al., 1993) and a patient with a missense mutation in a homologous region of ABD1, L172H, was diagnosed with the milder BMD (Hamed et al., 2005).

Disease-causing mutations in ABD1 were expected to disrupt actin binding activity (Norwood et al., 2000). However, many missense mutations in this domain, including L54R and L172H, did not show large differences in actin binding affinity but instead demonstrated increased thermodynamic instability and aggregation (Henderson et al., 2010; Singh et al., 2010). Additionally, myoblast cell culture models expressing L54R or L172H dystrophins revealed missense-mutant dystrophin levels that were inversely proportional to *in vitro* stability and disease severity of the corresponding patients (Talsness et al., 2015). Treatment of these cell lines with proteasome inhibitors or heat shock activators resulted in increased missense-mutant dystrophin levels suggesting that the mutations cause misfolding and are targeted to the proteasome. Because it is not therapeutically practical to treat chronic patients with broad-spectrum proteasome inhibitors over the course of their lifetime, research has more recently focused on inhibitors specific to ubiquitin-conjugating enzymes unique for a given disease target (Weathington and Mallampalli, 2014). Therefore, we performed an siRNA screen to identify the ubiquitin-conjugating enzymes that may specifically target misfolded dystrophins to the proteasome.

In addition to understanding the molecular/cellular pathomechanism associated with missense-mutant dystrophins, there is also a need to understand the consequences of missense mutations within the context of an animal model. The first animal model with a missense mutation in dystrophin was reported in a line of pigs harboring a point mutation in exon 41 resulting in full-length

dystrophin with the amino acid change R1958W (Hollinger et al., 2014). Phenotypically, the R1958W pigs appear to most closely model mildly-affected BMD patients and express dystrophin at 30% of wild-type levels. While this porcine model will likely be a valuable tool in muscular dystrophy research and therapy development, there currently is no animal model that harbors a missense mutation reported in any patients with Duchenne or Becker muscular dystrophy. Here we report the generation of two novel transgenic mouse models expressing missense dystrophins reported in human DMD (L54R) and BMD (L172H) patients, which we previously modeled in cultured myoblasts (Talsness et al., 2015). Analysis of hemizygous L54R and L172H mice on the dystrophin-null *mdx* background, as well as a homozygous L172H line, revealed that disease severity inversely correlates with expression levels of dystrophin protein, corroborating the results from the cell culture models. These mouse models are valuable platforms to continue understanding the mechanism of dystrophin protein regulation and to develop new therapies to treat Duchenne and Becker muscular dystrophy.

Materials and Methods

siRNA screen in myoblast model

The L54R mutant dystrophin C2C12 cell line was grown according to (Talsness et al., 2015). Cells were seeded to 600,000 and adhered for 4 hours before being treated with mouse ON-TARGETplus siRNA library for Ubiquitin Conjugating Enzymes Subsets 1, 2, and 3 (Dharmacon). Cells were treated with 40nM siRNA pools according to manufacturer's protocol or treated with 1uM bortezomib as a positive control. After 48 hours, cells were trypsinized and resuspended with 50ul microliters fluorescence-activated cell sorting (FACS) staining medium: phosphate-buffered saline (PBS) (Mediatech, Inc., Manassas, VA) containing 2% fetal bovine serum (FBS; HyClone, Logan, UT) supplemented with 1 ug/mL Propidium Iodide. FACS analysis was performed on a BD FACSAriaII (BD Biosciences, San Diego, CA) and data were analyzed using FlowJo (FlowJo LLC, Ashland, OR).

Cloning and mouse generation

Full-length mouse dystrophin cDNA (with missense mutations L54R and L172H) was subcloned into the Gateway system Entry vector (Life Technologies). The cDNA was then recombined into a vector containing the human skeletal alpha-actin (HSA) promoter and Vp1 intron that had been adapted to the Gateway system. The expression cassette was cut out of the vector with restriction enzymes and sent to the University of Cincinnati Transgenic Mouse Core (L54R) or The Scripps Research Institute Mouse Genetics Core (L172H) for pronuclear

injection into fertilized eggs. Injected eggs were transplanted into pseudopregnant mice. Progeny were screened for the transgene by genomic PCR. Transgenic mice were crossed onto the *mdx* background (mL54R and mL172H), and transgenic male progeny were analyzed. Homozygous mice were generated by breeding transgene positive males with transgene positive females. Progeny were then analyzed for homozygosity by genomic quantitative PCR using HSA transgene promoter specific primers (see below). All analyses were performed on mice 10-14 weeks of age.

RT-qPCR

Tissue was pulverized with mortar and pestle in liquid nitrogen. RNA was isolated with the Aurum Total RNA Fatty and Fibrous Tissue (BioRad 732-6870). Total RNA was reverse transcribed into cDNA using the iScript™ Advanced cDNA Synthesis Kit (Biorad 170-8843). cDNA was amplified using SsoAdvanced™ Universal SYBR® Green Supermix (Biorad 172-5270). Primers for endogenous mouse dystrophin: Forward [TGGCAGATGATTTGGGCAGA] and Reverse [CCATGCGGGAATCAGGAGTT]. Primers for transgenic mouse dystrophin (for HSA transgene promoter): Forward [ACAATGTAGAAGGGTGGGCG] and Reverse [GCGTAGAATCGAGACGCGAGG]. Primers for intragenic mouse dystrophin: Forward [GCGCCAACACAAAGGACGCC] and Reverse [GCTTCAGCCTGGGGCTGCTC]. All measurements were relative to reference transcript Hprt: Forward [CCCTGGTTAAGCAGTACAGCCCC] and Reverse

[GGCCTGTATCCAACACTTCGAGAGG]. Primers for RT-qPCR of the siRNA positive hits are listed in the table below. Measurements were collected with the C1000 Touch Thermal Cycler (Biorad) and analyzed with the CFX Manager software (Biorad).

Target	Forward Primer	Reverse Primer
ASB5	AAGCTGGGGCTAATGCAAAC	CAGGACTCCAGTTGGGCTTT
VPS41	GCCGAGTATGACCGACCAAA	CCCATTCGGCTCAGAAGGTA
Amn1	GTCAGCTCCTGGAACTATGTCT	GTTATCCGACCCCGAATGCT
FBXO33	TTGGCAATTCATGGTTACACCG	GCCCAGTGATACCTGCTCAA
FBXO16	GCTGCTGAGGTGTTGTCTTTC	GATGGTTGAGAGGTGTCCAGG
Zfand5	GTCACTCAGCCCAGTCCATC	GCAGTCAAACCCTGTAAGGC
SCEL	CAATCAACCAAGACGCCAGC	TGTGCTTGGAGAGGCATTGT
NSD1	TCCAGAAGTACCCACCGACT	GCGCATCAGACGACCTTTAG
PHF5A	GGTGTGGCTATCGGAAGACT	CGGCCCTGGTAAGATCCATAG
MYLIP	TACAGGAGCAGACAAGGCAT	TGTATTGGGCGGTGTTCTGG
Pcgf3	CCAGGAAGCGGAAATGAGGA	TGGTTTCACCATTTCGGGGA
Rnf182	GGCTCTCGATCCTCCCATCG	AAGGGCAGCTGAAGGATCTGAC
TRAF2	GCTACTGCTCCTTCTGCCTG	TGGAAAGGCCGAACTACTCTC

Western blot analysis

Tissue was pulverized with mortar and pestle in liquid nitrogen. Tissue was then lysed with 1% SDS solution with added protease inhibitors [100nM Aprotonin,

10mg/ml E-64, 100μM Leupeptin, 1mM PMSF, 1μg/ml Pepstatin] proportional to mass of the tissue pellet. Protein concentration was measured by A_{280} absorbance. Equal concentrations of lysate were then separated by electrophoresed at 150V for 1 hour, then transferred to PVDF membrane at 100V/0.7Amp for 1 hour. Membranes were blocked in either [5% non-fat milk in phosphate buffered saline 0.1% Tween solution] or [5% Bovine Serum Albumin in tris buffered saline 0.1% Tween solution] depending on the primary antibody for 1 hour. Primary antibodies used were anti-Dys1 (Leica) at 1:100, anti-Dys2 (Leica) at 1:100, anti-utrophin (Santa Cruz 8A4) at 1:100, anti-α-dystroglycan (Millipore 05-593) at 1:1000, anti-β-dystroglycan (vector labs VP-B205) at 1:100, anti-dystrobrevin (BD labs 610766) at 1:1000, anti-syntrophin (Abcam 11425) at 1:1000, anti-pan actin C4 (Seven Hills Bioreagent LMAB-C4) at 1:5000, anti-Desmin D93F5 (Cell Signaling 5332) at 1:1000, anti-Hsp40 C64B4 (Cell Signaling 4871) at 1:1000, anti-Hsp70 (Cell Signaling 4872) at 1:1000, anti-Hsp90 (abcam 19021) at 1:1000, anti-Phosph-Hsp90α (Cell Signaling 3488) at 1:1000, anti-Phospho-Hsp27 (Cell Signaling 9709) at 1:1000, anti-Fbxo33 at 1:500 (Abcam ab90046), and anti-Amn1 at 1:500 (Boster Bio A15649). Blots were then incubated in secondary antibodies anti-mouse or anti-rabbit IgG Dylight® 800 (Cell Signaling) at 1:10,000 in blocking buffer. Secondary antibody signal was visualized on Licor's Odyssey® Infrared Imaging System and band density calculated with Odyssey Software v2.1.

Immunofluorescent analysis

Quadriceps and gastrocnemius muscles were dissected, frozen in melting isopentane, and embedded in optimum cutting temperature (OCT) compound submerged in liquid nitrogen. Transverse sections of 10 µm were cut on a Leica CM3050 cryostat, air dried, and then fixed in 4% paraformaldehyde for 10 minutes. Sections were washed with PBS (150mM NaCl, 8 mM NaH_2PO_4, 42 mM Na_2HPO_4) before being blocked with 5% goat serum/0.1% Triton X-100 for 30 minutes. A secondary block in Rodent Block M (Biocare Medical) was also performed for 30 minutes. The sections were then incubated with primary antibodies overnight at 4°C. Primary antibody dilutions were: NCL-Dys1 (1:20) (Leica), NCL-Dys2 (1:20) (Leica), Rb2 (1:20), Utrophin (1:50) (Santa Cruz), α-Dystroglycan (1:50) (Millipore), β-Dystroglycan (1:50) (Vector Labs), Dystrobrevin (BD Biosciences), nNOS (1:50) (Invitrogen), and Laminin (1:1000) (Sigma). Sections were then washed with PBS and incubated with Alexa Fluor 488- or Alexa Fluor 568-conjugated secondary antibodies (1:500 dilutions) for 30 minutes at 37°C. Sections were washed with PBS and coverslips were applied with a drop of Prolong Gold antifade reagent with DAPI (Molecular Probes). Images were collected on a Deltavision PersonalDV microscope equipped with a 20x/0.75 objective (Applied Precision) and viewed with GIMP (GNU Image Manipulation Program) software.

Histology and CNF count

Cryosections were cut from the same blocks prepared for immunofluorescence at 10µm thickness. Sections were stained with hematoxylin and eosin-phloxine and

imaged on Leica DM5500 microscope at 200x total magnification. A total of at least 250 fibers were imaged from each muscle of each mouse and then centrally nucleated fibers (CNF) counted as a percentage of the total.

Serum CK analysis

Serum samples of the mice were collected by cheek bleed. The samples were diluted 1:20 and then serum creatine kinase (CK) activity analyzed using CK DT slides (Ortho-Clinical Diagnostics) and a Kodak Ektachem DT 60 Analyzer. CK activity is reported as U/L.

Forelimb grip strength

Mice were gripped at the base of their tail and positioned to grab the DFE series digital force gauge (Chatillon) with grip bar attachment. Once the mouse was gripping the bar with both hands, the mouse was slowly with consistent force pulled perpendicularly away from the grip bar. Five trials were run per mouse and the average force was calculated.

Whole body tension

Mice were placed between parallel barriers, allowing only for forward movement. A slipknot suture was used to attach the base of the mouse tail to a fixed range force transducer (BioaPac Systems). The tail of the mouse was then lightly pinched and the subsequent force evoked was measured. Five minute traces were collected and the top 5 peaks were averaged for each mouse and then normalized to body weight. Protocol adapted from (Carlson and Makiejus, 1990).

Activity after exercise

Mice were acclimatized to the treadmill for 3 consecutive days, for 5 minutes at 0m/min followed by 5 minutes at 9m/min at 0° decline. On the fourth day, baseline pre-exercise activity was assessed for 30 minutes using laser-sensor activity cages (AccuScan Instruments Inc.). Mice were then acclimatized to the treadmill for 5 minutes at 0m/min at 15° decline. Without the use of electrical shock, mice were then encouraged to walk on the treadmill for 5 min at 5m/min followed by 10 minutes at 15m/min. After exercise, activity was measured for 30 minutes. Total number of vertical episodes were counted and post-exercise activity reported as a percentage of the pre-exercise activity.

Eccentric contraction analysis

Mice were anesthetized with sodium pentobarbitoal and the extensor digitorum longus (EDL) muscle dissected out. Silk suture was used to attach the proximal tendon to a static structure and the distal tendon to a force transducer (Model 300B-LR, Aurora Scientific). The EDL was suspended in Ringer's solution [120.5mM NaCl, 4.8mM KCl, 1.2mM $MgSO_4$ 1.2mM Na_2HPO_4, 20.4mM $NaHCO_3$, 10mM glucose, 10mM pyruvate, 1.5mM $CaCl_2$], while 95% O_2/5% CO_2 was bubbled in. Muscles were lengthened to an optimal tension and this set as the optimal length (L_0). Maximal twitch and tetanus were measured. For 10% length change experiments, the EDL muscle was subjected to an eccentric contraction protocol consisting of 5 or 10 maximal tetanic stimulations (5.7ms pulses at 150Hz for 200 ms) while lengthening from 95% to 105% of the L_0 at 0.5 lengths per second. For 5% length change experiments, the EDL muscle was subjected

to an eccentric contraction protocol consisting of 10 maximal tetanic stimulations (5.7ms pulses at 150Hz for 200 ms) while lengthening from 97.5% to 102.5% of the L_0. Three minutes recovery was allowed between each eccentric contraction and maximum force recorded. Force production was plotted as percentage of the first contraction.

Statistics

All statistical calculation were performed with JMP® statistics software. Data are presented as mean ± standard error of the mean. To determine significance for all data with three or more groups, one-way ANOVA analysis was performed with $\alpha=0.05$. Upon significance of the ANOVA, the Tukey post hoc test was performed with all pairs of data at $\alpha=0.05$.

Results

The myoblast cell line expressing GFP-tagged L54R dystrophin was used to screen a commercial library of 512 E1, E2, and E3 ligases (Dharmacon/GE Life Sciences Ubiquitin Conjugation Subsets 1, 2, and 3) through fluorescence activated cell sorting (FACS, Figure 3.1). Sixteen positive hits were identified as those with fluorescence values significantly above a background threshold of 2.5% (Figure 3.2) and were replicated in an identical but separate siRNA treatment and FACS analysis. The positive hits of the screen are listed in Table 3.1. The majority of the hits are either confirmed or putative E3 ligases with only three E2 ligases identified in the screen (Ube2e3, DCN1, and Ube2i). Of the 16 positive hits, 9 were subsequently validated by RT-qPCR to show significant transcript knockdown in cells after siRNA treatment (Figure 3.3) and 5 of the E3 ligases further showed increased GFP-dystrophin fluorescence above the background when knocked down in the L172H cell line (Table 3.1).

To further characterize the E3 ligases implicated by the screen to target missense-mutant dystrophin to the proteasome, we generated transgenic mice expressing the L54R or L172H missense mutations in full-length dystrophin driven by the human skeletal actin (HSA) promoter and bred them onto the dystrophin-deficient *mdx* mouse line (labeled as mL54R and mL172H mice). Tibialis anterior (TA), gastrocnemius, and heart tissues were analyzed by RT-qPCR and Western blot for dystrophin transcript and protein levels (Figure 3.4). The L54R mice had comparable levels of dystrophin transcript compared to wild

type mice (Figure 3.4A) but only 7-9% of wild type protein levels (Figure 3.4E). Transcript levels in L172H mice were also comparable to wild type (Figure 3.4B) but mutant protein levels were only 44% of wild type (Figure 3.4F). L54R and L172H protein levels were remarkably similar to the levels measured in the corresponding myoblast cell culture model (13% for L54R and 46% for L172H).

The mL54R and mL172H mouse lines were analyzed for quantity and localization of several components of the dystrophin glycoprotein complex (DGC) compared to wild type and *mdx* mice (Figure 3.5). Both mL54R and mL172H lines did not exhibit rescue of DGC component expression by western blot but did show proper localization at the membrane. Interestingly, utrophin expression in transgenic lines was similar to *mdx* but nNOS expression was increased and was membrane-localized in mL172H mice. Quadriceps muscle sections were stained with H&E and assessed for histological signs of dystrophy (Figure 3.6A). The mL54R line showed dystrophic features similar to *mdx*. The mL172H was also dystrophic, but possibly to a lesser degree. To quantify the histological features, the fibers which are centrally-nucleated (CNF) were counted as a percentage of total fibers (Figure 3.6B). The data revealed that *mdx* had significantly more CNFs than wild type, as expected. The mL54R and mL172H lines also had significantly increased CNFs over wild type, but with lower average values than *mdx*. Indeed mL172H quadriceps had significantly lower CNFs than both *mdx* and mL54R. Across the four phenotypes, CNF values were inversely proportional to the quantity of dystrophin protein measured (Figure 3.4) and

consistent with the severity of patient muscular dystrophy symptoms modeled by each line.

The transgenic mL54R and mL172H lines were assessed for several physiological impairments associated with muscular dystrophy in the *mdx* mouse, including grip strength, whole body tension, activity after exercise, and eccentric contraction-induced force loss (Figure 3.7) (Petrof et al., 1993; Connolly et al., 2001; Kobayashi et al., 2008). Wild type mice displayed an average grip strength of 32 mN/g (Figure 3.7A), while all three dystrophic lines (*mdx*, mL54R, mL172H) had significantly decreased grip strengths. Whole body tension, which measures the force of both the proximal and distal muscles in all four limbs at once, for wild type mice showed approximately 140mN/g of tension (Figure 3.7B). The *mdx* line gave a large range of variability, but each of the transgenic lines mL54R and mL172H were significantly decreased compared to wild type. The activity levels of mice were monitored before and after exercise (Figure 3.7C), and it was found that each of the dystrophic lines were significantly less active than wild type. As a final assessment of physiological performance, extensor digitorum longus (EDL) muscle was analyzed *ex vivo* for force loss after eccentric contraction (Figure 3.7D). Wild type mice maintained the same level of force after 5 eccentric contractions, while *mdx*, mL54R, and mL172H all dropped to approximately 20% of initial force by the 5^{th} eccentric contraction. A summary of all the *ex vivo* parameters measured (Table 3.2) shows that all three of the dystrophic models were significantly different than wild type for specific force,

change in specific force after eccentric contractions, and total force drop during eccentric contraction. Together, these data indicate that neither missense mutant line was different from *mdx* suggesting that the L54R and L172H dystrophin proteins cannot restore physiologic function.

Because we previously showed in the myoblast models of L54R and L172H dystrophins that the mutant proteins were being targeted to the proteasome (Talsness et al., 2015), we treated the mL54R and mL172H mouse models with several different proteasome inhibitors at various concentrations and by multiple delivery methods according to protocols previously published (Table 3.3, Gazzerro et al., 2010; Yang et al., 2011; Stessman et al., 2013; Hurchla et al., 2013). None of the treatments showed evidence of an increase in dystrophin protein levels by Western blot (Figure 3.8). These results suggest that use of proteasome inhibitors is not a viable option for testing whether increasing missense dystrophin levels in muscle improved any of the dystrophic parameters or confirming whether mutant dystrophin protein was being targeted to the proteasome.

To determine if the missense mutations in dystrophin were stimulating the heat shock pathway, the relative abundance of the major heat shock proteins was measured by western blot analysis (Figure 3.9). Quantification from three separate sets of animals revealed no difference in the levels of Hsp40, Hsp70, Hsp90, or Hsp27P. Hsp90P levels were almost undetectable. While there was no significant increase, Hsp27P showed an upward trend for the mL54R line,

indicating that there may be a slight perturbance to the heat shock pathway. The lack of global heat shock response was similar to the missense myoblast model, and leaves the heat shock pathway as a possible therapeutic target for increasing dystrophin protein levels.

Given the ineffectiveness of proteasome inhibitors to elevate mutant dystrophin levels in the mL54R and mL172H mouse models (Table 3.3), we tested whether mice homozygous for the L172H missense mutant dystrophin transgene (mhomL172H) expressed more dytrophin than hemizygous mL172H animals and compared the phenotypes of mhomL172H animals with mL172H littermates. By Western blot, skeletal muscle from mhomL172H mice expressed significantly more dystrophin (~1.5X) than mL172H muscle (Figure 3.10). Histologically, mhomL172H mice showed similar fiber size and shape to mL172H, but showed a further significant decrease in the number of centrally nucleated fibers (Figure 3.11A-B). The mhomL172H animals demonstrated a modest but still significant protection from eccentric contraction-induced force loss compared to *mdx* and hemizygous littermates (Figure 3.11C). Protection was even more evident when the eccentric contraction protocol was adjusted to a 5% length change (Figure 3.11D) compared to our standard 10% length change protocol (Figure 3.11C). Comparison of *ex vivo* parameters to other mouse models showed significant improvement in specific force of the homozygous mice over mL172H mice (Table 3.2). Furthermore, homozygous mice had significant improvement in specific force, change in specific force, and force drop

compared to *mdx*, a change that was not seen for mL172H mice.

Based on our *in vitro* studies in myoblasts that missense dystrophins are targeted to the proteasome (Talsness et al., 2015), we analyzed muscle tissue from each mouse line for changes in expression of the 5 E3 ligases identified from the siRNA screen (Table 3.1). Western blots of Rnf182, VPS41, and Zfand5 using the commercially-available antibodies did not show specific bands of the expected molecular weight (data not shown). While the levels of FBXO33 did not vary in a pattern consistent with the level of dystrophin expressed, Amn1 immunoreactivity increased proportional to the amount of missense protein expressed (Figure 3.12). These data suggest that Amn1 may be involved in regulating the level of missense mutant dystrophins and/or their targeting to the proteasome for degradation.

Discussion

Using an siRNA screen in cultured myoblasts, we have identified five E3 ligases that may be involved in targeting missense dystrophins to the proteasome. Rnf182, or ring-finger like protein 182, has been shown to have E3 ubiquitin ligase activity *in vitro*, interacts with a complex that functions in gap junctions and neurotransmitter release channels, and has altered expression in Alzheimer's disease (Liu et al., 2008). Zfand5, also known as Znf216, is a zinc-finger and AN1-like domain containing protein that has been shown to interact with IKKgamma (Huang et al., 2004) and, more notably, has been implicated in muscle atrophy (Hishiya et al., 2006). VPS41 is a part of the regulated secretory pathway and endocytic pathways in mammalian cells(Wada, 2013) but contains a RING-H2 domain present in a number of ubiquitin ligases(McVey Ward et al., 2001). FBXO33 is a component of the SCF (Skp1/Cul1/F-box) E3 ubiquitin ligase (Lutz et al., 2006), was identified as a seizure response gene (Flood et al., 2004) and as a target of the DUX4 transcription factor that is activated in facioscapulohumeral muscular dystrophy (Geng et al., 2012). Amn1 has been implicated in cell cycle regulation and a putative interactor with the E3 ligase APC (anaphase-promoting complex) (Wang et al., 2003). With the exception of FBXO33, the E3 ligases we identified have not been previously associated with muscular dystrophy and none of them have been reported to bind to or ubiquitinate dystrophin.

We have also generated two novel transgenic mouse lines, representing severe DMD (L54R) and mild BMD (L172H) caused by missense mutations in dystrophin. The original reports of missense mutations L54R and L172H were more than a decade apart from each other and therefore could not be compared side by side (Prior et al., 1993; Hamed et al., 2005). While the physiology of the patients was well reported, the molecular analysis was minimal, with both groups estimating that the patient expressed 20% dystrophin levels. Here we measured steady state dystrophin levels of 7-9% for L54R and 44% for L172H. These results correlate with the level of protein seen in the cell culture models and dystrophin expression can be ascribed to the degree of *in vitro* misfolding as seen by differential scanning fluorimetry (Talsness et al., 2015). The mL54R line presented with biochemical, histological, and physiological phenotypes synonymous with the *mdx* mouse, whereas the mL172H line was more consistent with an improved, BMD-like phenotype. Therefore dystrophin protein abundance inversely correlates with disease severity in mice and we believe this is the major mechanism of disease.

Previous studies on the relationship between dystrophin protein expression and disease phenotype have also shown that disease severity inversely correlates with dystrophin protein levels (Wells et al., 1995; Phelps et al., 1995). Transgenic mice expressing only 20% of full-length or a therapeutic mini-dystrophin demonstrated rescue of dystrophic phenotype. Our mL172H mouse line expressing 40% dystrophin levels should thus theoretically be able to

ameliorate the dystrophic phenotype but instead only shows partial improvement in some parameters, suggesting that the L172H mutation disrupts dystrophin function in addition to protein stability. Other studies of dystrophin levels using non-transgenic mouse models with varying levels of dystrophin demonstrated that as little as 5% of wild-type dystrophin is sufficient to partially protect from some of the dystrophic phenotypes (Li et al., 2008; van Putten et al., 2012), suggesting that the L54R mutant expressed at 7-9% with no protection also has disrupted functionality.

To address the question of quality (functionality) versus quantity (dystrophin levels), we sought to increase dystrophin protein levels by treating mice with various proteasome inhibitors and heat shock activators as seen in the myoblast cell culture models. In all cases, there was no evidence of increased dystrophin protein upon treatment. One study on the use of proteasome inhibitors in *mdx* mice showed an improvement in muscle phenotype and an increase in DGC complex members at the plasma membrane (Bonuccelli et al., 2003) but we did not see a similar response. It is possible that the drugs are not at sufficient levels to inhibit the proteasome in muscle to produce the intended effect of increased dystrophin protein, leading us to generate homozygous transgenic mice to genetically increase missense dystrophin levels. We hypothesized that a homozygous L54R mouse would not produce high enough dystrophin levels to see an improvement, thus we focused our efforts on generating and characterizing the L172H homozygous line. The homozygous mice showed >1.5

fold increase in dystrophin levels compared to hemizygous littermates, demonstrating that L172H mutant dystrophin levels are able to be manipulated. The homozygous L172H line showed significant improvements in central nucleation, specific force, and eccentric contraction-induced force drop compared to hemizygous mice, indicating that higher levels of missense dystrophin are able to partially compensate for impaired functionality.

Finally, we were able to detect FBXO33 and Amn1 proteins in muscle tissue of wild-type, *mdx*, and missense dystrophin transgenic lines and observed that Amn1 levels increase as levels of missense dystrophin increase, with the highest level of expression in the homozygous L172H line. These data support our hypothesis that missense dystrophin proteins are being regulated by the ubiquitin-proteasome pathway. In future studies, we aim to knockdown Amn1 levels in our mice and evaluate the effect on missense dystrophin expression.

In summary, this work establishes two novel mouse models of missense dystrophins and, in particular for the L172H line, establishes the first animal model of BMD incorporating a mutation found in a patient. The proposed primary mechanism of disease in these models is through degradation of misfolded missense dystrophin proteins via the ubiquitin-proteasome pathway. The implications of this work are not limited to missense mutants only but can also apply to other potentially misfolded dystrophin proteins, such as internally deleted dystrophins (Henderson et al., 2011; McCourt et al., 2015) found in BMD

patients, those miniaturized dystrophins under investigation as therapeutic constructs for gene therapy, or in exon skipping therapies.

Figures

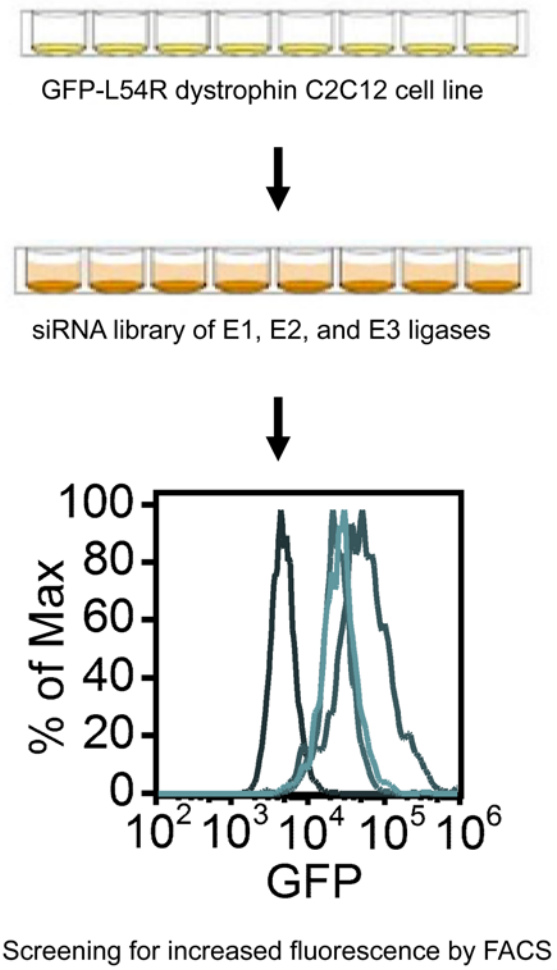

Figure 3.1: Experimental design for siRNA screen. The transgenic C2C12 cell line expressing GFP-L54R dystrophin was used to screen a library of 512 siRNAs targeting E1, E2, and E3 ligases. Fluorescence activated cell sorting (FACS) was used to screen for increased GFP fluorescence indicating an increase in L54R dystrophin protein levels.

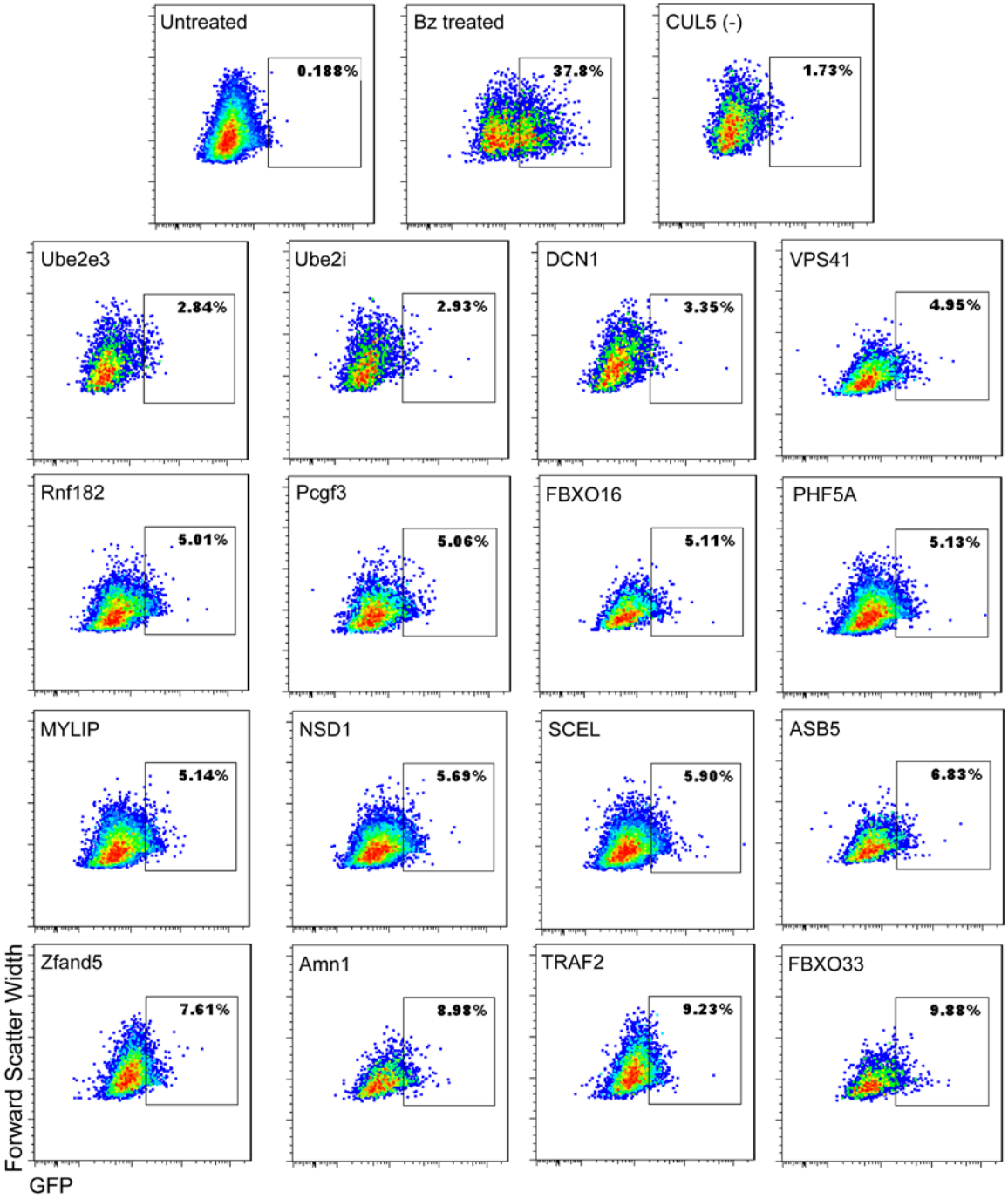

Figure 3.2: FACS plots of positive hits from siRNA screen. FACS plots generated from FlowJo of untreated cells, 1μM bortezomib (Bz) treated cells, a representative negative hit of below the 2.5% GFP threshold (CUL5), and the 16 positive hits above the threshold in order of increasing GFP fluorescence.

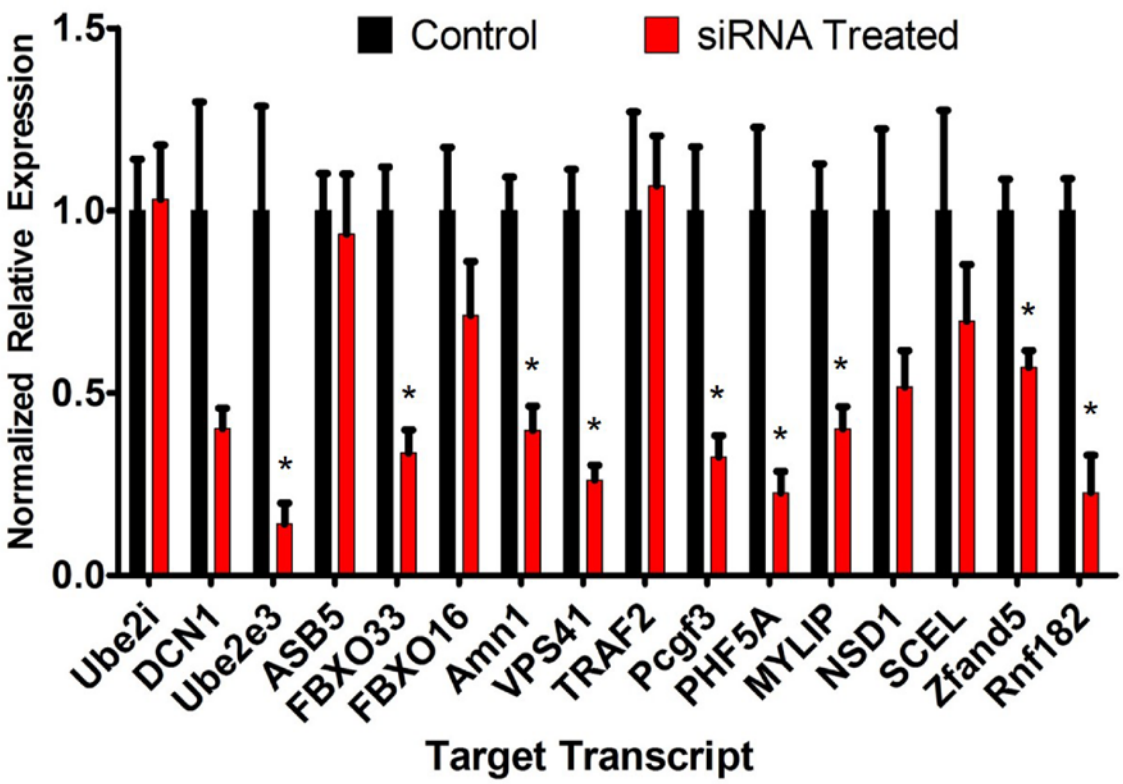

Figure 3.3: Validation of specific siRNA knockdown of 16 positive hits. RT-qPCR analysis of siRNA treated cells for each of the 16 positive hits compared to untreated cells. ANOVA $F<0.05$, * $p<0.05$ to untreated control.

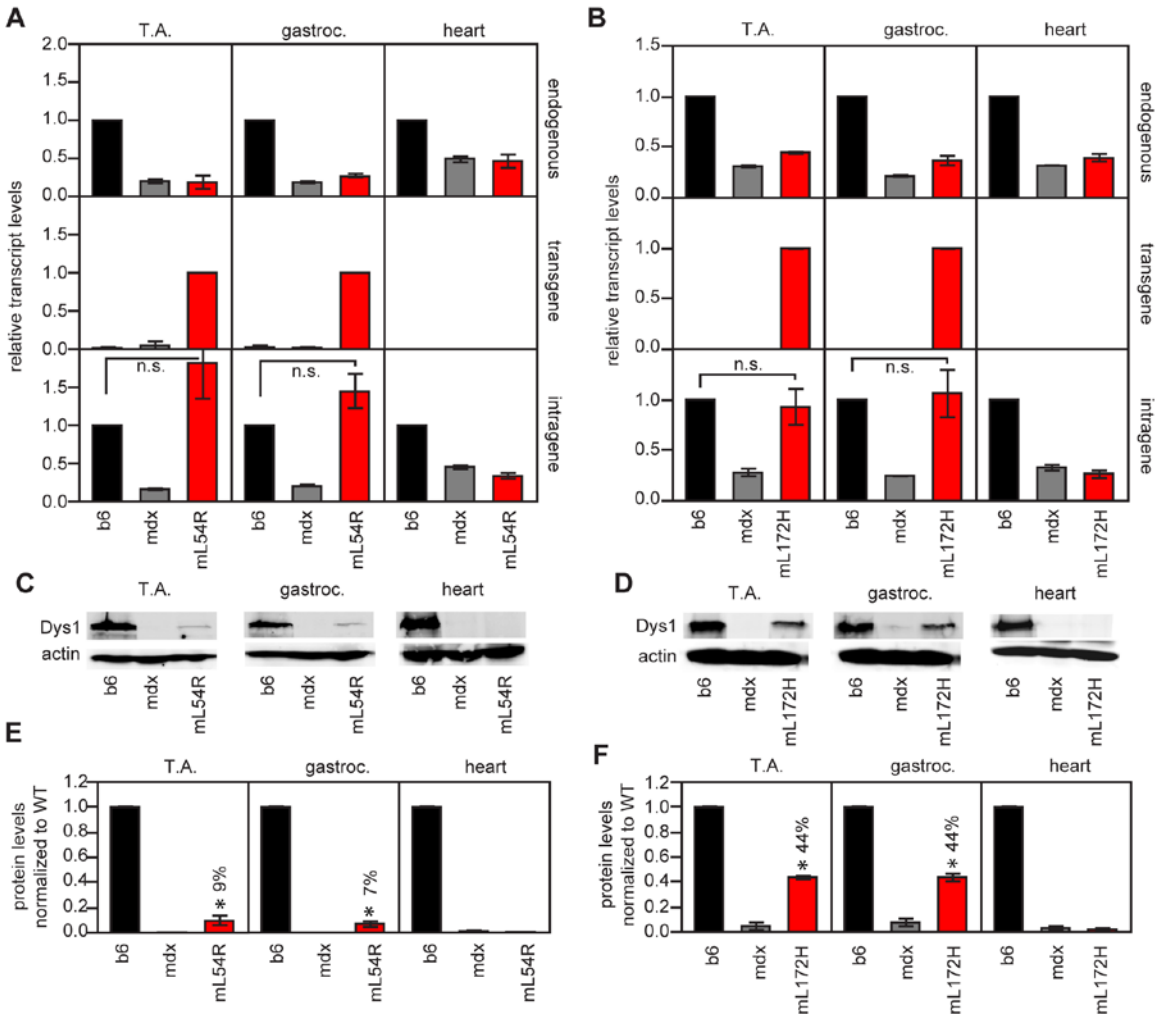

Figure 3.4: RNA and protein expression levels in transgenic mouse lines. (A) and **(B)** RT-qPCR analysis for mouse lines L54R and L172H respectively. Top panel shows amplification within the 3'UTR of endogenous mouse dystrophin. Middle panel shows amplification within the 3'UTR of the transgenic dystrophin. Bottom panel shows amplification within the coding region of dystrophin, amplifying both endogenous and transgenic dystrophin. n=3 separate animals for each line. ANOVA analysis of the intragene amplifications were $F<0.05$ for both L54R and L172H lines. Post hoc analysis between wild type and transgenic were n.s. (not significant). **(C)** and **(D)** Representative western blot analyses of mouse lines L54R and L172H respectively. **(E)** and **(F)**

Quantification of western blots from n=3 separate animals for each line. ANOVA analysis for both lines gave $F<0.05$. Post hoc analysis $*p<0.05$ compared to wild type.

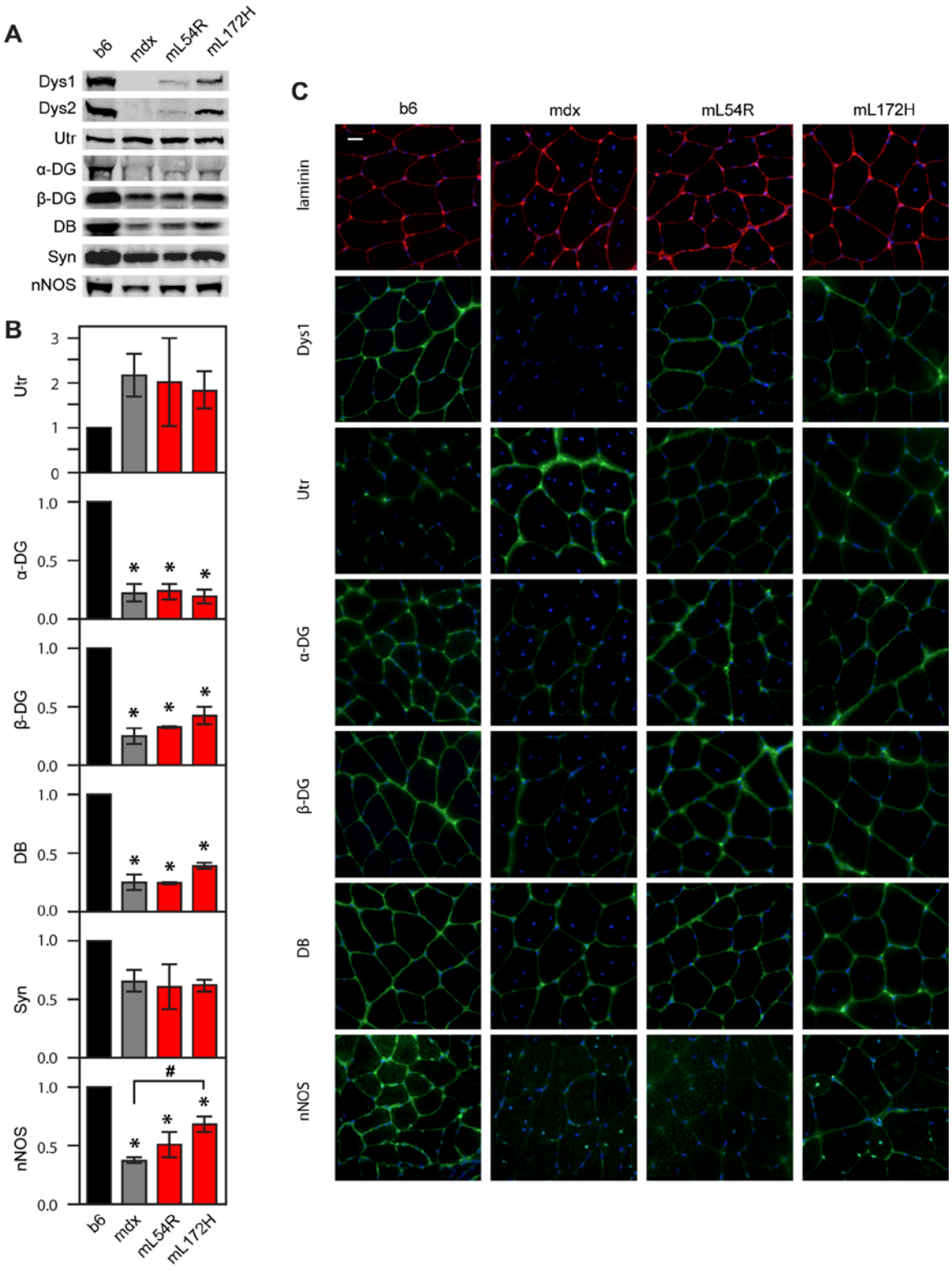

Figure 3.5: Expression levels and localization of components in the Dystrophin Glycoprotein Complex. (A-C) Utr = utrophin, α-DG = alpha-dystroglycan, β-DG = beta-

dystroglycan, DB = dystrobrevin, Syn = syntrophin, nNOS = neuronal nitric oxide synthase. **(A)** Representative western blot analyses for several components of the DGC in tibialis anterior muscle, including two different antibodies for dystrophin corroborating results found in Figure 4.2. **(B)** Quantification of western blots for n=3 separate animals for each line. Values are all normalized to wild type for each blot. ANOVA with significance of $F<0.05$ were analyzed with post hoc statistics. ✱$p<0.05$ compared to wild type. #$p<0.05$ between *mdx* and L172H. **(C)** Immunofluorescent analysis of components of the DGC in quadriceps muscle. Scale bar = 20μm.

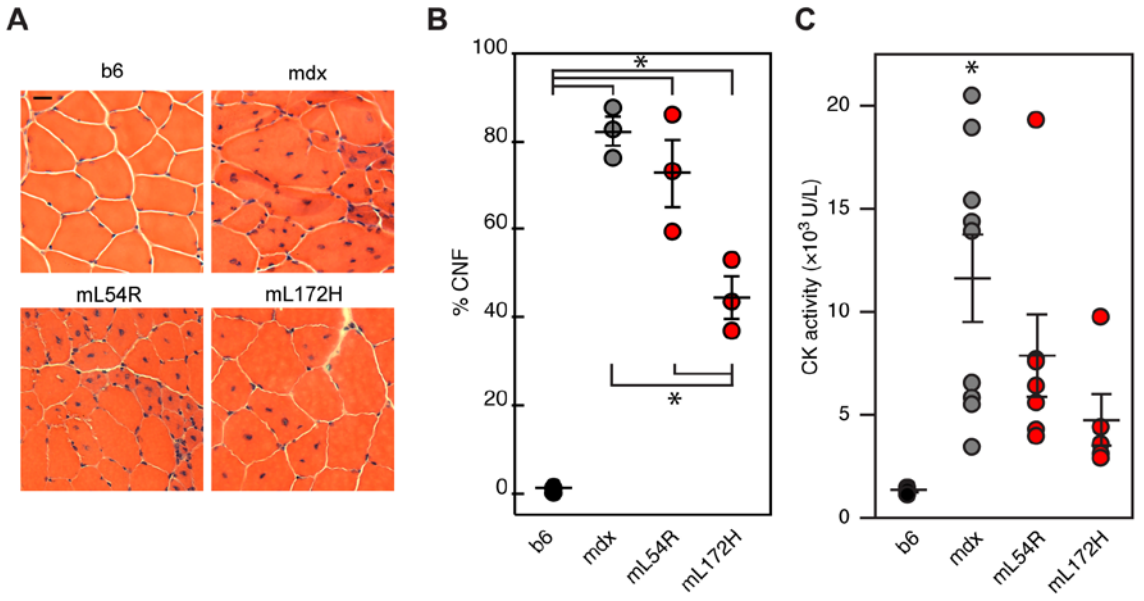

Figure 3.6: Fiber morphology and permeability. (A) Representative quadriceps muscle sections stained with H&E and imaged at 20x magnification. Scale bar = 20μm. **(B)** Quantification of centrally nucleated fibers (CNF) as a percentage of the total fibers. A minimum of 250 fibers were counted for each mouse. n=5 for b6 and *mdx*, n=6 for mL54R and mL172H. ANOVA analysis was significant at $F<0.0001$. Post hoc analysis gave ✱$p<0.001$ for wild type versus all disease models, and for mL172H versus *mdx* and mL54R. **(C)** Serum creatine kinase (CK) activity from cheek bleeds of individual mice. n=5 for b6, n=9 for mdx, n=7 for mL54R, n=9 for mL172H. ANOVA analysis was significant at $F<0.01$. Post-hoc analysis gave ✱$p<0.01$ for wild type versus *mdx*. Both transgenic lines were not statistically different from wild type.

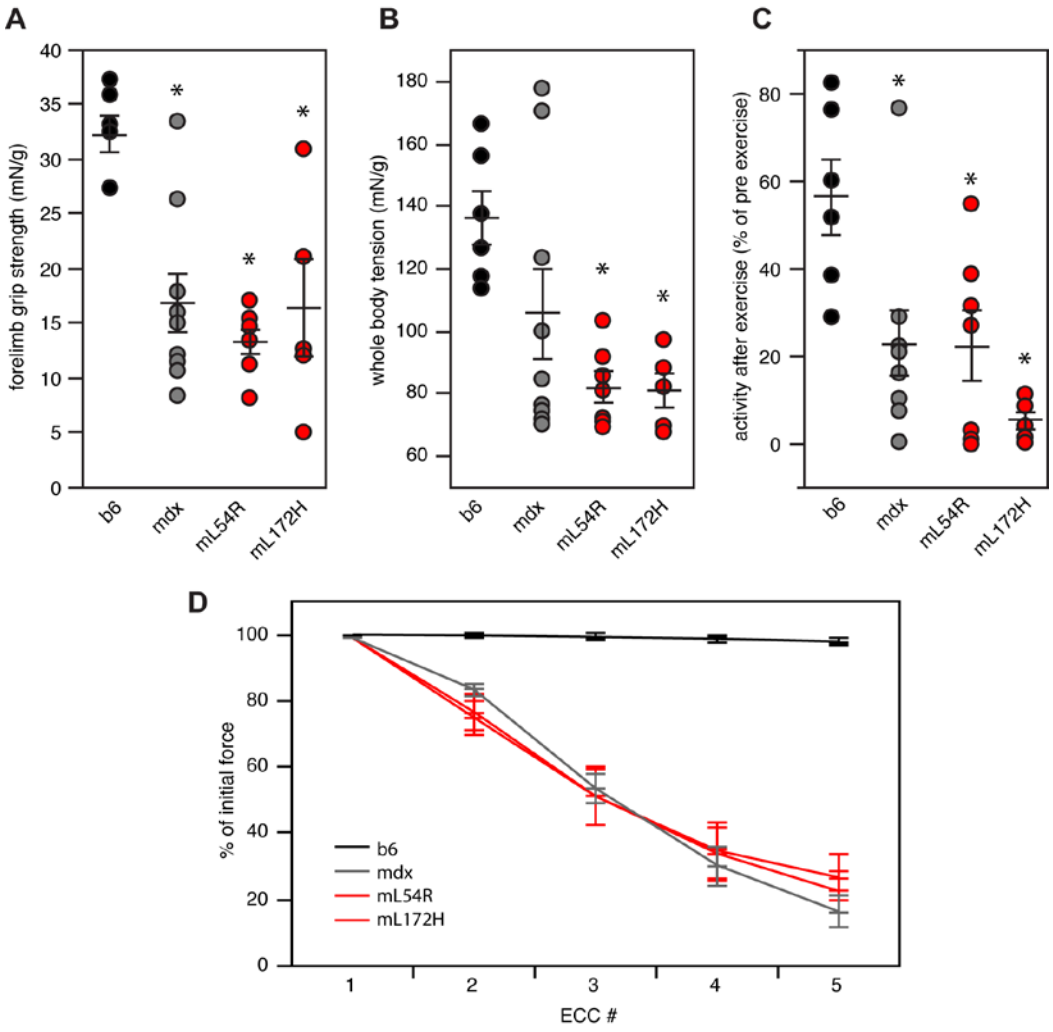

Figure 3.7: Physiology of transgenic mouse models. (A-C) n=6 for b6, n=9 for *mdx*, n=7 for mL54R, n=5 for mL172H. **(A)** Forelimb grip strength analysis. Individual points are an average of 5 trials for each mouse. ANOVA was significant at F<0.001. Post hoc analysis gave ✱p<0.005 compared to wild type. **(B)** Whole body tension analysis. Individual points are an average of 5 trials for each mouse. ANOVA was significant at F<0.01. Post hoc analysis gave ✱p<0.05 compared to wild type. **(C)** Activity after exercise analysis. ANOVA was significant at F<0.005. Post hoc analysis gave ✱p<0.05 compared to wild type. **(D)** *Ex vivo* EDL force measurement during eccentric contraction. n=4 for b6, n=5 for mdx, n=6 for mL54R, n=5 for mL172H. Data for b6 mice taken from Belanto et al. (PNAS 2014). For ECC 2-5, all three dystrophic models were significantly different than wild type.

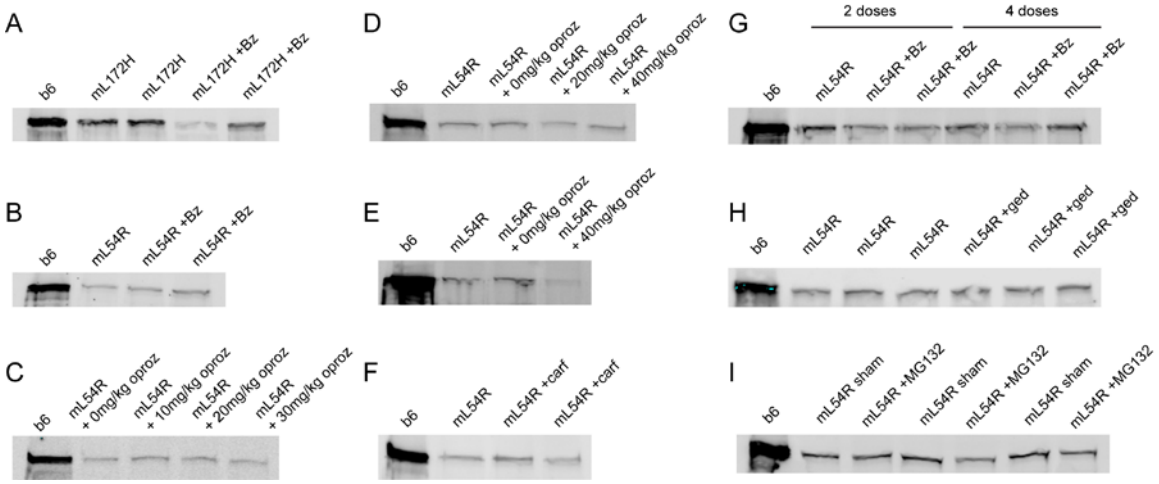

Figure 3.8: Dystrophin western blot analysis of drug-treated mice. Dystrophin western blot analysis of quad muscle lysates from mice treated with sham (solvent only) or various proteasome inhibitors (bortezomib – Bz, oprozomib – oproz, carfilzomib – carf, and MG132) or a heat shock activator (gedunin – ged) compared to an untreated b6 wild type mouse. Dosages, solvents, and delivery methods are outlined in Table 3.3.

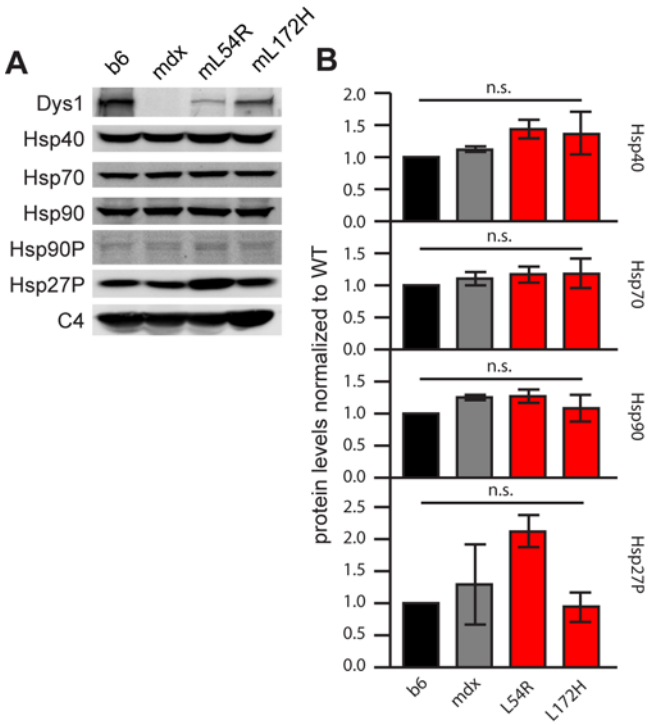

Figure 3.9: Effect of missense mutations on the heat shock pathway of the mice. **(A)** Representative western blots of heat shock proteins in each of the mouse lines from tibialis anterior muscle. Hsp90P was barely detectable. **(B)** Quantification of n=3 sets of mice. ANOVA analysis for each protein was not significant.

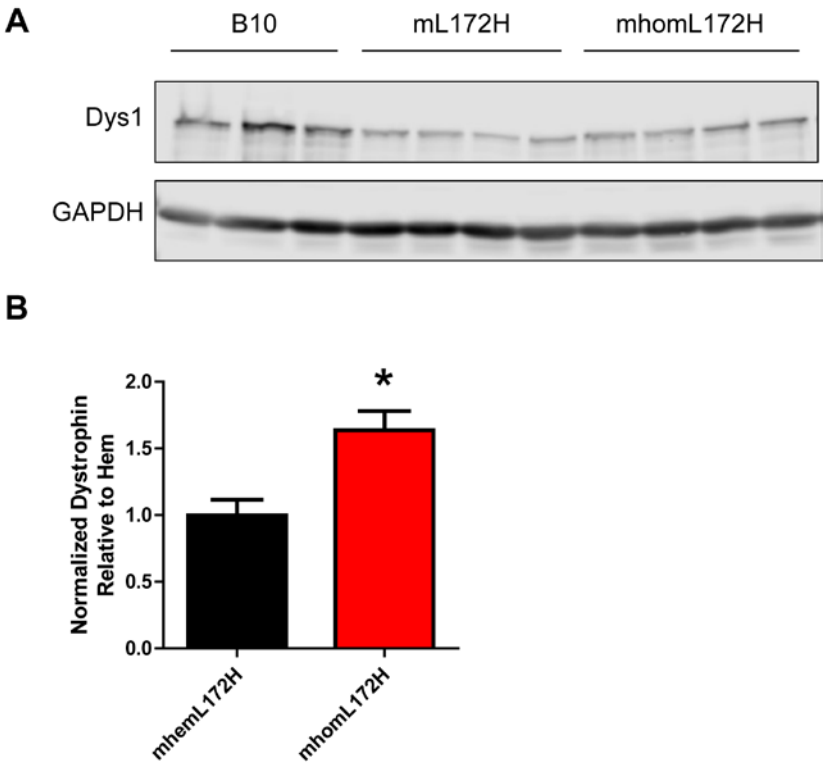

Figure 3.10: Protein expression levels in transgenic homozygous L172H mice. (A) western blot of wild-type (B10, n=3), hemizygous littermates (mL172H, n=4), and homozygous mice (mhomL172H, n=4) with GAPDH loading control **(B)** Quantification of western blots. Unpaired t-test, * $p<0.05$.

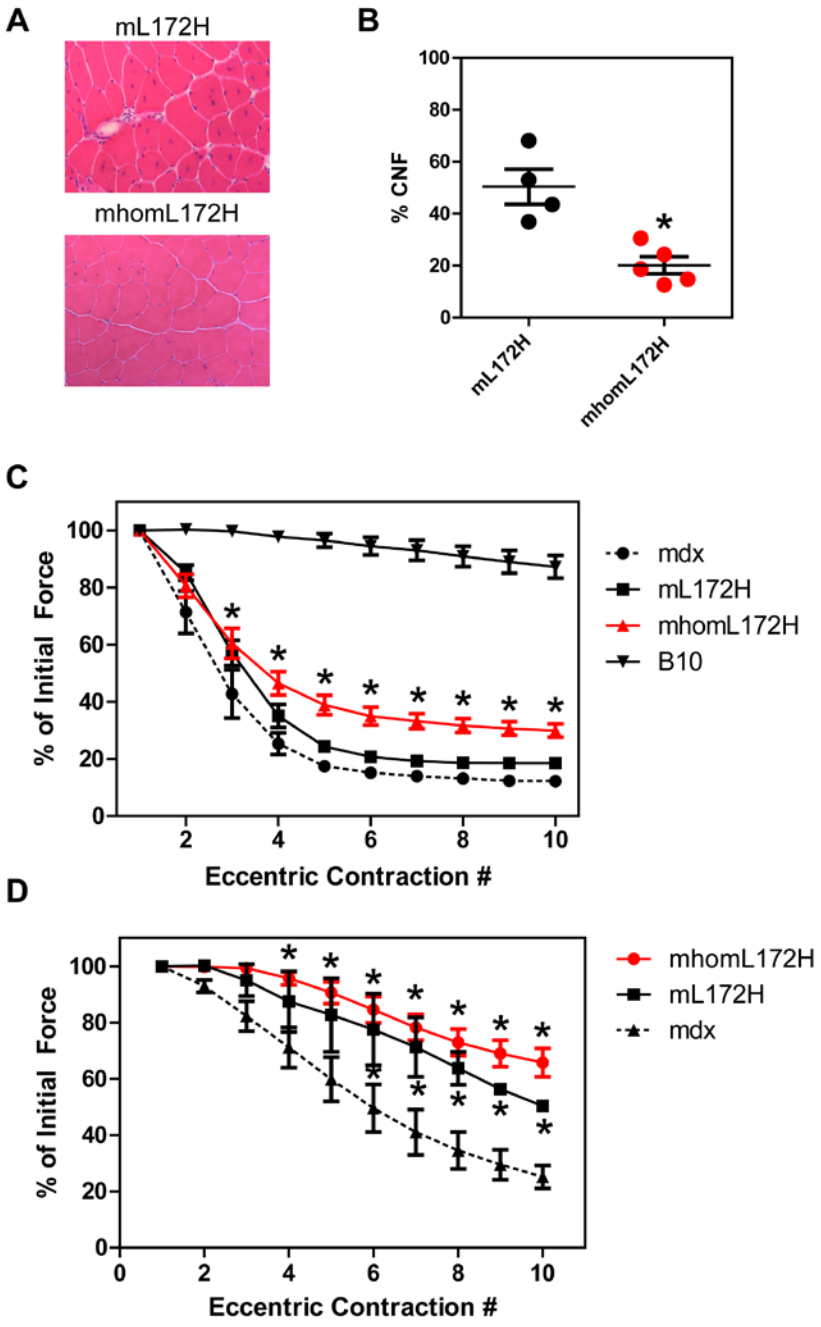

Figure 3.11: Histological and physiological analysis of transgenic homozygous L172H mice. (A) Representative quadriceps muscle sections from homozygous mice (mhomL172H) and hemizygous mice (mL172H) stained with H&E and imaged at 20x magnification. Scale bar = 20µm. (**B)** Quantification of centrally nucleated fibers (CNF) as a percentage of the total fibers. A minimum of 250 fibers were counted for each

mouse (n=3). Unpaired t-test, ✱p<0.05. **(C-D)** *Ex vivo* EDL force measurement during eccentric contraction at 10% lengthening (**C**) or 5% lengthening (**D**). B10 n=3, *mdx* n=3, mhemL172H n=6 (10%) or n=3 (5%), mhomL172H n=10 (10%) or n=4 (5%); ANOVA, post hoc analysis gave ✱p<0.05 compared to *mdx*.

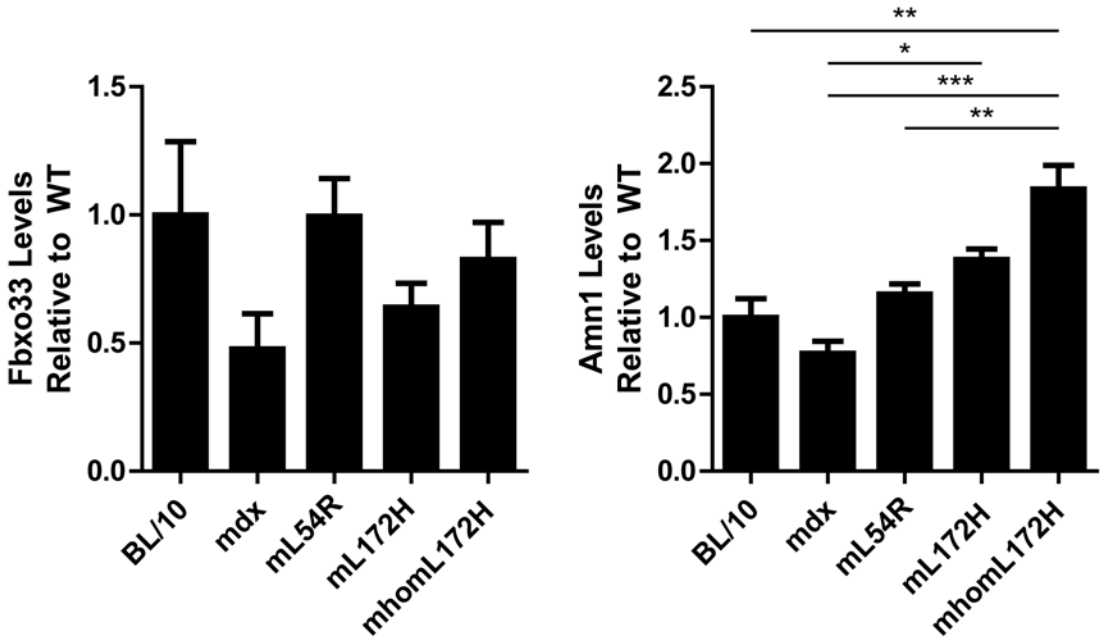

Figure 3.12: FBXO33 and Amn1 protein expression levels in transgenic mouse models. (A) Western blot of wild-type (B10, n=3), mL54R (n=3), hemizygous littermates (mL172H, n=3) and homozygous L172H (mhomL172H, n=3). **(B)** Quantification of western blots. One-way ANOVA, * $p<0.05$, ** $p<0.01$, *** $p<0.001$

Gene	Gene Accession	%GFP L54R	Sig. KD by RT-qPCR	%GFP L172H
Ube2i	NM_011665	2.93	ns	0.153
DCN1	NM_178896	3.35	ns	0.06
Ube2e3	NM_009454	2.84	*	0.073
ASB5	NM_029569	6.83	ns	0.162
VPS41	NM_172120	4.95	*	0.116
Amn1	NM_001113424	8.98	*	0.135
FBXO33	NM_001033156	9.88	*	0.146
FBXO16	NM_015795	5.11	ns	0.246
Zfand5	NM_009551	7.61	*	0.407
SCEL	NM_022886	5.90	ns	0.193
NSD1	NM_008739	5.69	ns	0.208
PHF5A	NM_026737	5.13	*	0.026
MYLIP	NM_153789	5.14	*	0.029
Pcgf3	NM_172716	5.06	*	0.052
Rnf182	NM_183204	5.01	*	0.163
TRAF2	NM_009422	4.23	ns	0.162

Table 3.1: Summary of positive hits from siRNA screen. Table of the 16 positive hits (above 2.5% GFP threshold in L54R cell line) with gene accession numbers, significant (*) or not significant (ns) knockdown by RT-qPCR, and %GFP in L172H cell line. Hits in red are those with both significant knockdown by RT-qPCR and above a 0.06% threshold in L172H cell line.

	b6	mdx	mL54R	mL172H	mhomL172H
EDL mass (mg)	12.8 ± 0.4	16.3 ± 1.5	14.2 ± 0.8	13.5 ± 0.7	12.4 ± 1.8
L_0 (mm)	13.3 ± 0.2	12.3 ± 0.1	12.4 ± 0.1	12.9 ± 0.1	13.0 ± 1.1
CSA (cm^2)	0.021 ±0.001	0.029 ± 0.003	0.025 ± 0.001	0.022 ± 0.001	0.021 ± 0.002
passive stiffness (N/m)	13.9 ± 0.9	16.8 ± 1.0	14.2 ± 0.6	15.8 ± 0.7	13.9 ± 3.2
active stiffness (N/m)	755.7 ± 36.2	720.7 ± 31.8	695.4 ± 38.2	785.5 ± 20.6	-
P_0 (mN)	448.5 ± 8.8	416.8 ± 31.5	414.7 ± 29.5	393.2 ± 34.7	403.8 ± 43.1
specific P_0 (N/cm^2)	21.8 ± 0.5	14.8 ± 0.8 #	16.9 ± 0.5 #	17.4 ± 0.9 #	19.6 ± 1.3 # † ǂ
ΔP_0 (%)	11.1 ± 3.1	82.8 ± 5.4 #	75.8 ± 5.8 #	73.6 ± 4.4 #	79.1 ± 2.4 # †
force drop (%)	2.1	75.1 ± 4.3 #	69.5 ± 5.5 #	65.7 ± 2.1 #	61.1 ± 10.7 # †

Table 3.2: Summary of *ex vivo* EDL parameters. For measurements of specific force, change in specific force, and force drop during eccentric contractions ANOVA was significant at $F<0.01$. Post hoc analysis gave # $p<0.05$ compared to wild type, † $p<0.05$ compared to *mdx*, ǂ $p<0.05$ compared to mL172H.

Panel	Drug	Dosing Schedule	Solvent	Route
A	Bortezomib	1mg/kg, every 3.5 days for 2 weeks	PBS slurry	Tail vein injection
B	Bortezomib	0.6mg/kg, every 3.5 days for 2 weeks	PBS slurry	Tail vein injection
C	Oprozomib	10, 20, or 30mg/kg, everyday for 3 days	1% DMSO, 1% Tween80, 30% PEG1500	Oral gavage
D	Oprozomib	20 or 40mg/kg, everyday for 3 days	5% DMSO, 5% Tween80	Oral gavage
E	Oprozomib	40mg/kg, everyday for 10 days	1% carbyoxymethyl-cellulose, 5% DMSO, 5% Tween80	Oral gavage
F	Carfilzomib	5mg/kg, everyday for 3 days	15% captisol, 10mM citrate	Intraperitoneal injection
G	Bortezomib	1mg/kg, every 3.5 days for 2 or 4 weeks	10% DMSO, 0.9% NaCl	Intraperitoneal injection
H	Gedunin	5mg/kg, everyday for 3 days	5% DMSO, 10% captisol, 10mM citrate	Intraperitoneal or intramuscular injection
I	MG132	Everyday for 10 days	PBS slurry	Intramuscular injection

Table 3.3: Protocols for drug treatment of mice from Figure 3.8. Specific dosages, solvents, and delivery routes for each panel of Figure 3.8.

Chapter 4

Distinct mechanical properties in homologous spectrin-like repeats of utrophin*

*Co-first author manuscript with Sayan Ghosal, to be submitted to *Nature Letters* in May 2017

Jackie McCourt performed the cloning, protein expression, purification, circular dichroism analysis of all utrophin proteins, and drafted the manuscript. Sayan Ghosal set up the atomic force miscrosope, performed all pulling experiments on utrophin proteins and the titin reference protein, performed the analysis on collected data for full-length utrophin, Utr NT-R10, Utr R11-CT, and Utr R1-10, and helped in drafting the manuscript. Sivaraman Rajaganapathy performed pulling experiments and analysis of Utr R11-22 and R1-22 and generated final figures for the manuscript.

Synopsis

Patients with Duchenne muscular dystrophy (DMD) lack the protein dystrophin (Koenig et al., 1989), which is a critical molecular component of the dystrophin-glycoprotein complex (DGC). Dystrophin is hypothesized to function as a molecular shock absorber or spring that mechanically stabilizes the sarcolemma of striated muscle through interaction with the cortical actin cytoskeleton via its N-terminal half with the transmembrane protein α-dystroglycan via its C-terminus (Rybakova and Ervasti, 1997; Ervasti, 2007). Utrophin is a fetal homologue of dystrophin that can subserve many dystrophin functions (Matsumura et al., 1992; Rybakova et al., 2002b) and is therefore under active investigation as a dystrophin replacement therapy for DMD (Guiraud et al., 2015). Here, we report the first mechanical characterization of utrophin using atomic force microscopy (AFM). Our data indicate that the mechanical properties of spectrin-like repeats of utrophin are more in line with the Ig-like repeats of titin rather than those reported for repeats in spectrin or dystrophin. Despite exhibiting identical thermal denaturation profiles (Henderson et al., 2011), we also measured markedly different mechanical characteristics for the spectrin repeats within the N-terminal actin-binding half of utrophin compared to those in the C-terminal dystroglycan-binding half. Spectrin repeats in the N-terminal half displayed a “brittle” behavior where the unfolding forces of individual repeats were remarkably uniform upon extension. In contrast, spectrin repeats in the C-terminal half exhibited characteristics of a stiffening spring with unfolding forces increasing dramatically with extension. AFM measurements of full-length utrophin demonstrate mechanical properties most consistent with the C-terminal half showing increasing resistive force upon extension but with much larger forces. Our results demonstrate dramatic differences in the mechanical properties of two structurally homologous utrophin constructs both dominated by repetitive spectrin-like motifs and

suggest that utrophin may function as a stiff elastic element in series with titin at the myotendinous junction.

Introduction

Duchenne muscular dystrophy (DMD) is a fatal muscle disease afflicting one in every 4000 boys (Mendell et al., 2012) and is caused by mutations in the DMD gene encoding the 427 kDa cytoplasmic protein dystrophin (Hoffman et al., 1987). Dystrophin is predominantly expressed in striated muscle and through interaction with the dystrophin-glycoprotein complex (DGC) at the muscle cell membrane, or sarcolemma (Ervasti, 2003). Disease-causing mutations in the DMD gene lead to an absence or loss of function of dystrophin, resulting in loss of sarcolemmal integrity and muscle fiber death (Rybakova et al., 2000).

Dystrophin is composed of three major functional domains: the N-terminal calponin homology actin binding domain (ABD1), a large central rod domain containing triple helical spectrin-like repeats, and the cysteine-rich C-terminal (CRCT) domain that binds the transmembrane dystroglycan complex and other proteins. It has long been hypothesized that dystrophin acts as a molecular spring or shock absorber to mechanically stabilize the sarcolemma during muscle contraction (Ervasti, 2007). Because the homologous protein utrophin can compensate for dystrophin deficiency in the *mdx* mouse model (Tinsley et al., 1998), pharmacologic upregulation of utrophin is under investigation as a therapeutic approach for DMD (Guiraud et al., 2015). While many of the biochemical and biophysical properties of dystrophin and utrophin have been characterized, only two studies have mechanically characterized dystrophin (Bhasin et al., 2005; Krieger et al., 2010) and no studies have investigated the mechanical properties of utrophin. Here, we report atomic force microscopy analysis of single protein molecules representing the N-terminal actin-binding half (Utr NT-R10), the C-terminal dystroglycan-binding half (Utr R11-CT), and full-length utrophin (Figure 4.1A).

Methods

Cloning

Full-length mouse utrophin was previously cloned from an existing vector into a pENTR/D-TOPO vector (Invitrogen™) with an 8-amino acid FLAG-tag (DYKDDDDK) added to the N-terminus of utrophin for use in purification(Guo et al., 1996; Rybakova et al., 2002a). All utrophin truncation constructs were PCR amplified using primers designed around adjacent repeats for the desired deletion based on reported repeat and domain boundaries(Winder et al., 1995). The PCR products were circularized using T4 polynucleotide kinase and T4 DNA ligase (New England BioLabs) and sequence verified. Using the Gateway Recombination system (Life Technologies), the deletion constructs were recombined into the pDEST8 destination vector and subsequently transformed into DH10Bac competent *E. coli* and purified according to the manufacturer's protocol.

Protein expression and purification

Sf9 insect cells were maintained at 1 x 10^6 cells/mL in Sf-900™ II SFM (Life Technologies). Purified Baculovirus was transfected using Cellfectin® II (Life Technologies) and high-titer viral stocks were generated through successive infections of Sf9 cells in 3.5 cm plates (P0), 10 cm plates (P1), and 250 mL of 1 x 10^6 cells/mL suspended cells (P2). Ten mL of P2 virus were used to infect 250 mL of 1 x 10^6 cells/mL and cultured for 72-hour post-infection to maximize protein expression. Infected cells were centrifuged at 1,000 x *g* for 3 minutes and re-suspended in lysis buffer containing phosphate buffered saline (PBS), 1% Triton, and a cocktail of protease inhibitors [100nM Aprotinin, 10mg/mL E-64, 10μM Leupeptin, 1mM PMSF, 1μg/mL Pepstatin]. The lysate was centrifuged at 14,000 x *g* for 10 min at 4ºC and the supernatant applied to an anti-FLAG M2 agarose column (Sigma Aldrich). The column was washed with >10 column

volumes of PBS and bound protein eluted with PBS containing protease inhibitors and 100μg/mL FLAG peptide. After dialysis overnight in 2L of PBS at pH 7.5, the purified protein was concentrated using the Amicon Centrifugal Filter unit (UFC801024) and protein concentration was determined using A_{280} and extinction coefficients calculated from the amino acid compositions for each construct. Concentrated proteins were run on a 3-12% SDS polyacrylamide gradient gel and run at 150V for 1 hour. Gels were stained with Coomassie blue stain and visualized using Licor's Odyssey® Infrared Imaging System.

Circular Dichroism

Each purified protein was centrifuged at 14,000 x *g* for 10 minutes at 4ºC and the supernatant diluted to 0.4 mg/mL using PBS. Absorption spectra were acquired with a Jasco J-815 spectropolarimeter, initially at 20°C as controlled by a Peltier device, from 200 to 260nm wavelength. Spectra were then acquired at 1°C temperature intervals from 20-90°C and the characteristic ellipticity at alpha-helical wavelength (θ_{222}) recorded. Molar ellipticity, [θ], was calculated using the following equation: $[\theta] = \theta / (10 \times c \times l)$ where c is the molar concentration of the sample (mole/L) and *l* is the path-length in cm. Molar ellipticity (with units of degrees, cm squared per decimole) was plotted against wavelength for the circular dichroism (CD) spectra. Ellipticity at 222nm (θ_{222}) was normalized, plotted against temperature, and fit by regression analysis in Sigma Plot (Systat Software, Inc.) using equations for two state unfolding (Legardinier et al., 2009).

Atomic Force Microscopy

The single molecule force spectroscopy experiments were performed utilizing a MFP-3D atomic force microscope (AFM) from Oxford Instruments. The AFM setup contains a flexible cantilever with a sharp tip, a laser-photodiode based sensor which measures the

position of the cantilever tip, and a piezo electric nano-positioner which can move a substrate in three spatial directions with respect to the cantilever base (Binnig et al., 1986). We used a soft BioLever (BL-RC-150VB) from Asylum Research with a typical spring constant of 6 pN/nm and a 25±12 nm tip radius coated with Cr/Au. A droplet (~100 µl) of the protein solution is employed on freshly cleaved mica substrate and allowed to settle for 10 minutes before commencing the experiment to ensure that some proteins get adsorbed on the mica surface. The cantilever tip is brought towards the mica surface, pressed against the surface for 3 seconds with a force ranging from 1000-2000 pN and then retracted with a specified retraction velocity. The approach-retraction cycle is repeated. During such a cycle, if a part of a protein molecule gets attached to the cantilever tip with another part adsorbed on the substrate, the interior is stretched during the retraction phase of the cantilever. The pulling force on the molecule is balanced by the force on the cantilever which can be measured by observing the deflection of the cantilever tip when the cantilever spring constant is known. The exact spring constant is measured before the pulling experiments by analyzing the thermal response of cantilever deflection. Forced extension causes the folded domains in the molecule to unfold, which can be detected by a characteristic saw-tooth pattern observed in the cantilever deflection (Rief et al., 1999) vs separation curve. Data from 300-500 successful force spectroscopy experiments are collected for each protein construct which reveal the statistical behavior of the unfolding forces of these molecules.

Data Analysis

Data from each of the successful protein pulling experiments are collected and analyzed using the Igor Pro software from Oxford Instruments. Collected data include the separation of the cantilever base from the substrate surface from which the extension of the molecule is calculated. The data also include the measured deflection of the

cantilever tip as a function of separation. Since the cantilever deflection is proportional to the force applied on it, the measured deflection can be converted to the force acting on the cantilever by multiplying by the spring constant of the cantilever. The extension of protein molecules in between successive unfolding events is fit with the worm like chain (WLC) models in Igor Pro software. The WLC model (Rief et al., 1999), which relates the force (*F*) exerted on the molecule to its extension (x) is shown in Equation 1.

$$F(x) = \frac{k_B T}{P}\left(\frac{1}{4\left(1-\frac{x}{L}\right)^2} - \frac{1}{4} + \frac{x}{L}\right) \quad (1)$$

The parameters of the model are the persistence length (*P*) and the contour length (*L*), whose statistics have been obtained for each utrophin construct. *T* is the temperature and k_B the Boltzmann constant. As a validation of our experimental setup and data analysis procedure, we also extracted the statistics of the persistent length and contour length for the reference protein titin I27O which matched well with the data reported in existing literature (Carrion-Vazquez et al., 1999).

Results

Previous atomic force microscopy studies have defined the mechanical properties of titin as a “stiff’ spring (Rief et al., 1997; Carrion-Vazquez et al., 1999) and spectrin as a “soft” spring (Rief et al., 1999; Law et al., 2003b; a). In such experiments, the mechanical extensibility of single protein molecules is measured and the unfolding forces of individual domains upon extension are collected over a large number of experiments to obtain statistical properties of unfolding behaviors. We first obtained AFM data for a recombinant titin reference protein (Figure 4.2) and spectrin (Figure 4.3) that agree well with previously published values (Carrion-Vazquez et al., 1999; Rief et al., 1999). AFM data for Utr NT-R10, Utr R11-CT and utrophin all showed characteristic saw-tooth patterns of individual domain unfolding (Figure 4.1B-D). From the force versus extension curves, we initially observed that the range of unfolding forces for utrophin proteins was significantly larger than the unfolding forces reported for spectrin and even in fragments of dystrophin (100 – 2000 pN in Figure 4.1B-D versus <50 pN; Bhasin et al., 2005; Krieger et al., 2010). More interestingly, Utr NT-R10 showed uniform unfolding forces upon extension whereas Utr R11-CT and full-length utrophin showed increasing unfolding forces with extension.

To determine if these initial observations were consistent statistically, we collected data for 300 – 500 successful pulling experiments for each protein construct and analyzed the force distribution and contour length, and persistence length (Figure 4.4 and 4.5). The overall unfolding force distributions between the utrophin constructs do not show significant differences (Figure 4.4A-C). However, analysis of the force distribution as a function of the unfolding event count within individual force traces revealed unique behaviors for Utr NT-R10 and Utr R11-CT (Figure 4.6). For Utr NT-R10, the force distributions for increasing unfolding events overlapped with each other (Figure 4.6A),

demonstrating a “brittle” behavior. The force distributions for Utr R11-CT (Figure 4.6B) and full-length utrophin (Figure 4.6C) were right-shifted and broadened as the unfolding event increased, demonstrating a stiffening spring behavior. The mechanical differences demonstrated between Utr NT-R10 and Utr R11-CT are in striking contrast to previously published circular dichroism data showing nearly identical thermal melt profiles for these same proteins (Henderson et al., 2011).

One explanation for the different mechanical properties of Utr NT-R10 and Utr R11-CT is that their 10-12 homologous spectrin-like repeats are controlled by long-range intra-protein communication from the unique ABD1 and/or CRCT terminating domains. Thus, we expressed and purified (Figure 4.7A-B) three new utrophin constructs deleted for ABD1 (Utr R1-10), CRCT (Utr R11-22) or both ABD1 and CRCT (Utr R1-22). Circular dichroism spectroscopy revealed highly similar thermal melt profiles for all three constructs (Figure 4.7C). Despite the absence of terminal ABD1 and/or CRCT domains, all three utrophin constructs maintained the brittle, or stiffening behaviors (Figure 4.7D-F) observed with the original domain-terminated constructs (Figure 4.6A-C).

Finally, we plotted the average peak forces as a function of unfolding events obtained from 300-500 successful pulling experiments (Figure 4.8 and Figure 4.9). Figure 4.9 visually demonstrates the striking differences between the N-terminal half (red and green plots) and C-terminal half (blue and cyan plots) of utrophin independent of their unique terminating domains (ABD1 and CRCT, respectively). Our results suggest the sequences of homologous spectrin-like repeats within the N-terminal and C-terminal halves of utrophin encode information that dramatically influences their respective mechanical behaviors. Additionally, Figure 4.9 reveals that full-length utrophin both with and without its terminating domains (pink and black plots) exhibits mechanical behavior directed by the C-terminal half.

Discussion

In comparison to single molecule force spectroscopy data for other spectrin-like repeat containing proteins (Bhasin et al., 2005; Krieger et al., 2010), our results for utrophin reveal much higher forces of unfolding and stiffening behavior more similar to the mechanically stiff spring titin (Zhu et al., 2009; Kellermayer et al., 2003). The consistently linear increase in the contour length with increasing unfolding events (Figure 4.10) as well as contour length peak values that are consistent with single repeats (Figure 4.5) argues against the possibility that the high unfolding forces observed for utrophin are due to simultaneous unfolding of multiple repeats. It is more likely that the differences in measured forces of unfolding of spectrin repeat-containing proteins are influenced by sequence differences. Of the spectrin family of proteins, dystrophin and utrophin exhibit lower sequence similarity in comparison to the other family members (alpha-actinin, alpha-spectrin, and beta-spectrin) (Nicolas et al., 2014). Dystrophin and utrophin also have much weaker conservation between repeat units, with a lower number of conserved residues and greater number of insertions compared to repeats within the spectrins (Winder et al., 1995). Our data are the first to demonstrate markedly different mechanical behaviors for structurally homologous spectrin-like repeats within the same molecule.

In vivo mechanical studies of plasma membrane adhesion complexes such as integrins and cadherins have revealed unfolding forces that were more within the ~25 pN range of those measured for repeats in spectrin, or dystrophin measured *in vitro* (Chang et al., 2016; Buckley et al., 2014; Bhasin et al., 2005). The surprisingly high unfolding forces of utrophin measured here, particularly in Utr R11-CT and full-length utrophin, suggest that utrophin is too stiff to also function as a spring that protects the sarcolemma from mechanical stress. Alternatively, the stiffness of utrophin is more consistent with its

localization to the myotendinous junction (MTJ) (Ohlendieck et al., 1991), the primary site of muscle force transmission to bone where perhaps utrophin may function in series with titin as a restorative elastic element (Charvet et al., 2012).

Figures

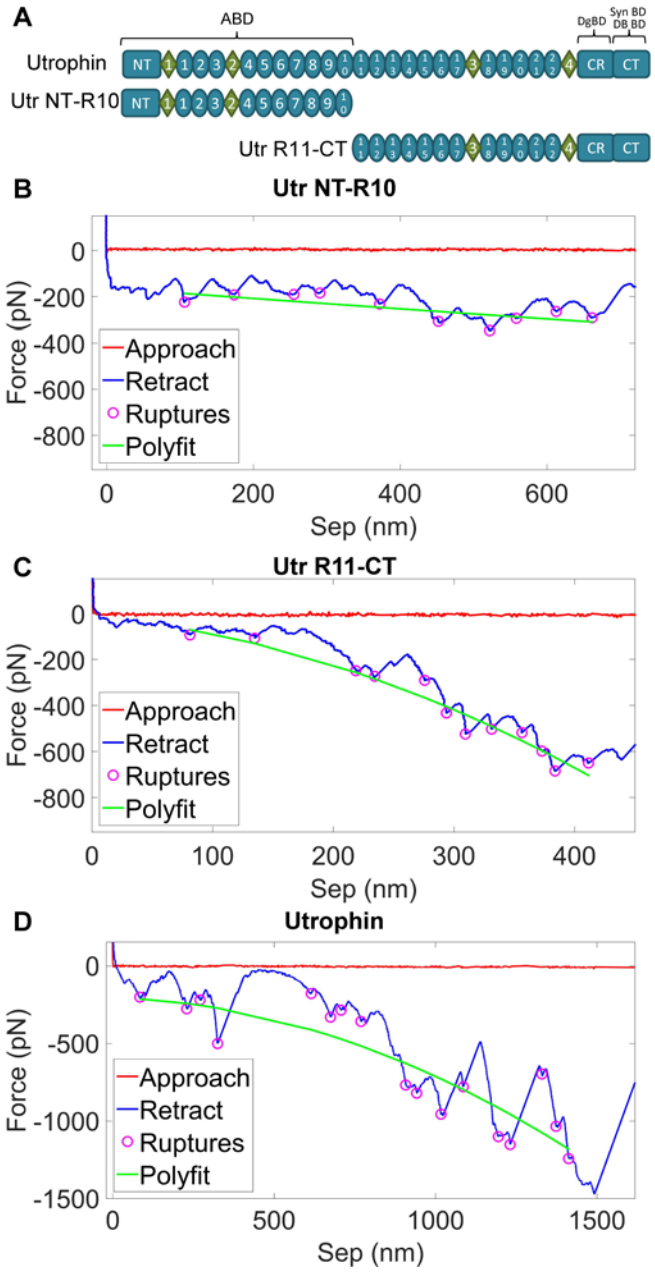

Figure 4.1: AFM extension characteristics of utrophin terminal constructs. (A) Schematic of constructs analyzed by AFM. **(B)** Force vs extension representative trace curve for the N-terminal half of utrophin, Utr NT-R10, shows uniform unfolding forces upon extension. **(C)** Force vs extension representative trace curve for the C-terminal half

of utrophin, Utr R11-CT, shows increasing unfolding forces upon extension. **(D)** Force vs extension representative trace curve for full-length utrophin, Utr FL, also shows progressive increases in unfolding forces upon extension.

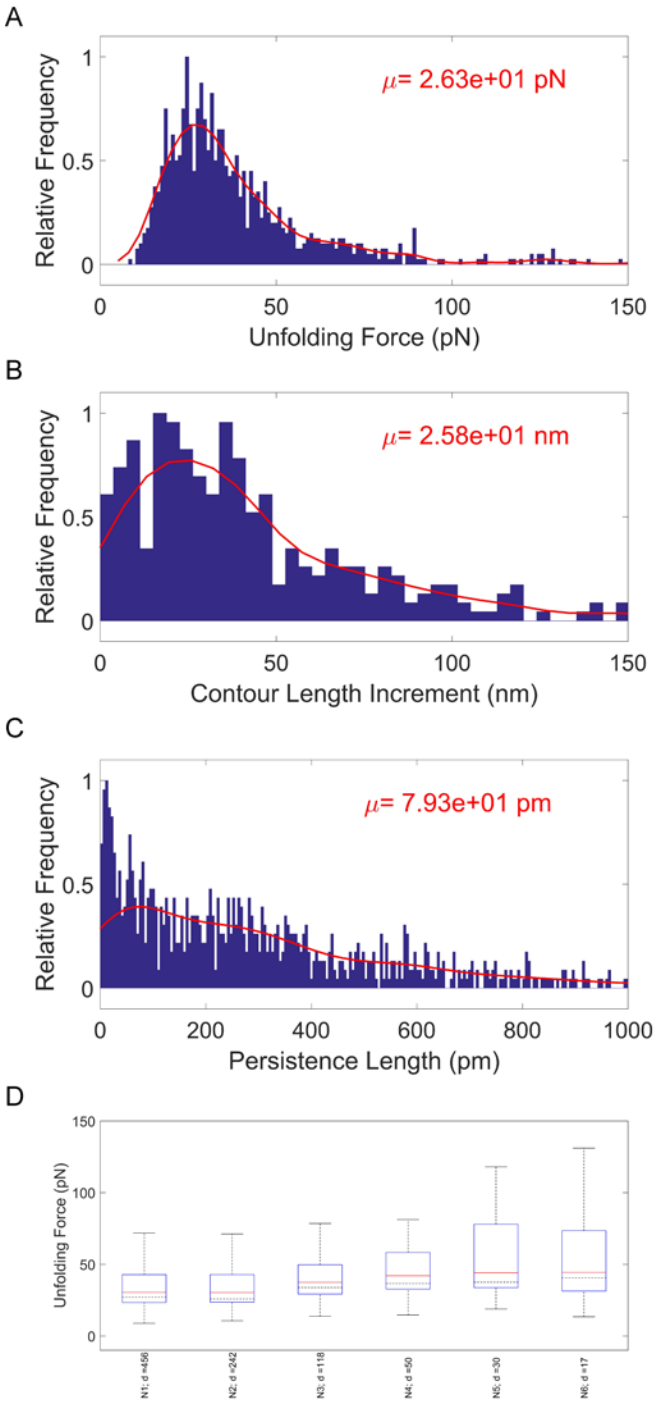

Figure 4.2: Statistics of Titin I27O™ from AthenaES® (an AFM Reference Protein with 8 repeats of the Ig 27 domain of human titin) (A) Histogram of unfolding forces with the mode at 220 pN when pulled at 1um/s with a cantilever of spring constant 6.67

pN/nm. This matches closely with the reported value of 224 pN (Carrion-Vazguez et al., 1999). (**B)** The histogram of contour length increments indicates that the most probable value is 27.5 nm, while 28.4 nm was the corresponding reported value (Carrion-Vazguez et al., 1999). **(C)** The peak persistence length was measured to be 309 pm compared to the reported value of 390±70 pm (Carrion-Vazguez et al., 1999). **(D)** Box plots of the unfolding forces classified based on the unfolding count, with the red line indicating the median value and the dotted black line indicating the mode. The edges of the box represent the 25% and 75% percentiles, with the whisker plots marking the minimum and maximum recorded values excluding the outliers. Titin behaves like a stiff but 'brittle' spring, with the unfolding forces (mode) ranging from 200 pN to 250 pN (a 25% increase) for unfolding counts of 1 to 8 respectively.

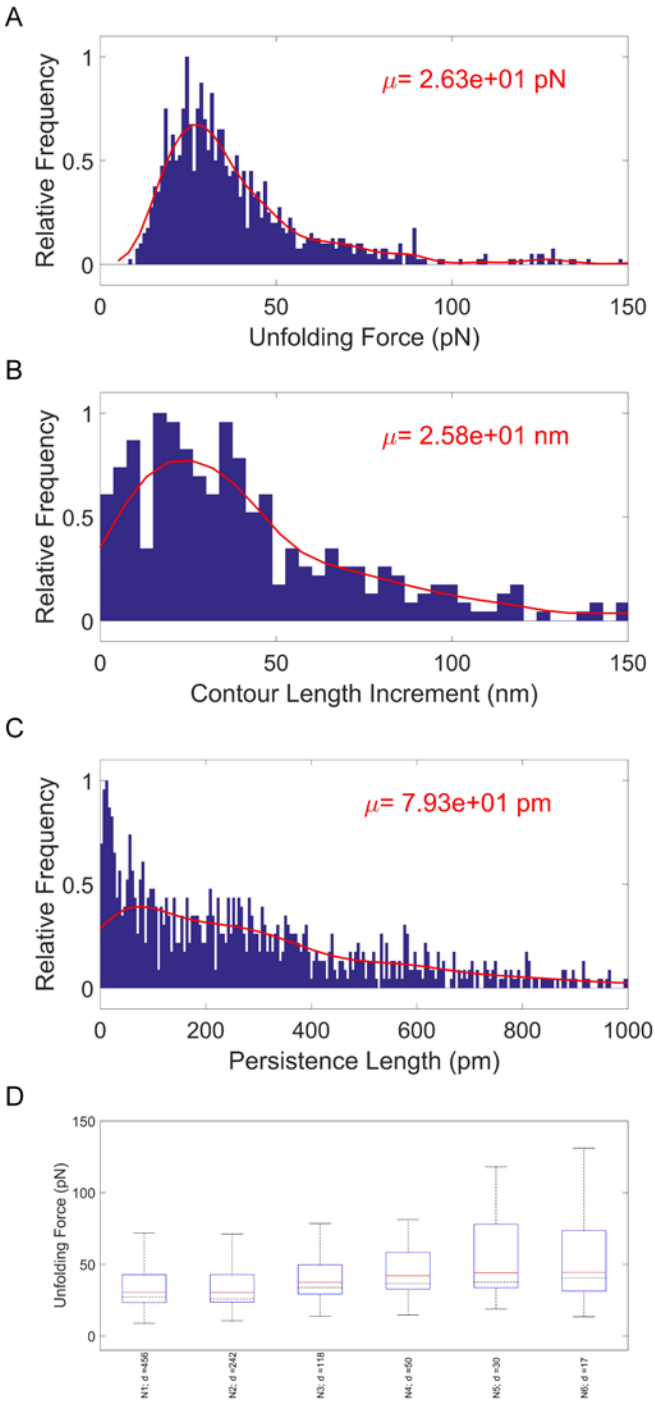

Figure 4.3: Statistics of Spectrin extracted from human erythrocytes from SIGMA-ALDRICH®. (A) Unfolding force histogram shows that a mode of 26.3 pN for spectrin, when pulled at 0.25 um/s with a cantilever of spring constant 6.88 pN/nm. A value of 28

pN was reported in literature under similar conditions (Rief et al., 1999). **(B)** The most probable contour length increment was found to be 25.8 nm, consistent with a value of 31.7 nm from the earlier report (Rief et al., 1999). **(C)** The persistence length mode was measured at 79.3 pm. **(D)** The unfolding forces vary from 26 pN for the first unfolding event to 40 pN for the sixth (a 54% increase), indicating that the molecule exhibits a mildly stiffening spring behavior.

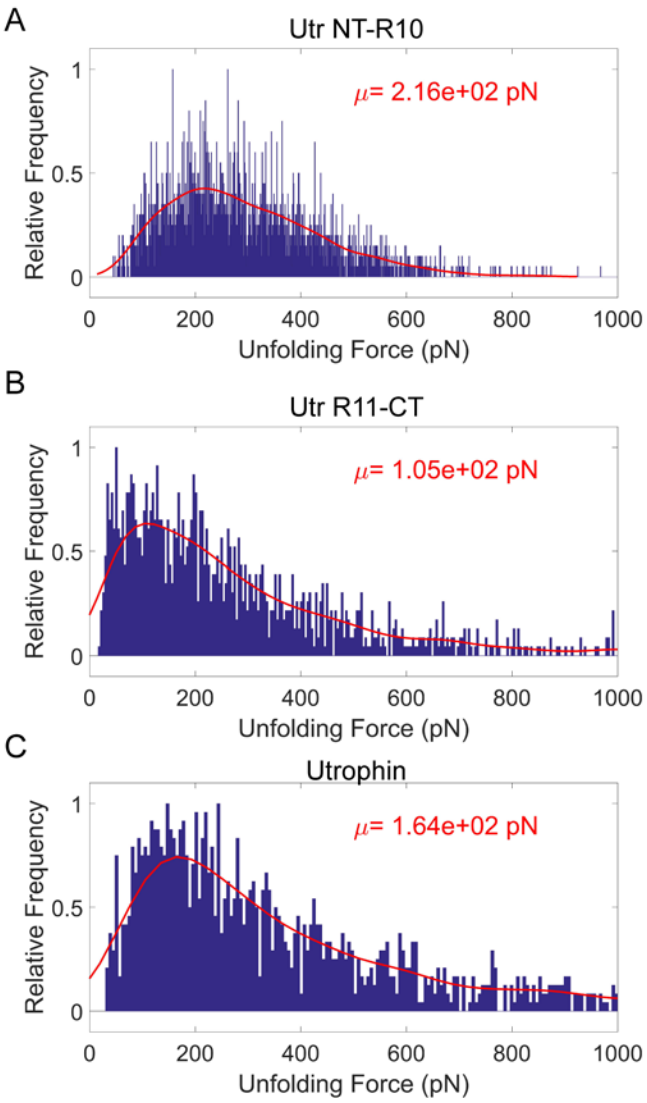

Figure 4.4: Unfolding Force histograms for Utr NT-R10, Utr R11-CT, and full-length utrophin. The unfolding forces are reported for a pulling speed of 1 um/s with cantilever spring constants between 5.04-9.06 pN/nm.

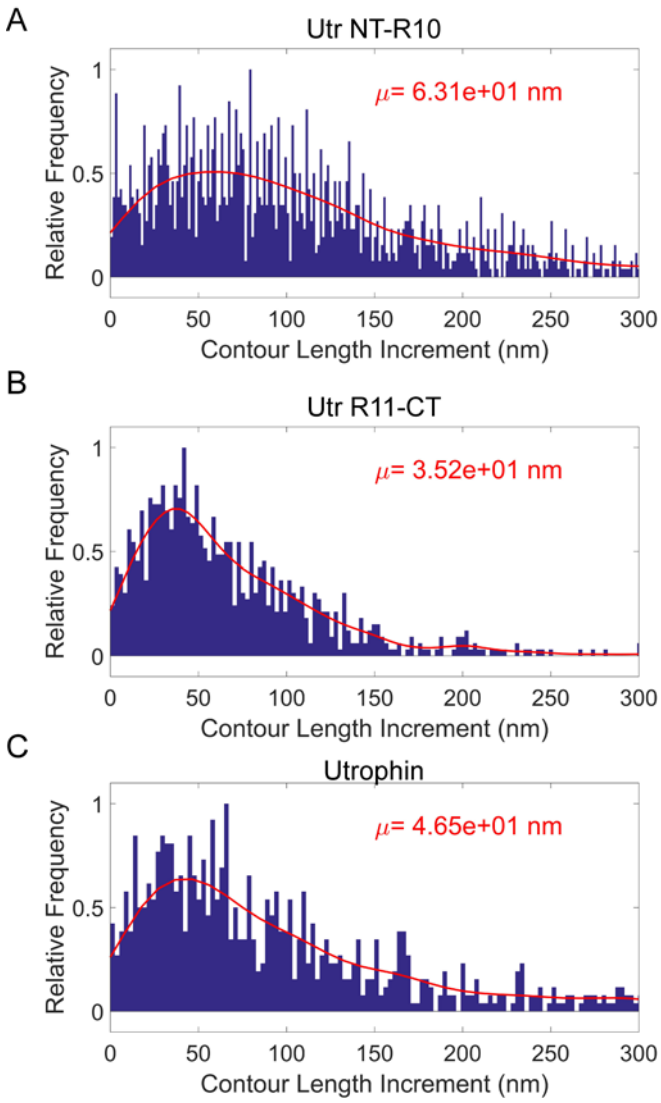

Figure 4.5: Contour Length Increment histograms for Utr NT-R10, Utr R11-CT, and full-length utrophin. The most probable contour length increments range between 35.2 to 63.1 nm.

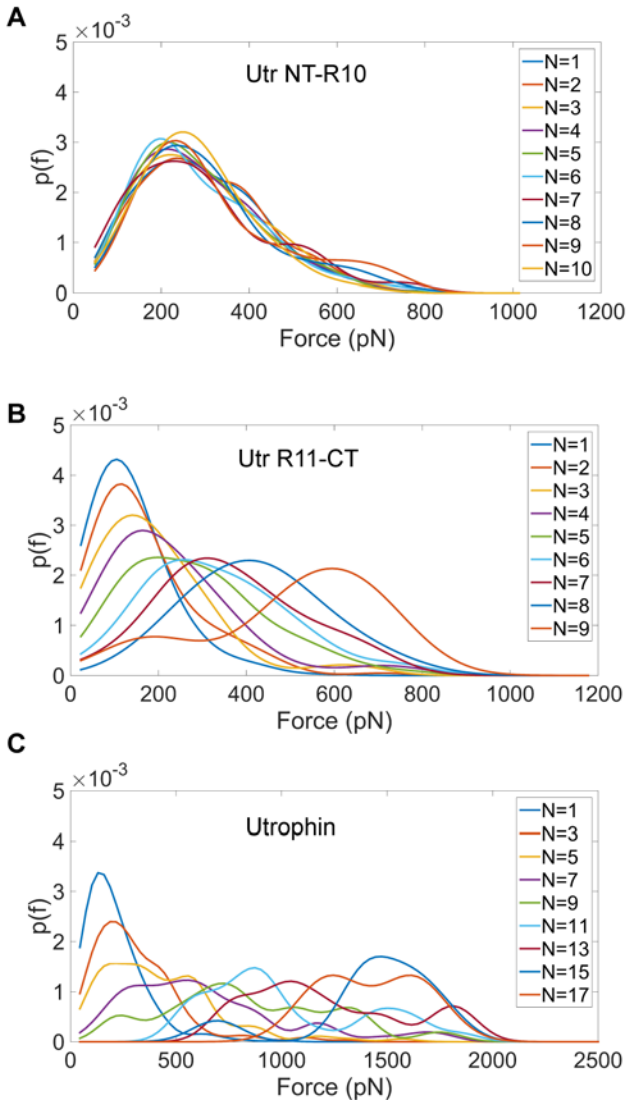

Figure 4.6: Unfolding force distributions for utrophin terminal constructs reveal markedly different mechanical behaviors. (A) The plot of the probability distribution of unfolding force (**p(f)**) vs the unfolding force for Utr NT-R10 is shown. Here, 'N' in the legend represents the unfolding event count. For example, the distribution corresponding to N = 4 represents the distribution of the 4th unfolding event. For Utr NT-R10, the distributions have significant overlap, indicating that the unfolding forces remain uniform across unfolding events (referred in this paper as 'brittle'). **(B)** The distributions for Utr R11-CT differ both in their peak locations and widths across the different unfolding

events. We observe that the peak of the distributions shifts right with increasing unfolding events, resulting in a stiffening spring behavior. **(C)** The full length utrophin largely shows behavior similar to Utr R11-CT, a stiffening spring, with increasing distribution widths and a shift of the peak towards the right with increasing unfolding events.

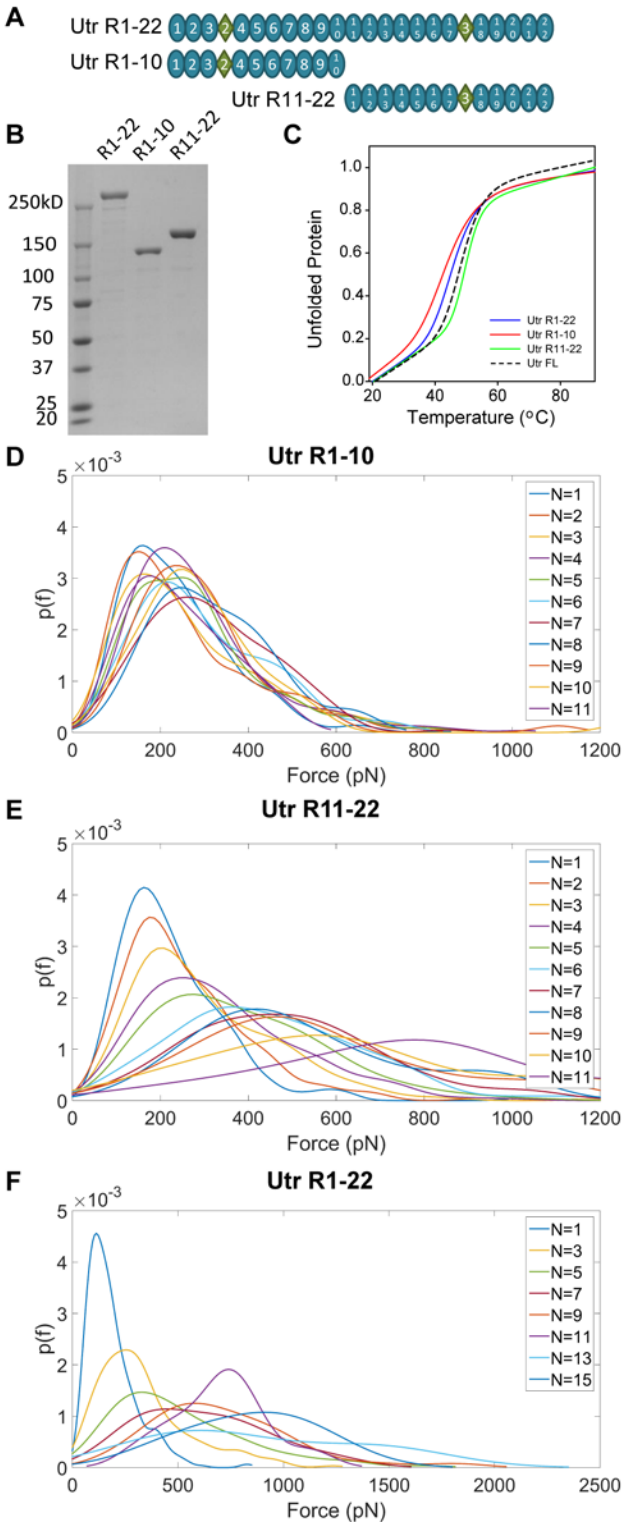

Figure 4.7: Unique mechanical behavior of utrophin halves is maintained upon deletion of the terminal domains. (A) Schematic of constructs lacking terminal

domains. **(B)** Coomassie-stained gel of 5ug aliquots of purified utrophin proteins. **(C)** Circular dichroism melt curves of terminally-deleted utrophin constructs exhibit similar thermal melting compared to full-length utrophin. **(D)** Probability distributions vs unfolding forces for the actin binding half of utrophin without the N-terminus (Utr R1-10) maintains a brittle behavior compared to Utr NT-R10 (Figure 4.6A). The distributions for the different unfolding events overlap, with closely located peaks. **(E)** The dystroglycan-binding half with the C-terminus removed (Utr R11-22) does not produce a substantial difference in its stiffening spring characteristic compared to Utr R11-CT (Figure 4.6B). **(F)** Similar to its halves, utrophin without the N and C termini (Utr R1-22) does not exhibit a change in behavior compared to full length utrophin (Figure 4.6C), and maintains a stiffening spring behavior.

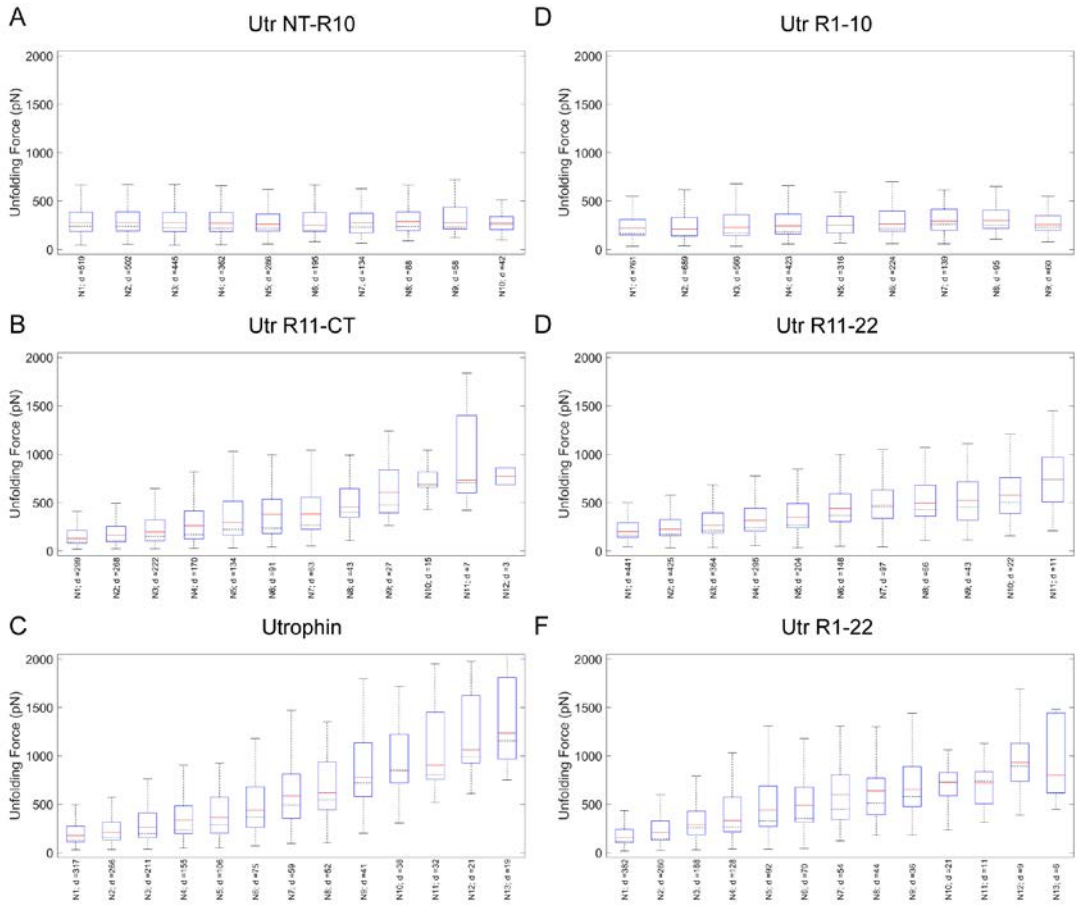

Figure 4.8: Box plots of unfolding forces as a function of unfolding count. Unfolding events are represented as 'Ni', i = {1,2,3…} and 'd' denotes the number of pulling experiments that resulted in 'Ni' events. Utr NT-R10 and Utr R1-R10 can be seen to exhibit 'brittle' behavior, wherein the unfolding force for the 10th unfolding event is comparable to that of the 1st unfolding event. The dystroglycan-binding halves of utrophin (Utr R11-CT and UTR R11-R22) show a significantly different 'stiffening' spring behavior, wherein the unfolding forces have a 3 to 5-fold increase for the 10th unfolding event compared to the 1st. The full length Utrophin variants (two halves combined together to form Utr FL and Utr R1-R22) show a strongly stiffening spring behavior with 4 to 6-fold increases for the 10th unfolding events compared to their 1st.

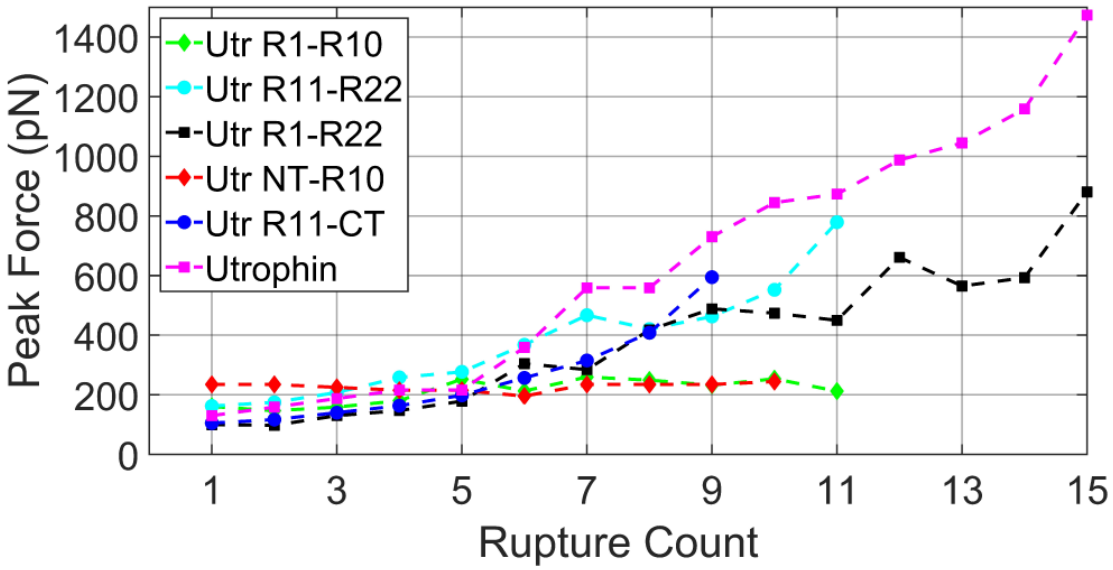

Figure 4.9: Comparison of peak unfolding force vs unfolding event count shows brittle vs stiffening behavior of utrophin constructs. Peak unfolding force expressed as a function of the number of domains unfolded (Rupture Count). Data is averaged over 300-500 successful pulling experiments for each protein construct. Utr NT-R10 and R1-10 show brittle behavior whereas Utr FL, Utr R1-22, Utr R11-CT, and Utr R1-22 all show stiffening spring behavior.

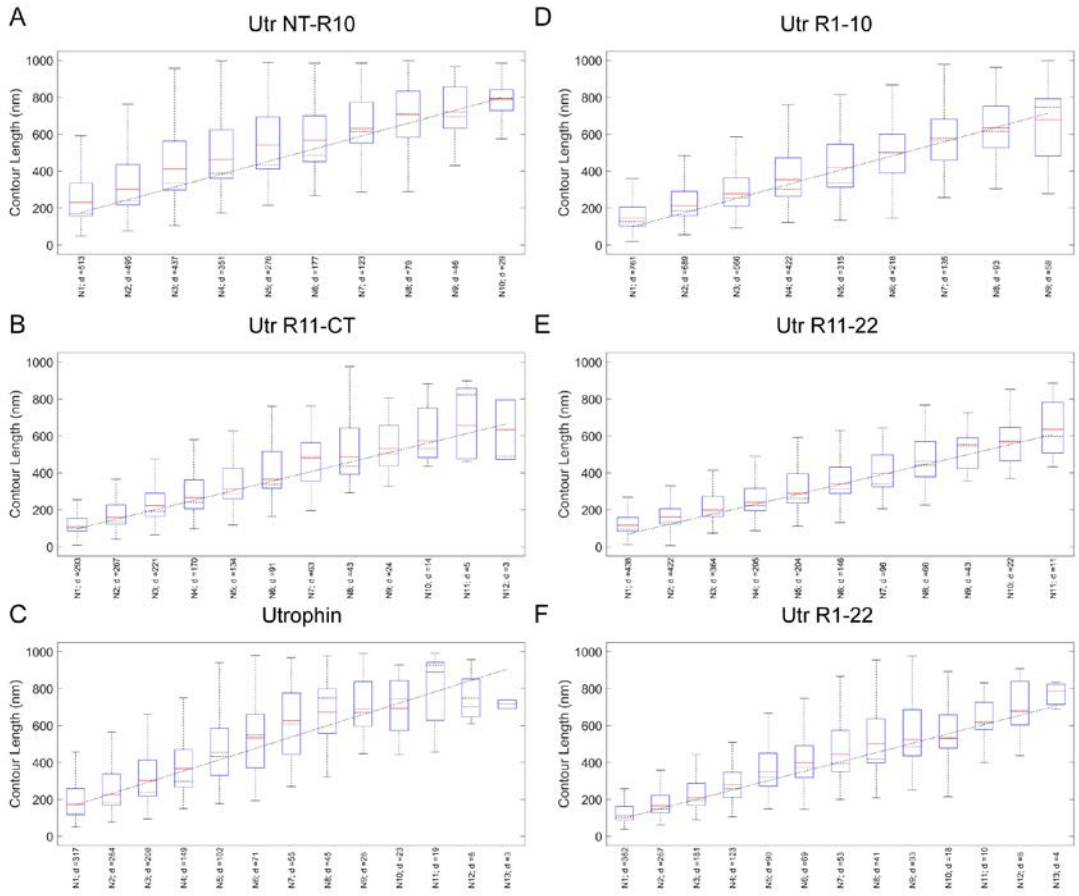

Figure 4.10: Box plots of contour lengths as a function of unfolding count. These figures show contour length increasing linearly with unfolding events, where unfolding events are represented as ‘Ni’, i = {1,2,3…} and ‘d’ denotes the number of pulling experiments that resulted in ‘Ni’ events. A nearly linear increase in the contour length is expected as the unfolding events occur.

Chapter 5

Conclusions and Discussion

Thesis Findings

In addressing the questions proposed at the beginning of my thesis, my major findings are as follows:

How do deletions present in therapeutically relevant, internally truncated dystrophins affect in vitro protein stability?

Dystrophin stability is context-dependent: relatively unaffected by small deletions at natural exon boundaries but sensitive to larger and more complex rearrangements from deletions present in gene therapy constructs.

How are missense dystrophin proteins regulated in murine models of DMD and BMD missense mutants?

Missense dystrophin protein abundance inversely correlates with disease severity and positively correlates with levels of an E3 ubiquitin ligase identified in an siRNA screen for dystrophin-specific ubiquitin-conjugating enzymes, supporting our hypothesis that missense mutants are targeted to the proteasome for degradation.

What are the mechanical properties of full-length utrophin and functionally relevant utrophin fragments?

We demonstrated that there are dramatic differences in the mechanical properties of two structurally homologous utrophin constructs both dominated by repetitive spectrin-like motifs and that full-length utrophin exhibits unfolding forces and stiffening behavior more similar to titin than to spectrin.

Analysis of Dystrophin Protein Stability *In Vitro* and *In Vivo*

Despite its large size, full-length dystrophin is a highly stable protein, demonstrating cooperative unfolding as measured by circular dichroism spectroscopy (Henderson et al., 2010). However, a meta-analysis of similar *in vitro* thermodynamic measurements of dystrophin spectrin-like repeats, functional domains, and exon-skipped fragments reveals substantial heterogeneity with a broad range of stabilities compared to full-length dystrophin (see Chapter 1, Figure 1.4) (Bhasin et al., 2005; Legardinier et al., 2008, 2009; Ruszczak et al., 2009; Krieger et al., 2010; Mirza et al., 2010; Henderson et al., 2011; Sahni et al., 2012). We have shown here that internally deleted dystrophins representing therapeutic micro-dystrophins also display variability in *in vitro* stability while exon-skipped dystrophins exhibit stability profiles congruent with the full-length protein (Chapter 2, McCourt et al. 2015).

The variability we see in thermodynamic stability of AAV gene therapy micro-dystrophins appears to be dependent on the nature of the non-native junction created by the internal deletion. In comparing our data to studies on the same micro-dystrophins in *mdx* mice and the GRMD dog model, it is surprising that proteins displaying significant instability *in vitro* demonstrate significant efficacy in rescuing the dystrophic phenotype in mouse and dog models, even for the μH2 and ΔH2-R15ΔCT constructs exhibiting the greatest instability (Wang et al., 2007; Lai et al., 2009; Banks et al., 2010; Wang et al., 2012; Lai et al., 2013; Shin et al., 2013). The levels of micro-dystrophins expressed in animal models, however, were substantially higher than native dystrophin in wild-type mice, raising the possibility that putatively misfolded micro-dystrophins are evading the protein quality control pathways *in vivo*. The stability profile for the Δ3990 construct was most similar to full-length dystrophin and that showed similar efficacy in *mdx* mice was used in a clinical trial that reported minimal recombinant dystrophin expression

associated with a strong immune response to dystrophin. Clinical trials of optimized micro-dystrophins are expected in the near future. It is evident from our work together with pre-clinical animal studies and a single clinical trial that it is difficult to predict clinical efficacy from *in vitro* and *in vivo* murine models and requires additional understanding of how micro-dystrophins behave in the complex environment of a human muscle cell.

The exon-skipped dystrophins analyzed in our study represent the predicted protein products of anti-sense oligonucleotide (ASO) and morpholino drugs targeting out-of-frame deletions around exon 45 or 51 that could potentially treat 8% and 13% of DMD patients, respectively (Aartsma-Rus et al., 2009). Natural history studies on BMD patients with deletions mimicking those in DMD patients treated with exon-skipping drugs suggested that deletions spanning exon 45 were associated with lower levels of dystrophin and a more severe phenotype than those spanning exon 51 (Findlay et al., 2015; Bello et al., 2016). Interestingly, both exon-45 and exon-51 skipped dystrophins in our study displayed *in vitro* stabilities consistent with full-length dystrophin suggesting that *in vitro* stability does not predict functionality *in vivo*. Additional clinical data for exon-51 skipped dystrophins is now available following the recent approval of the morpholino drug, eteplirsen. The primary endpoint for the clinical trial was dystrophin restoration and western blot analysis of dystrophin levels in patients treated with the drug revealed increases in dystrophin protein from 0.28% to 0.93% (Aartsma-Rus and Krieg, 2017; Center for Drug Evaluation and Research, Application Number: 206488Orig1s000, 2016). Additionally, initial analysis of functional improvement as measured by the 6-minute walk test demonstrated a slower decrease in the distance walked for eteplirsen-treated patients but the significance of this result is debated. Despite the lack of robust dystrophin restoration and clinical improvement, the small increase in dystrophin levels establishes that eteplirsen is producing its intended effect. There are several factors that

might be influencing eteplirsen's efficiency including drug uptake, pharmacokinetics, targeting efficiency, as well as protein stability. Thus, continuing to determine how deletions resulting from exon-skipping affect protein stability *in vivo* is important for optimizing exon-skipping therapies.

To address the consequences of dystrophin instability *in vivo*, we have generated two novel transgenic mouse models expressing missense mutant dystrophins reported in human DMD (L54R) and BMD (L172H) patients (Chapter 3). The L54R and L172H missense mutants were previously evaluated in cultured myoblasts and shown to have missense-mutant dystrophin levels that were inversely proportional to *in vitro* stability and disease severity of the corresponding patients (Talsness et al., 2015). Analysis of the L54R and L172H mouse lines as well as a homozygous L172H mouse revealed that disease severity inversely correlates with expression levels of dystrophin protein.

Because missense dystrophin protein was increased in response to proteasome inhibition in the cell culture models, we hypothesized that the L54R and L172H proteins were also being targeted for degradation to the proteasome in the mouse lines. The ubiquitin-proteasome pathway is the major pathway for selective protein degradation as a means of quality control and protein homeostasis and is a highly specific and coordinated cascade of events involving ubiquitin-conjugating enzymes (Cohen-Kaplan et al., 2016). Ubiquitin-conjugating enzymes are categorized as ubiquitin-activating enzymes (E1), ubiquitin-conjugating enzymes (E2), or ubiquitin protein ligases (E3) and together, an E1, E2, and E3 ligase coordinate the transfer of a ubiquitin molecule to a specific target protein (Iconomou and Saunders, 2016). To determine the specific ligases involved in targeting missense dystrophins to the proteasome, we used an siRNA library of over 500 E1, E2, and E3 ligases in cultured myoblasts and identified five E3 ligases – Rnf182, VPS41, Zfand5, Amn1, and FBXO33. We detected Amn1 and FBXO33 proteins

in muscle tissues from our mouse lines and measured significant increases in both Amn1 and FBXO33 in the missense mouse lines compared to wild type and *mdx* mice. Amn1 protein levels also correlated with the amount of missense dystrophin present. Since treatment of mice with broad-spectrum proteasome inhibitors did not increase missense dystrophin levels in the mice, we plan to continue to investigate the role of the five putative dystrophin-specific E3 ligases in missense dystrophin biology in mouse models and in patients with the goal of establishing new therapeutic targets.

In future studies, we aim to determine whether knocking out or knocking down any of the E3 ligases causes an increase in dystrophin levels in mice. Of the five E3 ligases we identified, there is currently only a knockout mouse of Zfand5 available that would be used for generating a knockout model on the transgenic missense dystrophin background (Hishiya et al., 2006). We will utilize siRNAs in complex with atelocollagen for cell delivery to target Rnf182, VPS41, Amn1, and FBXO33 for knockdown in muscle (Kawakami et al., 2013) and analyze for E3 ligase levels, dystrophin protein levels, dystrophin ubiquitination, and improvement in dystrophic phenotype. A recent study on miRNA regulation of dystrophin identified dystrophin-targeting miRNAs that inversely correlated with dystrophin protein levels in *mdx* mice treated with exon skipping morpholinos, the GRMD canine model, and patient biopsies (Fiorillo et al., 2015). Therefore, we will measure dystrophin-targeting miRNAs in muscle tissues from L54R, L172H, and homozygous L172H mice. To apply our studies to human patients, we will evaluate dystrophin-specific E3 ligase expression in BMD patient samples that have reduced dystrophin expression.

The overall aim of our proposed studies is identification of a therapeutic target for missense dystrophins but any findings would have implications for other mutation types and other therapeutic strategies. Protein instability caused by in-frame deletions found in

BMD patients can manifest as decreased dystrophin expression and thus inhibiting the degradation of dystrophin by the proteasome would be clinically beneficial (Anthony et al., 2011). Furthermore, dystrophin-specific E3 ligase inhibition could be used as an adjuvant treatment to exon-skipping drugs or gene therapies to optimize dystrophin restoration.

Mechanical Properties of Muscle Proteins

In contrast to dystrophin, utrophin displays uniform thermal stability upon internal deletion or terminal truncation (Henderson et al., 2011). However, in the first ever mechanical characterization of utrophin presented in Chapter 4, we measured remarkably different mechanical stabilities for terminal halves of utrophin by atomic force microscopy (AFM). The N-terminal half that binds actin filaments displayed uniform unfolding forces upon extension, demonstrating a “brittle” behavior. The C-terminal half and full-length utrophin showed increasing unfolding forces with extension that is characteristic of stiffening spring behavior. We determined that the observed mechanical differences are not influenced by the unique amino- and carboxy-terminal domains but rather are likely influenced by sequence differences in the spectrin-like repeats themselves, a phenomenon that has not been previously reported for other spectrin repeats. Indeed, the spectrin-like repeats of dystrophin and utrophin have much weaker conservation between repeat units compared to repeats within the spectrins (Winder et al., 1995).

Another surprising finding from our study was that unfolding forces measured for utrophin are much higher than those measured for spectrin and fragments of the dystrophin central rod domain (>100 pN compared to ~25 pN) (Rief et al., 1999; Bhasin et al., 2005; Krieger et al., 2010). The high unfolding forces of utrophin are not consistent with forces measured for plasma membrane adhesion complexes such as integrins and cadherins where forces do not exceed 25 pN, likely ruling out a spring-like mechanical role for utrophin at the membrane. The mechanical properties of utrophin are more consistent with the mechanically stiff muscle protein, titin that has unfolding forces in the range of 100-300 pN (Rief et al., 1997; Kellermayer et al., 2003; Zhu et al., 2009). In adult skeletal muscle, utrophin is localized to the myotendinous junction (MTJ) where

titin functions as a restorative elastic element (Ohlendieck et al., 1991; Charvet et al., 2012).

Titin is a giant muscle protein that spans the distance from the Z-disk to the M-line of a sarcomere with functions including regulation of assembly and length of the thick filament, signaling, and development of passive force (reviewed in Granzier and Labeit 2007). The elasticity of titin can be attributed to structures in the I-band composed of repeated immunoglobulin (Ig) domains made of β-sandwich folds and a PEVK (rich in proline, glutamate, valine, arginine) domain containing coiled structures (Linke et al., 1998; Linke and Grutzner, 2008). Experiments on stretch-induced translational movement using antibodies against the I-band components demonstrated that the Ig-domains and PEVK domains contribute differently to the elasticity of titin (Linke et al., 1996). At short sarcomere lengths and low passive force, the Ig domains are lengthened whereas at moderate to long sarcomere lengths and high passive force, the PEVK domain lengthens while the remaining Ig domains resist force. By AFM, Ig domains display increasing unfolding forces upon extension (Kellermayer et al., 2003), characteristic of stiffening spring behavior and similar to what we observed for the C-terminal half and full-length utrophin proteins. AFM measurements for the PEVK domain show unfolding forces that are uniform upon extension, a property that is comparable to what we observed the N-terminal actin-binding half of utrophin. Interestingly, the PEVK domain of titin also binds actin (Yamasaki et al., 2001; Kulke et al., 2001; Linke et al., 2002; Nagy et al., 2004). Based on our initial observations on comparing mechanical properties and localization of utrophin and titin, we hypothesize that utrophin may be acting in series with titin at the myotendinous junction.

Here we report novel findings on the properties of structurally homologous spectrin-like repeats in utrophin and on the potential function of utrophin at the

myotendinous junction. In future studies, we aim to optimize our AFM protocols to more efficiently attach protein molecules to the cantilever tip. We will design protein constructs with N- and C-terminal sequence tags (SpyTag and yBBr) that provide chemistries for covalent linkages to the cantilever tip and the substrate base (Yin et al., 2006; Li et al., 2014), ensuring secure attachment at the termini for more efficient and complete extension. We will continue to design and evaluate utrophin spectrin-like repeat constructs to establish a mechanism of mechanical stability differences. Analysis of R6-15, R4-13, R8-17, and R18-22 are some of the constructs we propose in order to determine the influence of N-terminal vs C-terminal repeats on mechanical properties. Much of the work in our lab has focused on the differences between dystrophin and utrophin thus we will extend our AFM studies on functionally- and therapeutically relevant dystrophins as well as full-length dystrophin. To address our hypothesis that utrophin is acting in series with titin, we aim to evaluate utrophin-deficient mice for myotendinous junction defects, particularly passive stiffness. A mouse line deficient for both utrophin and α7 integrin has already been investigated and shown to have myotendinous junction defects (Welser et al., 2009) but any conclusions about the unique role of utrophin are confounded by an α7 integrin phenotype. Our proposed future studies will provide critical assessment of the mechanical functions of utrophin and dystrophin.

References

Aartsma-Rus, A., I. Fokkema, J. Verschuuren, I. Ginjaar, J. van Deutekom, G.-J. van Ommen, and J.T. den Dunnen. 2009. Theoretic applicability of antisense-mediated exon skipping for Duchenne muscular dystrophy mutations. *Hum. Mutat.* 30:293–9. doi:10.1002/humu.20918.

Aartsma-Rus, A., and A.M. Krieg. 2017. FDA Approves Eteplirsen for Duchenne Muscular Dystrophy: The Next Chapter in the Eteplirsen Saga. *Nucleic Acid Ther.* 27:1–3. doi:10.1089/nat.2016.0657.

A Study of the Safety, Tolerability & Efficacy of Long-term Administration of Drisapersen in US & Canadian Subjects.

Albrecht, D.E., and S.C. Froehner. 2002. Syntrophins and dystrobrevins: defining the dystrophin scaffold at synapses. *Neurosignals.* 11:123–129. doi:65053.

Alter, J., F. Lou, A. Rabinowitz, H. Yin, J. Rosenfeld, S.D. Wilton, T.A. Partridge, and Q.L. Lu. 2006. Systemic delivery of morpholino oligonucleotide restores dystrophin expression bodywide and improves dystrophic pathology. *Nat. Med.* 12:175–7. doi:10.1038/nm1345.

Amann, K.J., B.A. Renley, and J.M. Ervasti. 1998. A cluster of basic repeats in the dystrophin rod domain binds F-actin through an electrostatic interaction. *J. Biol. Chem.* 273:28419–23.

Anthony, K., S. Cirak, S. Torelli, G. Tasca, L. Feng, V. Arechavala-Gomeza, A. Armaroli, M. Guglieri, C.S. Straathof, J.J. Verschuuren, A. Aartsma-Rus, P. Helderman-van den Enden, K. Bushby, V. Straub, C. Sewry, A. Ferlini, E. Ricci, J.E. Morgan, and F. Muntoni. 2011. Dystrophin quantification and clinical correlations in Becker muscular dystrophy: implications for clinical trials. *Brain*. 134:3547–59. doi:10.1093/brain/awr291.

Ayalon, G., J.Q. Davis, P.B. Scotland, and V. Bennett. 2008. An ankyrin-based mechanism for functional organization of dystrophin and dystroglycan. *Cell*. 135:1189–1200. doi:10.1016/j.cell.2008.10.018.

Banks, G.B., L.M. Judge, J.M. Allen, and J.S. Chamberlain. 2010. The polyproline site in hinge 2 influences the functional capacity of truncated dystrophins. *PLoS Genet.* 6:e1000958. doi:10.1371/journal.pgen.1000958.

Belanto, J.J., T.L. Mader, M.D. Eckhoff, D.M. Strandjord, G.B. Banks, M.K. Gardner, D.A. Lowe, and J.M. Ervasti. 2014. Microtubule binding distinguishes dystrophin from utrophin. *Proc. Natl. Acad. Sci. U. S. A.* 111:5723–8. doi:10.1073/pnas.1323842111.

Bello, L., P. Campadello, A. Barp, M. Fanin, C. Semplicini, G. Soraru, L. Caumo, C. Calore, C. Angelini, and E. Pegoraro. 2016. Functional changes in Becker muscular dystrophy: implications for clinical trials in dystrophinopathies. *Sci. Rep.* 6:32439. doi:10.1038/srep32439.

Bengtsson, N.E., J.K. Hall, G.L. Odom, M.P. Phelps, C.R. Andrus, R.D. Hawkins, S.D. Hauschka, J.R. Chamberlain, and J.S. Chamberlain. 2017. Muscle-specific CRISPR/Cas9 dystrophin gene editing ameliorates pathophysiology in a mouse model for Duchenne muscular dystrophy. *Nat. Commun.* 8:14454. doi:10.1038/ncomms14454.

Bhasin, N., R. Law, G. Liao, D. Safer, J. Ellmer, B.M. Discher, H.L. Sweeney, and D.E. Discher. 2005a. Molecular extensibility of mini-dystrophins and a dystrophin rod construct. *J. Mol. Biol.* 352:795–806. doi:10.1016/j.jmb.2005.07.064.

Bhasin, N., R. Law, G. Liao, D. Safer, J. Ellmer, B.M. Discher, H.L. Sweeney, and D.E.

Discher. 2005b. Molecular extensibility of mini-dystrophins and a dystrophin rod construct. *J. Mol. Biol.* 352:795–806. doi:10.1016/j.jmb.2005.07.064.

Bhosle, R.C., D.E. Michele, K.P. Campbell, Z. Li, and R.M. Robson. 2006. Interactions of intermediate filament protein synemin with dystrophin and utrophin. *Biochem. Biophys. Res. Commun.* 346:768–77. doi:10.1016/j.bbrc.2006.05.192.

Binnig, Quate, and Gerber. 1986. Atomic force microscope. *Phys. Rev. Lett.* 56:930–933. doi:10.1103/PhysRevLett.56.930.

Bladen, C.L., D. Salgado, S. Monges, M.E. Foncuberta, K. Kekou, K. Kosma, H. Dawkins, L. Lamont, A.J. Roy, T. Chamova, V. Guergueltcheva, S. Chan, L. Korngut, C. Campbell, Y. Dai, J. Wang, N. Barisic, P. Brabec, J. Lahdetie, M.C. Walter, O. Schreiber-Katz, V. Karcagi, M. Garami, V. Viswanathan, F. Bayat, F. Buccella, E. Kimura, Z. Koeks, J.C. van den Bergen, M. Rodrigues, R. Roxburgh, A. Lusakowska, A. Kostera-Pruszczyk, J. Zimowski, R. Santos, E. Neagu, S. Artemieva, V.M. Rasic, D. Vojinovic, M. Posada, C. Bloetzer, P.-Y. Jeannet, F. Joncourt, J. Diaz-Manera, E. Gallardo, A.A. Karaduman, H. Topaloglu, R. El Sherif, A. Stringer, A. V Shatillo, A.S. Martin, H.L. Peay, M.I. Bellgard, J. Kirschner, K.M. Flanigan, V. Straub, K. Bushby, J. Verschuuren, A. Aartsma-Rus, C. Beroud, and H. Lochmuller. 2015. The TREAT-NMD DMD Global Database: analysis of more than 7,000 Duchenne muscular dystrophy mutations. *Hum. Mutat.* 36:395–402. doi:10.1002/humu.22758.

Blake, D.J., D.R. Love, J. Tinsley, G.E. Morris, H. Turley, K. Gatter, G. Dickson, Y.H. Edwards, and K.E. Davies. 1992. Characterization of a 4.8kb transcript from the Duchenne muscular dystrophy locus expressed in Schwannoma cells. *Hum. Mol. Genet.* 1:103–109.

Bodanovsky, A., N. Guttman, H. Barzilai-Tutsch, O. Genin, O. Levy, M. Pines, and O. Halevy. 2014. Halofuginone improves muscle-cell survival in muscular dystrophies. *Biochim. Biophys. Acta*. 1843:1339–1347. doi:10.1016/j.bbamcr.2014.03.025.

Bonuccelli, G., F. Sotgia, W. Schubert, D.S. Park, P.G. Frank, S.E. Woodman, L. Insabato, M. Cammer, C. Minetti, and M.P. Lisanti. 2003. Proteasome inhibitor (MG-132) treatment of mdx mice rescues the expression and membrane localization of dystrophin and dystrophin-associated proteins. *Am. J. Pathol.* 163:1663–1675. doi:10.1016/S0002-9440(10)63523-7.

Briguet, A., I. Courdier-Fruh, M. Foster, T. Meier, and J.P. Magyar. 2004. Histological parameters for the quantitative assessment of muscular dystrophy in the mdx-mouse. *Neuromuscul. Disord.* 14:675–682. doi:10.1016/j.nmd.2004.06.008.

Buckley, C.D., J. Tan, K.L. Anderson, D. Hanein, N. Volkmann, W.I. Weis, W.J. Nelson, and A.R. Dunn. 2014. Cell adhesion. The minimal cadherin-catenin complex binds to actin filaments under force. *Science*. 346:1254211. doi:10.1126/science.1254211.

Bulfield, G., W.G. Siller, P.A. Wight, and K.J. Moore. 1984. X chromosome-linked muscular dystrophy (mdx) in the mouse. *Proc. Natl. Acad. Sci. U. S. A.* 81:1189–1192.

Bushby, K., R. Finkel, B. Wong, R. Barohn, C. Campbell, G.P. Comi, A.M. Connolly, J.W. Day, K.M. Flanigan, N. Goemans, K.J. Jones, E. Mercuri, R. Quinlivan, J.B. Renfroe, B. Russman, M.M. Ryan, M. Tulinius, T. Voit, S.A. Moore, H. Lee Sweeney, R.T. Abresch, K.L. Coleman, M. Eagle, J. Florence, E. Gappmaier, A.M. Glanzman, E. Henricson, J. Barth, G.L. Elfring, A. Reha, R.J. Spiegel, M.W. O'donnell, S.W. Peltz, and C.M. Mcdonald. 2014. Ataluren treatment of patients with nonsense mutation dystrophinopathy. *Muscle Nerve*. 50:477–487.

doi:10.1002/mus.24332.
Call, J.A., J.M. Ervasti, and D.A. Lowe. 2011. TAT-μUtrophin mitigates the pathophysiology of dystrophin and utrophin double-knockout mice. *J. Appl. Physiol.* 111:200–5. doi:10.1152/japplphysiol.00248.2011.
Campbell, C., H.J. McMillan, J.K. Mah, M. Tarnopolsky, K. Selby, T. McClure, D.M. Wilson, M.L. Sherman, D. Escolar, and K.M. Attie. 2016. Myostatin inhibitor ACE-031 treatment of ambulatory boys with Duchenne muscular dystrophy: Results of a randomized, placebo-controlled clinical trial. *Muscle Nerve*. doi:10.1002/mus.25268.
Carlson, C.G., and R. V Makiejus. 1990. A noninvasive procedure to detect muscle weakness in the mdx mouse. *Muscle Nerve*. 13:480–4. doi:10.1002/mus.880130603.
Carrion-Vazquez, M., A.F. Oberhauser, S.B. Fowler, P.E. Marszalek, S.E. Broedel, J. Clarke, and J.M. Fernandez. 1999. Mechanical and chemical unfolding of a single protein: a comparison. *Proc. Natl. Acad. Sci. U. S. A.* 96:3694–3699.
Center for Drug Evaluation and Research, Application Number: 206488Orig1s000. 2016.
Chamberlain, J.S., and G.M. Benian. 2000. Muscular dystrophy: the worm turns to genetic disease. *Curr. Biol.* 10:R795-7.
Chang, A.C., A.H. Mekhdjian, M. Morimatsu, A.K. Denisin, B.L. Pruitt, and A.R. Dunn. 2016. Single Molecule Force Measurements in Living Cells Reveal a Minimally Tensioned Integrin State. *ACS Nano*. 10:10745–10752. doi:10.1021/acsnano.6b03314.
Charvet, B., F. Ruggiero, and D. Le Guellec. 2012. The development of the myotendinous junction. A review. *Muscles. Ligaments Tendons J.* 2:53–63.
Cohen-Kaplan, V., I. Livneh, N. Avni, C. Cohen-Rosenzweig, and A. Ciechanover. 2016. The ubiquitin-proteasome system and autophagy: Coordinated and independent activities. *Int. J. Biochem. Cell Biol.* 79:403–418. doi:10.1016/j.biocel.2016.07.019.
Cohn, R.D., and K.P. Campbell. 2000. Molecular basis of muscular dystrophies. *Muscle Nerve*. 23:1456–71.
Connolly, A.M., R.M. Keeling, S. Mehta, A. Pestronk, and J.R. Sanes. 2001. Three mouse models of muscular dystrophy: the natural history of strength and fatigue in dystrophin-, dystrophin/utrophin-, and laminin alpha2-deficient mice. *Neuromuscul. Disord.* 11:703–712.
Consolino, C.M., and S. V Brooks. 2004. Susceptibility to sarcomere injury induced by single stretches of maximally activated muscles of mdx mice. *J. Appl. Physiol.* 96:633–638. doi:10.1152/japplphysiol.00587.2003.
Cooper, B.J., N.J. Winand, H. Stedman, B.A. Valentine, E.P. Hoffman, L.M. Kunkel, M.O. Scott, K.H. Fischbeck, J.N. Kornegay, and R.J. Avery. 1988. The homologue of the Duchenne locus is defective in X-linked muscular dystrophy of dogs. *Nature*. 334:154–156. doi:10.1038/334154a0.
Deconinck, A.E., J.A. Rafael, J.A. Skinner, S.C. Brown, A.C. Potter, L. Metzinger, D.J. Watt, J.G. Dickson, J.M. Tinsley, and K.E. Davies. 1997. Utrophin-dystrophin-deficient mice as a model for Duchenne muscular dystrophy. *Cell*. 90:717–727.
Dennett, X., L.K. Shield, L.J. Clingan, and D.A. Woolley. 1988. Becker and Duchenne muscular dystrophy: a comparative morphological study. *Aust. Paediatr. J.* 24 Suppl 1:15–20.
van Deutekom, J.C., A. a Janson, I.B. Ginjaar, W.S. Frankhuizen, A. Aartsma-Rus, M. Bremmer-Bout, J.T. den Dunnen, K. Koop, A.J. van der Kooi, N.M. Goemans, S.J. de Kimpe, P.F. Ekhart, E.H. Venneker, G.J. Platenburg, J.J. Verschuuren, and G.-J.B. van Ommen. 2007. Local dystrophin restoration with antisense oligonucleotide

PRO051. *N. Engl. J. Med.* 357:2677–86. doi:10.1056/NEJMoa073108.
Dowling, P., K. Culligan, and K. Ohlendieck. 2002. Distal mdx muscle groups exhibiting up-regulation of utrophin and rescue of dystrophin-associated glycoproteins exemplify a protected phenotype in muscular dystrophy. *Naturwissenschaften*. 89:75–78.
Ervasti, J.M. 2003. Costameres: the Achilles' heel of Herculean muscle. *J. Biol. Chem.* 278:13591–4. doi:10.1074/jbc.R200021200.
Ervasti, J.M. 2007. Dystrophin, its interactions with other proteins, and implications for muscular dystrophy. *Biochim. Biophys. Acta*. 1772:108–17. doi:10.1016/j.bbadis.2006.05.010.
Ervasti, J.M., and K.P. Campbell. 1991. Membrane organization of the dystrophin-glycoprotein complex. *Cell*. 66:1121–1131.
Filareto, A., S. Parker, R. Darabi, L. Borges, M. Iacovino, T. Schaaf, T. Mayerhofer, J.S. Chamberlain, J.M. Ervasti, R.S. McIvor, M. Kyba, and R.C.R. Perlingeiro. 2013. An ex vivo gene therapy approach to treat muscular dystrophy using inducible pluripotent stem cells. *Nat. Commun.* 4:1549. doi:10.1038/ncomms2550.
Findlay, A.R., N. Wein, Y. Kaminoh, L.E. Taylor, D.M. Dunn, J.R. Mendell, W.M. King, A. Pestronk, J.M. Florence, K.D. Mathews, R.S. Finkel, K.J. Swoboda, M.T. Howard, J.W. Day, C. McDonald, A. Nicolas, E. Le Rumeur, R.B. Weiss, and K.M. Flanigan. 2015. Clinical phenotypes as predictors of the outcome of skipping around DMD exon 45. *Ann. Neurol.* 77:668–674. doi:10.1002/ana.24365.
Fiorillo, A.A., C.R. Heier, J.S. Novak, C.B. Tully, K.J. Brown, K. Uaesoontrachoon, M.C. Vila, P.P. Ngheim, L. Bello, J.N. Kornegay, C. Angelini, T.A. Partridge, K. Nagaraju, and E.P. Hoffman. 2015. TNF-alpha-Induced microRNAs Control Dystrophin Expression in Becker Muscular Dystrophy. *Cell Rep.* 12:1678–1690. doi:10.1016/j.celrep.2015.07.066.
Flanigan, K.M. 2014. Duchenne and Becker muscular dystrophies. *Neurol. Clin.* 32:671–88, viii. doi:10.1016/j.ncl.2014.05.002.
Flood, W.D., R.W. Moyer, A. Tsykin, G.R. Sutherland, and S.A. Koblar. 2004. Nxf and Fbxo33: novel seizure-responsive genes in mice. *Eur. J. Neurosci.* 20:1819–1826. doi:10.1111/j.1460-9568.2004.03646.x.
Fukada, S., D. Morikawa, Y. Yamamoto, T. Yoshida, N. Sumie, M. Yamaguchi, T. Ito, Y. Miyagoe-Suzuki, S. Takeda, K. Tsujikawa, and H. Yamamoto. 2010. Genetic Background Affects Properties of Satellite Cells and mdx Phenotypes. *Am. J. Pathol.* 176:2414–2424. doi:10.2353/ajpath.2010.090887.
Gazzerro, E., S. Assereto, A. Bonetto, F. Sotgia, S. Scarfì, A. Pistorio, G. Bonuccelli, M. Cilli, C. Bruno, F. Zara, M.P. Lisanti, and C. Minetti. 2010. Therapeutic potential of proteasome inhibition in Duchenne and Becker muscular dystrophies. *Am. J. Pathol.* 176:1863–77. doi:10.2353/ajpath.2010.090468.
Geng, L.N., Z. Yao, L. Snider, A.P. Fong, J.N. Cech, J.M. Young, S.M. van der Maarel, W.L. Ruzzo, R.C. Gentleman, R. Tawil, and S.J. Tapscott. 2012. DUX4 activates germline genes, retroelements, and immune mediators: implications for facioscapulohumeral dystrophy. *Dev. Cell*. 22:38–51. doi:10.1016/j.devcel.2011.11.013.
Gowers, W. 1886. A manual of diseases of the nervous system. *London: Churchill*.
Grady, R.M., H. Teng, M.C. Nichol, J.C. Cunningham, R.S. Wilkinson, and J.R. Sanes. 1997. Skeletal and cardiac myopathies in mice lacking utrophin and dystrophin: a model for Duchenne muscular dystrophy. *Cell*. 90:729–738.
Granzier, H., and S. Labeit. 2007. Structure-function relations of the giant elastic protein

titin in striated and smooth muscle cells. *Muscle Nerve*. 36:740–755. doi:10.1002/mus.20886.
Guiraud, S., H. Chen, D.T. Burns, and K.E. Davies. 2015. Advances in genetic therapeutic strategies for Duchenne muscular dystrophy. *Exp. Physiol.* 100:1458–1467. doi:10.1113/EP085308.
Guo, W.X., M. Nichol, and J.P. Merlie. 1996. Cloning and expression of full length mouse utrophin: the differential association of utrophin and dystrophin with AChR clusters. *FEBS Lett.* 398:259–264.
Hamed, S., A. Sutherland-Smith, J. Gorospe, J. Kendrick-Jones, and E. Hoffman. 2005. DNA sequence analysis for structure/function and mutation studies in Becker muscular dystrophy. *Clin. Genet.* 68:69–79. doi:10.1111/j.1399-0004.2005.00455.x.
Harper, S.Q., M.A. Hauser, C. DelloRusso, D. Duan, R.W. Crawford, S.F. Phelps, H.A. Harper, A.S. Robinson, J.F. Engelhardt, S. V Brooks, and J.S. Chamberlain. 2002. Modular flexibility of dystrophin: implications for gene therapy of Duchenne muscular dystrophy. *Nat. Med.* 8:253–61. doi:10.1038/nm0302-253.
Heier, C.R., J.M. Damsker, Q. Yu, B.C. Dillingham, T. Huynh, J.H. Van der Meulen, A. Sali, B.K. Miller, A. Phadke, L. Scheffer, J. Quinn, K. Tatem, S. Jordan, S. Dadgar, O.C. Rodriguez, C. Albanese, M. Calhoun, H. Gordish-Dressman, J.K. Jaiswal, E.M. Connor, J.M. McCall, E.P. Hoffman, E.K.M. Reeves, and K. Nagaraju. 2013. VBP15, a novel anti-inflammatory and membrane-stabilizer, improves muscular dystrophy without side effects. *EMBO Mol. Med.* 5:1569–1585. doi:10.1002/emmm.201302621.
Heller, K.N., C.L. Montgomery, K.M. Shontz, K.R. Clark, J.R. Mendell, and L.R. Rodino-Klapac. 2015. Human alpha7 Integrin Gene (ITGA7) Delivered by Adeno-Associated Virus Extends Survival of Severely Affected Dystrophin/Utrophin-Deficient Mice. *Hum. Gene Ther.* 26:647–656. doi:10.1089/hum.2015.062.
Henderson, D.M., J.J. Belanto, B. Li, H. Heun-Johnson, and J.M. Ervasti. 2011. Internal deletion compromises the stability of dystrophin. *Hum. Mol. Genet.* 20:2955–63. doi:10.1093/hmg/ddr199.
Henderson, D.M., A. Lee, and J.M. Ervasti. 2010. Disease-causing missense mutations in actin binding domain 1 of dystrophin induce thermodynamic instability and protein aggregation. *Proc. Natl. Acad. Sci. U. S. A.* 107:9632–7. doi:10.1073/pnas.1001517107.
Hijikata, T., T. Murakami, H. Ishikawa, and H. Yorifuji. 2003. Plectin tethers desmin intermediate filaments onto subsarcolemmal dense plaques containing dystrophin and vinculin. *Histochem. Cell Biol.* 119:109–123. doi:10.1007/s00418-003-0496-5.
Hishiya, A., S. Iemura, T. Natsume, S. Takayama, K. Ikeda, and K. Watanabe. 2006. A novel ubiquitin-binding protein ZNF216 functioning in muscle atrophy. *EMBO J.* 25:554–564. doi:10.1038/sj.emboj.7600945.
Hoffman, E.P., R.H. Brown, and L.M. Kunkel. 1987. Dystrophin : The Protein Product of the Duchenne Muscular Dystrophy Locus. *Cell*. 51:919–928.
Hollinger, K., C.X. Yang, R.E. Montz, D. Nonneman, J.W. Ross, and J.T. Selsby. 2014. Dystrophin insufficiency causes selective muscle histopathology and loss of dystrophin-glycoprotein complex assembly in pig skeletal muscle. *FASEB J. Off. Publ. Fed. Am. Soc. Exp. Biol.* 28:1600–1609. doi:10.1096/fj.13-241141.
Hotta, A. 2015. Genome Editing Gene Therapy for Duchenne Muscular Dystrophy. *J. Neuromuscul. Dis.* 2:343–355. doi:10.3233/JND-150116.
Huang, J., L. Teng, L. Li, T. Liu, L. Li, D. Chen, L.-G. Xu, Z. Zhai, and H.-B. Shu. 2004. ZNF216 Is an A20-like and IkappaB kinase gamma-interacting inhibitor of

NFkappaB activation. *J. Biol. Chem.* 279:16847–16853. doi:10.1074/jbc.M309491200.
Hurchla, M.A., A. Garcia-Gomez, M.C. Hornick, E.M. Ocio, A. Li, J.F. Blanco, L. Collins, C.J. Kirk, D. Piwnica-Worms, R. Vij, M.H. Tomasson, A. Pandiella, J.F. San Miguel, M. Garayoa, and K.N. Weilbaecher. 2013. The epoxyketone-based proteasome inhibitors carfilzomib and orally bioavailable oprozomib have anti-resorptive and bone-anabolic activity in addition to anti-myeloma effects. *Leukemia*. 27:430–40. doi:10.1038/leu.2012.183.
Iconomou, M., and D.N. Saunders. 2016. Systematic approaches to identify E3 ligase substrates. *Biochem. J.* 473:4083–4101. doi:10.1042/BCJ20160719.
Ishikawa-Sakurai, M., M. Yoshida, M. Imamura, K.E. Davies, and E. Ozawa. 2004. ZZ domain is essentially required for the physiological binding of dystrophin and utrophin to beta-dystroglycan. *Hum. Mol. Genet.* 13:693–702. doi:10.1093/hmg/ddh087.
Jung, D., B. Yang, J. Meyer, J.S. Chamberlain, and K.P. Campbell. 1995. Identification and Characterization of the Dystrophin Anchoring Site on Beta-Dystroglycan. *J. Biol. Chem.* 270:27305–27310. doi:10.1074/jbc.270.45.27305.
Karijolich, J., and Y.-T. Yu. 2014. Therapeutic suppression of premature termination codons: mechanisms and clinical considerations (review). *Int. J. Mol. Med.* 34:355–362. doi:10.3892/ijmm.2014.1809.
Kawakami, E., N. Kawai, N. Kinouchi, H. Mori, Y. Ohsawa, N. Ishimaru, Y. Sunada, S. Noji, and E. Tanaka. 2013. Local applications of myostatin-siRNA with atelocollagen increase skeletal muscle mass and recovery of muscle function. *PLoS One*. 8:e64719. doi:10.1371/journal.pone.0064719.
Kellermayer, M.S.Z., C. Bustamante, and H.L. Granzier. 2003. Mechanics and structure of titin oligomers explored with atomic force microscopy. *Biochim. Biophys. Acta*. 1604:105–114.
Khurana, T.S., E.P. Hoffman, and L.M. Kunkel. 1990. Identification of a chromosome 6-encoded dystrophin-related protein. *J. Biol. Chem.* 265:16717–16720.
Kinali, M., V. Arechavala-Gomeza, L. Feng, S. Cirak, D. Hunt, C. Adkin, M. Guglieri, E. Ashton, S. Abbs, P. Nihoyannopoulos, M.E. Garralda, M. Rutherford, C. McCulley, L. Popplewell, I.R. Graham, G. Dickson, M.J.A. Wood, D.J. Wells, S.D. Wilton, R. Kole, V. Straub, K. Bushby, C. Sewry, J.E. Morgan, and F. Muntoni. 2009. Local restoration of dystrophin expression with the morpholino oligomer AVI-4658 in Duchenne muscular dystrophy: a single-blind, placebo-controlled, dose-escalation, proof-of-concept study. *Lancet Neurol.* 8:918–28. doi:10.1016/S1474-4422(09)70211-X.
Kleopa, K. a, A. Drousiotou, E. Mavrikiou, A. Ormiston, and T. Kyriakides. 2006. Naturally occurring utrophin correlates with disease severity in Duchenne muscular dystrophy. *Hum. Mol. Genet.* 15:1623–8. doi:10.1093/hmg/ddl083.
Kobayashi, Y.M., E.P. Rader, R.W. Crawford, N.K. Iyengar, D.R. Thedens, J.A. Faulkner, S. V Parikh, R.M. Weiss, J.S. Chamberlain, S.A. Moore, and K.P. Campbell. 2008. Sarcolemma-localized nNOS is required to maintain activity after mild exercise. *Nature*. 456:511–515. doi:10.1038/nature07414.
Koenig, M., A.H. Beggs, M. Moyer, S. Scherpf, K. Heindrich, T. Bettecken, G. Meng, C.R. Muller, M. Lindlof, and H. Kaariainen. 1989. The molecular basis for Duchenne versus Becker muscular dystrophy: correlation of severity with type of deletion. *Am. J. Hum. Genet.* 45:498–506.
Koenig, M., E.P. Hoffman, C.J. Bertelson, A.P. Monaco, C. Feener, and L.M. Kunkel.

1987. Complete cloning of the Duchenne muscular dystrophy (DMD) cDNA and preliminary genomic organization of the DMD gene in normal and affected individuals. *Cell*. 50:509–517.
Koenig, M., and L.M. Kunkel. 1990. Detailed analysis of the repeat domain of dystrophin reveals four potential hinge segments that may confer flexibility. *J. Biol. Chem.* 265:4560–6.
Koenig, M., A.P. Monaco, and L.M. Kunkel. 1988. The complete sequence of dystrophin predicts a rod-shaped cytoskeletal protein. *Cell*. 53:219–228.
Kohler, M., C.F. Clarenbach, C. Bahler, T. Brack, E.W. Russi, and K.E. Bloch. 2009. Disability and survival in Duchenne muscular dystrophy. *J. Neurol. Neurosurg. Psychiatry*. 80:320–325. doi:10.1136/jnnp.2007.141721.
Kornegay, J.N., J.R. Bogan, D.J. Bogan, M.K. Childers, J. Li, P. Nghiem, D.A. Detwiler, C.A. Larsen, R.W. Grange, R.K. Bhavaraju-Sanka, S. Tou, B.P. Keene, J.F.J. Howard, J. Wang, Z. Fan, S.J. Schatzberg, M.A. Styner, K.M. Flanigan, X. Xiao, and E.P. Hoffman. 2012. Canine models of Duchenne muscular dystrophy and their use in therapeutic strategies. *Mamm. Genome*. 23:85–108. doi:10.1007/s00335-011-9382-y.
Krieger, C.C., N. Bhasin, M. Tewari, A.E.X. Brown, D. Safer, H.L. Sweeney, and D.E. Discher. 2010a. Exon-skipped dystrophins for treatment of Duchenne muscular dystrophy: mass spectrometry mapping of most exons and cooperative domain designs based on single molecule mechanics. *Cytoskelet.* 67:796–807. doi:10.1002/cm.20489.
Krieger, C.C., N. Bhasin, M. Tewari, A.E.X. Brown, D. Safer, H.L. Sweeney, and D.E. Discher. 2010b. Exon-skipped dystrophins for treatment of Duchenne muscular dystrophy: mass spectrometry mapping of most exons and cooperative domain designs based on single molecule mechanics. *Cytoskeleton (Hoboken).* 67:796–807. doi:10.1002/cm.20489.
Kulke, M., S. Fujita-Becker, E. Rostkova, C. Neagoe, D. Labeit, D.J. Manstein, M. Gautel, and W.A. Linke. 2001. Interaction between PEVK-titin and actin filaments: origin of a viscous force component in cardiac myofibrils. *Circ. Res.* 89:874–881.
Kunkel, L.M., E. Bachrach, R.R. Bennett, J. Guyon, and L. Steffen. 2006. Diagnosis and cell-based therapy for Duchenne muscular dystrophy in humans, mice, and zebrafish. *J. Hum. Genet.* 51:397–406. doi:10.1007/s10038-006-0374-9.
Lai, Y., G. Thomas, Y. Yue, and H. Yang. 2009. Dystrophins carrying spectrin-like repeats 16 and 17 anchor nNOS to the sarcolemma and enhance exercise performance in a mouse model of muscular. *J. Clin. Investig.* 119. doi:10.1172/JCI36612.624.
Lai, Y., J. Zhao, Y. Yue, and D. Duan. 2012. α2 and α3 helices of dystrophin R16 and R17 frame a microdomain in the α1 helix of dystrophin R17 for neuronal NOS binding. *Proc. Natl. Acad. Sci. U. S. A.*
Lai, Y., J. Zhao, Y. Yue, and D. Duan. 2013. alpha2 and alpha3 helices of dystrophin R16 and R17 frame a microdomain in the alpha1 helix of dystrophin R17 for neuronal NOS binding. *Proc. Natl. Acad. Sci. U. S. A.* 110:525–530. doi:10.1073/pnas.1211431109.
Law, R., P. Carl, S. Harper, P. Dalhaimer, D.W. Speicher, and D.E. Discher. 2003a. Cooperativity in forced unfolding of tandem spectrin repeats. *Biophys. J.* 84:533–544. doi:10.1016/S0006-3495(03)74872-3.
Law, R., G. Liao, S. Harper, G. Yang, D.W. Speicher, and D.E. Discher. 2003b. Pathway shifts and thermal softening in temperature-coupled forced unfolding of spectrin

domains. *Biophys. J.* 85:3286–3293. doi:10.1016/S0006-3495(03)74747-X.
Legardinier, S., J.-F. Hubert, O. Le Bihan, C. Tascon, C. Rocher, C. Raguénès-Nicol, A. Bondon, S. Hardy, and E. Le Rumeur. 2008. Sub-domains of the dystrophin rod domain display contrasting lipid-binding and stability properties. *Biochim. Biophys. Acta*. 1784:672–82. doi:10.1016/j.bbapap.2007.12.014.
Legardinier, S., B. Legrand, C. Raguénès-Nicol, A. Bondon, S. Hardy, C. Tascon, E. Le Rumeur, and J.-F. Hubert. 2009a. A Two-amino Acid Mutation Encountered in Duchenne Muscular Dystrophy Decreases Stability of the Rod Domain 23 (R23) Spectrin-like Repeat of Dystrophin. *J. Biol. Chem.* 284:8822–32. doi:10.1074/jbc.M805846200.
Legardinier, S., C. Raguénès-Nicol, C. Tascon, C. Rocher, S. Hardy, J.-F. Hubert, and E. Le Rumeur. 2009b. Mapping of the lipid-binding and stability properties of the central rod domain of human dystrophin. *J. Mol. Biol.* 389:546–58. doi:10.1016/j.jmb.2009.04.025.
Li, D., A. Bareja, L. Judge, Y. Yue, Y. Lai, R. Fairclough, K.E. Davies, J.S. Chamberlain, and D. Duan. 2010. Sarcolemmal nNOS anchoring reveals a qualitative difference between dystrophin and utrophin. *J. Cell Sci.* 123:2008–13. doi:10.1242/jcs.064808.
Li, D., Y. Yue, and D. Duan. 2008. Preservation of muscle force in Mdx3cv mice correlates with low-level expression of a near full-length dystrophin protein. *Am. J. Pathol.* 172:1332–1341. doi:10.2353/ajpath.2008.071042.
Li, L., J.O. Fierer, T.A. Rapoport, and M. Howarth. 2014. Structural analysis and optimization of the covalent association between SpyCatcher and a peptide Tag. *J. Mol. Biol.* 426:309–317. doi:10.1016/j.jmb.2013.10.021.
Linke, W.A., and A. Grutzner. 2008. Pulling single molecules of titin by AFM--recent advances and physiological implications. *Pflugers Arch.* 456:101–115. doi:10.1007/s00424-007-0389-x.
Linke, W.A., M. Ivemeyer, P. Mundel, M.R. Stockmeier, and B. Kolmerer. 1998. Nature of PEVK-titin elasticity in skeletal muscle. *Proc. Natl. Acad. Sci. U. S. A.* 95:8052–8057.
Linke, W.A., M. Ivemeyer, N. Olivieri, B. Kolmerer, J.C. Ruegg, and S. Labeit. 1996. Towards a molecular understanding of the elasticity of titin. *J. Mol. Biol.* 261:62–71.
Linke, W.A., M. Kulke, H. Li, S. Fujita-Becker, C. Neagoe, D.J. Manstein, M. Gautel, and J.M. Fernandez. 2002. PEVK domain of titin: an entropic spring with actin-binding properties. *J. Struct. Biol.* 137:194–205. doi:10.1006/jsbi.2002.4468.
Liu, Q.Y., J.X. Lei, M. Sikorska, and R. Liu. 2008. A novel brain-enriched E3 ubiquitin ligase RNF182 is up regulated in the brains of Alzheimer's patients and targets ATP6V0C for degradation. *Mol. Neurodegener.* 3:4. doi:10.1186/1750-1326-3-4.
Lloyd, T.E., and J.P. Taylor. 2010. Flightless flies: Drosophila models of neuromuscular disease. *Ann. N. Y. Acad. Sci.* 1184:e1-20.
Long, C., L. Amoasii, A.A. Mireault, J.R. McAnally, H. Li, E. Sanchez-Ortiz, S. Bhattacharyya, J.M. Shelton, R. Bassel-Duby, and E.N. Olson. 2016. Postnatal genome editing partially restores dystrophin expression in a mouse model of muscular dystrophy. *Science (80-.).* 351:400–403. doi:10.1126/science.aad5725.
Long, C., J.R. McAnally, J.M. Shelton, A.A. Mireault, R. Bassel-Duby, and E.N. Olson. 2014. Prevention of muscular dystrophy in mice by CRISPR/Cas9-mediated editing of germline DNA. *Science*. 345:1184–1188. doi:10.1126/science.1254445.
Love, D.R., D.F. Hill, G. Dickson, N.K. Spurr, B.C. Byth, R.F. Marsden, F.S. Walsh, Y.H. Edwards, and K.E. Davies. 1989. An autosomal transcript in skeletal muscle with homology to dystrophin. *Nature*. 339:55–58. doi:10.1038/339055a0.

Lu, Q.L., A. Rabinowitz, Y.C. Chen, T. Yokota, H. Yin, J. Alter, A. Jadoon, G. Bou-Gharios, and T. Partridge. 2005. Systemic delivery of antisense oligoribonucleotide restores dystrophin expression in body-wide skeletal muscles. *Proc. Natl. Acad. Sci. U. S. A.* 102:198–203. doi:10.1073/pnas.0406700102.

Lutz, M., F. Wempe, I. Bahr, D. Zopf, and H. von Melchner. 2006. Proteasomal degradation of the multifunctional regulator YB-1 is mediated by an F-Box protein induced during programmed cell death. *FEBS Lett.* 580:3921–3930. doi:10.1016/j.febslet.2006.06.023.

Matsumura, K., J.M. Ervasti, K. Ohlendieck, S.D. Kahl, and K.P. Campbell. 1992. Assocation of dystrophin-related protein with dystrophin-associated proteins in mdx mouse muscle. *Nature*. 360:588–91.

McCourt, J.L., K.K. Rhett, M.A. Jaeger, J.J. Belanto, D.M. Talsness, and J.M. Ervasti. 2015. In vitro stability of therapeutically relevant, internally truncated dystrophins. *Skelet. Muscle*. 5:13. doi:10.1186/s13395-015-0040-z.

McGreevy, J.W., C.H. Hakim, M.A. McIntosh, and D. Duan. 2015. Animal models of Duchenne muscular dystrophy: from basic mechanisms to gene therapy. *Dis. Model. Mech.* 8:195–213. doi:10.1242/dmm.018424.

McVey Ward, D., D. Radisky, M.A. Scullion, M.S. Tuttle, M. Vaughn, and J. Kaplan. 2001. hVPS41 is expressed in multiple isoforms and can associate with vesicles through a RING-H2 finger motif. *Exp. Cell Res.* 267:126–134. doi:10.1006/excr.2001.5244.

Megeney, L.A., B. Kablar, K. Garrett, J.E. Anderson, and M.A. Rudnicki. 1996. MyoD is required for myogenic stem cell function in adult skeletal muscle. *Genes Dev.* 10:1173–1183.

Mendell, J. 2010. Dystrophin immunity in Duchenne's muscular dystrophy. *N. Engl. J. Med.* 1429–1437.

Mendell, J.R., C. Shilling, N.D. Leslie, K.M. Flanigan, R. al-Dahhak, J. Gastier-Foster, K. Kneile, D.M. Dunn, B. Duval, A. Aoyagi, C. Hamil, M. Mahmoud, K. Roush, L. Bird, C. Rankin, H. Lilly, N. Street, R. Chandrasekar, and R.B. Weiss. 2012. Evidence-based path to newborn screening for Duchenne muscular dystrophy. *Ann. Neurol.* 71:304–13. doi:10.1002/ana.23528.

Mirza, A., M. Sagathevan, N. Sahni, L. Choi, and N. Menhart. 2010. A biophysical map of the dystrophin rod. *Biochim. Biophys. Acta*. 1804:1796–809. doi:10.1016/j.bbapap.2010.03.009.

Moens, P., P.H. Baatsen, and G. Marechal. 1993. Increased susceptibility of EDL muscles from mdx mice to damage induced by contractions with stretch. *J. Muscle Res. Cell Motil.* 14:446–451.

Monaco, A.P., C.J. Bertelson, S. Liechti-Gallati, H. Moser, and L.M. Kunkel. 1988. An explanation for the phenotypic differences between patients bearing partial deletions of the DMD locus. *Genomics*. 2:90–95.

Muntoni, F., S. Torelli, and A. Ferlini. 2003. Review Dystrophin and mutations : one gene , several proteins , multiple phenotypes. 44:731–740.

Muthu, M., K. a. Richardson, and A.J. Sutherland-Smith. 2012. The Crystal Structures of Dystrophin and Utrophin Spectrin Repeats: Implications for Domain Boundaries. *PLoS One*. 7:e40066. doi:10.1371/journal.pone.0040066.

Nagy, A., P. Cacciafesta, L. Grama, A. Kengyel, A. Malnasi-Csizmadia, and M.S.Z. Kellermayer. 2004. Differential actin binding along the PEVK domain of skeletal muscle titin. *J. Cell Sci.* 117:5781–5789. doi:10.1242/jcs.01501.

Nelson, C.E., C.H. Hakim, D.G. Ousterout, P.I. Thakore, E.A. Moreb, R.M.C. Rivera, S.

Madhavan, X. Pan, F.A. Ran, W.X. Yan, A. Asokan, F. Zhang, D. Duan, and C.A. Gersbach. 2016. In vivo genome editing improves muscle function in a mouse model of Duchenne muscular dystrophy. *Science (80-.).* 351:403–407. doi:10.1126/science.aad5143.

Nicolas, A., O. Delalande, J.-F. Hubert, and E. Le Rumeur. 2014a. The spectrin family of proteins: a unique coiled-coil fold for various molecular surface properties. *J. Struct. Biol.* 186:392–401. doi:10.1016/j.jsb.2014.03.011.

Nicolas, A., C. Lucchetti-Miganeh, R. Ben Yaou, J.-C. Kaplan, J. Chelly, F. Leturcq, F. Barloy-Hubler, and E. Le Rumeur. 2012. Assessment of the structural and functional impact of in-frame mutations of the DMD gene, using the tools included in the eDystrophin online database. *Orphanet J. Rare Dis.* 7:45. doi:10.1186/1750-1172-7-45.

Nicolas, A., C. Raguenes-Nicol, R. Ben Yaou, S. Ameziane-Le Hir, A. Cheron, V. Vie, M. Claustres, F. Leturcq, O. Delalande, J.-F. Hubert, S. Tuffery-Giraud, E. Giudice, and E. Le Rumeur. 2014b. Becker muscular dystrophy severity is linked to the structure of dystrophin. *Hum. Mol. Genet.*

Niesen, F.H., H. Berglund, and M. Vedadi. 2007. The use of differential scanning fluorimetry to detect ligand interactions that promote protein stability. *Nat. Protoc.* 2:2212–21. doi:10.1038/nprot.2007.321.

Nonneman, D.J., T. Brown-Brandl, S.A. Jones, R.T. Wiedmann, and G.A. Rohrer. 2012. A defect in dystrophin causes a novel porcine stress syndrome. *BMC Genomics*. 13:233. doi:10.1186/1471-2164-13-233.

Norwood, F.L., a J. Sutherland-Smith, N.H. Keep, and J. Kendrick-Jones. 2000. The structure of the N-terminal actin-binding domain of human dystrophin and how mutations in this domain may cause Duchenne or Becker muscular dystrophy. *Structure*. 8:481–91.

Odom, G.L., P. Gregorevic, J.M. Allen, E. Finn, and J.S. Chamberlain. 2008. Microutrophin delivery through rAAV6 increases lifespan and improves muscle function in dystrophic dystrophin/utrophin-deficient mice. *Mol. Ther.* 16:1539–45. doi:10.1038/mt.2008.149.

Ohlendieck, K., and K.P. Campbell. 1991. Dystrophin-associated proteins are greatly reduced in skeletal muscle from mdx mice. *J. Cell Biol.* 115:1685–1694.

Ohlendieck, K., J.M. Ervasti, K. Matsumura, S.D. Kahl, C.J. Leveille, and K.P. Campbell. 1991. Dystrophin-related protein is localized to neuromuscular junctions of adult skeletal muscle. *Neuron*. 7:499–508.

Oudet, C., A. Hanauer, P. Clemens, T. Caskey, and J.L. Mandel. 1992. Two hot spots of recombination in the DMD gene correlate with the deletion prone regions. *Hum. Mol. Genet.* 1:599–603.

Ousterout, D.G., A.M. Kabadi, P.I. Thakore, W.H. Majoros, T.E. Reddy, and C.A. Gersbach. 2015. Multiplex CRISPR/Cas9-based genome editing for correction of dystrophin mutations that cause Duchenne muscular dystrophy. *Nat. Commun.* 6:6244. doi:10.1038/ncomms7244.

Pascual, J., M. Pfuhl, D. Walther, M. Saraste, and M. Nilges. 1997. Solution structure of the spectrin repeat: a left-handed antiparallel triple-helical coiled-coil. *J. Mol. Biol.* 273:740–51. doi:10.1006/jmbi.1997.1344.

Petrof, B.J., J.B. Shrager, H.H. Stedman, A.M. Kelly, and H.L. Sweeney. 1993. Dystrophin protects the sarcolemma from stresses developed during muscle contraction. *Proc. Natl. Acad. Sci. U. S. A.* 90:3710–3714.

Phase IIb Study of PRO045 in Subjects With Duchenne Muscular Dystrophy.

Phelps, S.F., M.A. Hauser, N.M. Cole, J.A. Rafael, R.T. Hinkle, J.A. Faulkner, and J.S. Chamberlain. 1995. Expression of full-length and truncated dystrophin mini-genes in transgenic mdx mice. *Hum. Mol. Genet.* 4:1251–1258.

Prins, K.W., J.L. Humston, A. Mehta, V. Tate, E. Ralston, and J.M. Ervasti. 2009. Dystrophin is a microtubule-associated protein. *J. Cell Biol.* 186:363–9. doi:10.1083/jcb.200905048.

Prior, T.W., A.C. Papp, P.J. Snyder, A.H. Burghes, C. Bartolo, M.S. Sedra, L.M. Western, and J.R. Mendell. 1993. A missense mutation in the dystrophin gene in a Duchenne muscular dystrophy patient. *Nat. Genet.* 4:357–360. doi:10.1038/ng0893-357.

van Putten, M., M. Hulsker, V.D. Nadarajah, S.H. van Heiningen, E. van Huizen, M. van Iterson, P. Admiraal, T. Messemaker, J.T. den Dunnen, P.A.C. 't Hoen, and A. Aartsma-Rus. 2012. The effects of low levels of dystrophin on mouse muscle function and pathology. *PLoS One*. 7:e31937. doi:10.1371/journal.pone.0031937.

Rahimov, F., and L.M. Kunkel. 2013. The cell biology of disease: cellular and molecular mechanisms underlying muscular dystrophy. *J. Cell Biol.* 201:499–510. doi:10.1083/jcb.201212142.

Rezniczek, G. a, P. Konieczny, B. Nikolic, S. Reipert, D. Schneller, C. Abrahamsberg, K.E. Davies, S.J. Winder, and G. Wiche. 2007. Plectin 1f scaffolding at the sarcolemma of dystrophic (mdx) muscle fibers through multiple interactions with beta-dystroglycan. *J. Cell Biol.* 176:965–77. doi:10.1083/jcb.200604179.

Ricotti, V., S. Spinty, H. Roper, I. Hughes, B. Tejura, N. Robinson, G. Layton, K. Davies, F. Muntoni, and J. Tinsley. 2016. Safety, Tolerability, and Pharmacokinetics of SMT C1100, a 2-Arylbenzoxazole Utrophin Modulator, following Single- and Multiple-Dose Administration to Pediatric Patients with Duchenne Muscular Dystrophy. *PLoS One*. 11:e0152840. doi:10.1371/journal.pone.0152840.

Rief, M., M. Gautel, F. Oesterhelt, J.M. Fernandez, and H.E. Gaub. 1997. Reversible unfolding of individual titin immunoglobulin domains by AFM. *Science*. 276:1109–1112.

Rief, M., J. Pascual, M. Saraste, and H.E. Gaub. 1999. Single molecule force spectroscopy of spectrin repeats: low unfolding forces in helix bundles. *J. Mol. Biol.* 286:553–561. doi:10.1006/jmbi.1998.2466.

Rigoletto, C., A. Prelle, P. Ciscato, M. Moggio, G. Comi, F. Fortunato, and G. Scarlato. 1995. Utrophin expression during human fetal development. *Int. J. Dev. Neurosci.* 13:585–593.

Rodrigues, M., Y. Echigoya, R. Maruyama, K.R.Q. Lim, S. Fukada, and T. Yokota. 2016. Impaired regenerative capacity and lower revertant fibre expansion in dystrophin-deficient mdx muscles on DBA/2 background. *Sci. Rep.* 6:38371. doi:10.1038/srep38371.

Ruszczak, C., A. Mirza, and N. Menhart. 2009. Differential stabilities of alternative exon-skipped rod motifs of dystrophin. *Biochim. Biophys. Acta*. 1794:921–8. doi:10.1016/j.bbapap.2009.02.016.

Rybakova, I.N., K.J. Amann, and J.M. Ervasti. 1996. A new model for the interaction of dystrophin with F-actin. *J. Cell Biol.* 135:661–72.

Rybakova, I.N., and J.M. Ervasti. 1997. Dystrophin-glycoprotein complex is monomeric and stabilizes actin filaments in vitro through a lateral association. *J. Biol. Chem.* 272:28771–8.

Rybakova, I.N., J.L. Humston, K.J. Sonnemann, and J.M. Ervasti. 2006. Dystrophin and utrophin bind actin through distinct modes of contact. *J. Biol. Chem.* 281:9996–

10001. doi:10.1074/jbc.M513121200.
Rybakova, I.N., J.R. Patel, K.E. Davies, P.D. Yurchenco, and J.M. Ervasti. 2002a. Utrophin Binds Laterally along Actin Filaments and Can Couple Costameric Actin with Sarcolemma When Overexpressed in Dystrophin-deficient Muscle. 13:1512–1521. doi:10.1091/mbc.01.
Rybakova, I.N., J.R. Patel, K.E. Davies, P.D. Yurchenco, and J.M. Ervasti. 2002b. Utrophin binds laterally along actin filaments and can couple costameric actin with sarcolemma when overexpressed in dystrophin-deficient muscle. *Mol. Biol. Cell*. 13:1512–1521. doi:10.1091/mbc.01-09-0446.
Rybakova, I.N., J.R. Patel, and J.M. Ervasti. 2000. The Dystrophin Complex Forms a Mechanically Strong Link between the Sarcolemma and Costameric Actin. *J. Cell Biol.* 150:1209–1214. doi:10.1083/jcb.150.5.1209.
Saadat, L., L. Pittman, and N. Menhart. 2006. Structural cooperativity in spectrin type repeats motifs of dystrophin. *Biochim. Biophys. Acta*. 1764:943–54. doi:10.1016/j.bbapap.2006.02.012.
Sahni, N., K. Mangat, E. Le Rumeur, and N. Menhart. 2012. Exon edited dystrophin rods in the hinge 3 region. *Biochim. Biophys. Acta*. 1824:1080–1089. doi:10.1016/j.bbapap.2012.06.011.
Sakamoto, M., K. Yuasa, M. Yoshimura, T. Yokota, T. Ikemoto, M. Suzuki, G. Dickson, Y. Miyagoe-Suzuki, and S. Takeda. 2002. Micro-dystrophin cDNA ameliorates dystrophic phenotypes when introduced into mdx mice as a transgene. *Biochem. Biophys. Res. Commun.* 293:1265–72. doi:10.1016/S0006-291X(02)00362-5.
Shin, J.-H., X. Pan, C.H. Hakim, H.T. Yang, Y. Yue, K. Zhang, R.L. Terjung, and D. Duan. 2013. Microdystrophin ameliorates muscular dystrophy in the canine model of duchenne muscular dystrophy. *Mol. Ther.* 21:750–757. doi:10.1038/mt.2012.283.
Sicinski, P., Y. Geng, A.S. Ryder-Cook, E.A. Barnard, M.G. Darlison, and P.J. Barnard. 1989. The molecular basis of muscular dystrophy in the mdx mouse: a point mutation. *Science*. 244:1578–1580.
Singh, S.M., N. Kongari, J. Cabello-Villegas, and K.M.G. Mallela. 2010. Missense mutations in dystrophin that trigger muscular dystrophy decrease protein stability and lead to cross-beta aggregates. *Proc. Natl. Acad. Sci. U. S. A.* 107:15069–74. doi:10.1073/pnas.1008818107.
Sonnemann, K.J., H. Heun-Johnson, A.J. Turner, K.A. Baltgalvis, D.A. Lowe, and J.M. Ervasti. 2009. Functional substitution by TAT-utrophin in dystrophin-deficient mice. *PLoS Med.* 6:e1000083. doi:10.1371/journal.pmed.1000083.
Stessman, H.A.F., L.B. Baughn, A. Sarver, T. Xia, R. Deshpande, A. Mansoor, S.A. Walsh, J.J. Sunderland, N.G. Dolloff, M.A. Linden, F. Zhan, S. Janz, C.L. Myers, and B.G. Van Ness. 2013. Profiling Bortezomib Resistance Identifies Secondary Therapies in a Mouse Myeloma Model. *Mol. Cancer Ther.* 12:1140–1150. doi:10.1158/1535-7163.MCT-12-1151.
Stone, M.R., A.O. Neill, D. Catino, and R.J. Bloch. 2005. Specific Interaction of the Actin-binding Domain of Dystrophin with Intermediate Filaments Containing Keratin 19. *Mol. Biol. Cell*. 16:4280–4293. doi:10.1091/mbc.E05.
Suzuki, A., M. Yoshida, H. Yamamoto, and E. Ozawa. 1992. Glycoprotein-binding site of dystrophin is confined to the cysteine-rich domain and the first half of the carboxy-terminal domain. *FEBS Lett.* 308:154–160.
Tabebordbar, M., K. Zhu, J.K.W. Cheng, W.L. Chew, J.J. Widrick, W.X. Yan, C. Maesner, E.Y. Wu, R. Xiao, F.A. Ran, L. Cong, F. Zhang, L.H. Vandenberghe, G.M. Church, and A.J. Wagers. 2016. In vivo gene editing in dystrophic mouse muscle

and muscle stem cells. *Science (80-.).* 351:407–411. doi:10.1126/science.aad5177.
Talsness, D.M., J.J. Belanto, and J.M. Ervasti. 2015. Disease-proportional proteasomal degradation of missense dystrophins. *Proc. Natl. Acad. Sci. U. S. A.* 112:12414–9. doi:10.1073/pnas.1508755112.
Tanabe, Y., K. Esaki, and T. Nomura. 1986. Skeletal muscle pathology in X chromosome-linked muscular dystrophy (mdx) mouse. *Acta Neuropathol.* 69:91–95.
Tinsley, J., N. Deconinck, R. Fisher, D. Kahn, S. Phelps, J.M. Gillis, and K. Davies. 1998. Expression of full-length utrophin prevents muscular dystrophy in mdx mice. *Nat. Med.* 4:1441–4. doi:10.1038/4033.
Tinsley, J.M., R.J. Fairclough, R. Storer, F.J. Wilkes, A.C. Potter, S.E. Squire, D.S. Powell, A. Cozzoli, R.F. Capogrosso, A. Lambert, F.X. Wilson, S.P. Wren, A. De Luca, and K.E. Davies. 2011. Daily Treatment with SMTC1100, a Novel Small Molecule Utrophin Upregulator, Dramatically Reduces the Dystrophic Symptoms in the mdx Mouse. *PLoS One*. 6:e19189. doi:10.1371/journal.pone.0019189.
Valentine, B.A., B.J. Cooper, J.F. Cummings, and A. deLahunta. 1986. Progressive muscular dystrophy in a golden retriever dog: light microscope and ultrastructural features at 4 and 8 months. *Acta Neuropathol.* 71:301–310.
Wada, Y. 2013. Vacuoles in mammals: a subcellular structure indispensable for early embryogenesis. *Bioarchitecture*. 3:13–19. doi:10.4161/bioa.24126.
Wang, B., J. Li, and X. Xiao. 2000. Adeno-associated virus vector carrying human minidystrophin genes effectively ameliorates muscular dystrophy in mdx mouse model. *Proc. Natl. Acad. Sci. U. S. A.* 97:13714–9. doi:10.1073/pnas.240335297.
Wang, Y., T. Shirogane, D. Liu, J.W. Harper, and S.J. Elledge. 2003. Exit from exit: resetting the cell cycle through Amn1 inhibition of G protein signaling. *Cell*. 112:697–709.
Wang, Z., C.S. Kuhr, J.M. Allen, M. Blankinship, P. Gregorevic, J.S. Chamberlain, S.J. Tapscott, and R. Storb. 2007. Sustained AAV-mediated dystrophin expression in a canine model of Duchenne muscular dystrophy with a brief course of immunosuppression. *Mol. Ther.* 15:1160–6. doi:10.1038/sj.mt.6300161.
Wang, Z., R. Storb, C.L. Halbert, G.B. Banks, T.M. Butts, E.E. Finn, J.M. Allen, A.D. Miller, J.S. Chamberlain, and S.J. Tapscott. 2012. Successful regional delivery and long-term expression of a dystrophin gene in canine muscular dystrophy: a preclinical model for human therapies. *Mol. Ther.* 20:1501–7. doi:10.1038/mt.2012.111.
Warner, L.E., C. DelloRusso, R.W. Crawford, I.N. Rybakova, J.R. Patel, J.M. Ervasti, and J.S. Chamberlain. 2002. Expression of Dp260 in muscle tethers the actin cytoskeleton to the dystrophin-glycoprotein complex and partially prevents dystrophy. *Hum. Mol. Genet.* 11:1095–105.
Way, M., B. Pope, R.A. Cross, J. Kendrick-Jones, and A.G. Weeds. 1992. Expression of the N-terminal domain of dystrophin in E. coli and demonstration of binding to F-actin. *FEBS Lett.* 301:243–5.
Weathington, N.M., and R.K. Mallampalli. 2014. Emerging therapies targeting the ubiquitin proteasome system in cancer. *J. Clin. Invest.* 124:6–12. doi:10.1172/JCI71602.
Wells, D.J., K.E. Wells, E.A. Asante, G. Turner, Y. Sunada, K.P. Campbell, F.S. Walsh, and G. Dickson. 1995. Expression of human full-length and minidystrophin in transgenic mdx mice: implications for gene therapy of Duchenne muscular dystrophy. *Hum. Mol. Genet.* 4:1245–1250.

Welser, J. V, J.E. Rooney, N.C. Cohen, P.B. Gurpur, C.A. Singer, R.A. Evans, B.A. Haines, and D.J. Burkin. 2009. Myotendinous junction defects and reduced force transmission in mice that lack alpha7 integrin and utrophin. *Am. J. Pathol.* 175:1545–1554. doi:10.2353/ajpath.2009.090052.

Winder, S.J., T.J. Gibson, and J. Kendrick-Jones. 1995. Dystrophin and utrophin: the missing links! *FEBS Lett.* 369:27–33.

Xu, L., K.H. Park, L. Zhao, J. Xu, M. El Refaey, Y. Gao, H. Zhu, J. Ma, and R. Han. 2016. CRISPR-mediated Genome Editing Restores Dystrophin Expression and Function in mdx Mice. *Mol. Ther.* 24:564–569. doi:10.1038/mt.2015.192.

Yamasaki, R., M. Berri, Y. Wu, K. Trombitas, M. McNabb, M.S. Kellermayer, C. Witt, D. Labeit, S. Labeit, M. Greaser, and H. Granzier. 2001. Titin-actin interaction in mouse myocardium: passive tension modulation and its regulation by calcium/S100A1. *Biophys. J.* 81:2297–2313. doi:10.1016/S0006-3495(01)75876-6.

Yamashita, K., A. Suzuki, Y. Satoh, M. Ide, Y. Amano, M. Masuda-Hirata, Y.K. Hayashi, K. Hamada, K. Ogata, and S. Ohno. 2010. The 8th and 9th tandem spectrin-like repeats of utrophin cooperatively form a functional unit to interact with polarity-regulating kinase PAR-1b. *Biochem. Biophys. Res. Commun.* 391:812–817. doi:10.1016/j.bbrc.2009.11.144.

Yang, J., Z. Wang, Y. Fang, J. Jiang, F. Zhao, H. Wong, M.K. Bennett, C.J. Molineaux, and C.J. Kirk. 2011. Pharmacokinetics, pharmacodynamics, metabolism, distribution, and excretion of carfilzomib in rats. *Drug Metab. Dispos.* 39:1873–82. doi:10.1124/dmd.111.039164.

Yin, J., A.J. Lin, D.E. Golan, and C.T. Walsh. 2006. Site-specific protein labeling by Sfp phosphopantetheinyl transferase. *Nat. Protoc.* 1:280–285. doi:10.1038/nprot.2006.43.

Young, C.S., M.R. Hicks, N.V. Ermolova, H. Nakano, M. Jan, S. Younesi, S. Karumbayaram, C. Kumagai-Cresse, D. Wang, J.A. Zack, D.B. Kohn, A. Nakano, S.F. Nelson, M.C. Miceli, M.J. Spencer, and A.D. Pyle. 2016. A Single CRISPR-Cas9 Deletion Strategy that Targets the Majority of DMD Patients Restores Dystrophin Function in hiPSC-Derived Muscle Cells. *Cell Stem Cell*. 18:533–540. doi:10.1016/j.stem.2016.01.021.

Zellweger, H., and A. Antonik. 1975. Newborn screening for Duchenne muscular dystrophy. *Pediatrics*. 55:30–34.

Zhu, Y., J. Bogomolovas, S. Labeit, and H. Granzier. 2009. Single molecule force spectroscopy of the cardiac titin N2B element: effects of the molecular chaperone alphaB-crystallin with disease-causing mutations. *J. Biol. Chem.* 284:13914–13923. doi:10.1074/jbc.M809743200.